NUTRIENT GRADIENTS IN THE RED SEA: THE COASTAL AREA OFF JEDDAH AND THE CENTRAL RED SEA

Dissertation in fulfilment of the requirements for the degree

Doctor rerum naturalium

of the

Faculty of Mathematics and Natural Sciences

at Kiel University

submitted by

DAVID PEÑA GARCÍA

Kiel, June 2022

First Examiner:	Prof. Dr. Roberto Mayerle
Second Examiner:	Prof. Dr. Christian Winter
Date of the oral examination:	June 29, 2022

SUMMARY

The present study deals with the nutrient situation in two different environments of the Red Sea: The polluted coastal waters off the Metropolitan Area of Jeddah/Saudi-Arabia and the strictly oligotrophic waters of the central Red Sea. The study was carried out by means of field campaigns, numerical modelling and *in situ* experiments. The overall objectives were: 1) the assessment of the nutrient gradients, the anthropogenic nutrient loads and the trophic status in the coastal waters of the Jeddah Metropolitan Area; 2) evaluation of the effect of nutrient load reduction or enhancement on coastal nutrient and phytoplankton biomass levels by means of numerical modelling, 3) investigation of the gradients of dissolved nutrients along a south-north transect in the central Red Sea, and 4) assessment of the importance of organic nitrogen transformation due to photomineralization in the central Red Sea.

Large amounts of wastewater rich in nutrients are discharged from the Jeddah Metropolitan Area into the adjacent coastal waters of the Red Sea. Daily loads of total nitrogen (TN) and phosphorus (TP) amount to ca. 6,564 kg N and 2,241 kg P, respectively, comprising 83 % of dissolved inorganic nitrogen and 33 % of dissolved phosphate. Steep gradients prevail nearshore, ranging from about 2,000 µM TN and 250 µM TP in the hypertrophic city lagoons to 6 µM TN and 0.4 µM TP in the oligotrophic open water offshore. It was found that sewage inputs from Jeddah's main outfall Al Khumra cause a widespread but moderate increase in surface nutrient concentrations due to the submerged diffuser pipe. The nutrient pool in the oligotrophic offshore water is dominated by dissolved organic and particulate forms, with nitrate frequently below the detection limit, indicating rapid transformation of inorganic nutrients. N:P ratios, as well as the comparison of nutrient levels with

half-saturation constants for phytoplankton growth, suggest that the limiting factor restricting primary production in the area is nitrogen.

A numerical model based on the Delft3D Modelling System was developed and applied to further study the impact of anthropogenic wastewater discharge on nutrient distribution and phytoplankton biomass in the coastal waters of the Jeddah Metropolitan Area. The model was coupled to an existing model covering the entire Red Sea. Transformation processes considered in the model were primarily nitrification, phosphorus and nitrogen remineralization, phytoplankton growth and mortality as well as nutrient uptake. The model was calibrated and validated using field data from two sampling campaigns. The good agreement obtained between field measurements and model results proves it adequacy as a tool in future research and management policies. Scenario runs to study the impact of reduction or increase in nutrient loads on coastal nutrient concentrations and on phytoplankton biomass were carried out. Modification of nitrogen loads resulted in a more pronounced effect on coastal phytoplankton biomass than changes in phosphorus loads. An 80% reduction in nitrogen discharges led to a 57 % decrease in both nutrient and chlorophyll-*a* concentrations in a confined area in the inner Jeddah bight. However, nutrient enhancement and phytoplankton biomass were still high when compared to the situation in pristine coastal waters.

The hydrographic structure along the transect in the central Red Sea was consistent with the typical winter pattern and characterized by the inflow of warm and less saline surface water from the Indian Ocean through the Bab-el-Mandeb strait. A common feature were the oligotrophic inorganic nitrogen and phosphorus concentrations in the upper mixed layer of the central Red Sea with a N:P ratio well below the Redfield value. Nitrate and phosphate surface concentrations were in most cases below the detection limit, but increased substantially below the upper mixed layer. Ammonium was completely depleted while nitrite exhibited a maximum located at about 40 to 80 m depths, being shallower and more pronounced in the south of the Red Sea.

Chlorophyll-*a* concentrations were very low in the upper mixed layer not exceeding 0.1 µg L^{-1} with exception of higher levels of ca. 0.3 µg L^{-1} observed at the northernmost stations. There was a typical deep chlorophyll maximum which reached up to 0.5 µg L^{-1} in the northern part of the central Red Sea.

Surface photomineralization of dissolved organic nitrogen in the central Red Sea averaged 1.7 µmol N m^{-3} d^{-1} and ranged between 1.0 and 2.7 µmol N m^{-3} d^{-1}. Integrated photomineralization in the euphotic zone averaged ca. 41.7 µmol N m^{-2} d^{-1}. When compared to other inorganic nitrogen sources e.g. turbulent intrusion from deeper waters, photomineralization is considered to be a process bringing only moderate amounts of bioavailable nitrogen to the strongly N-limited environment prevailing in the surface waters of the central Red Sea.

ZUSAMMENFASSUNG

Die vorliegende Arbeit befasst sich mit der Nährstoffsitution in zwei unterschiedlichen Gebieten des Roten Meeres: Die durch Abwassereinträge verschmutzten Küstengewässer vor der Metropolregion Jeddah/Saudi-Arabien und die ausgeprägt oligotrophen Gewässer des zentralen Roten Meeres. Im Zentrum der Untersuchungen standen: 1) die Ermittlung der Nährstoffgradienten, der anthropogenen Nährstoffeinträge und des Trophiegrades der Küstengewässer vor Jeddah; 2) die numerische Modellierung der Auswirkungen einer Erhöhung oder Reduzierung der Nährstoffeinträge auf die Nährstoffverteilung und Phytoplanktonbiomasse im Küstenwasser; 3) die Verteilung gelöster Nährstoffe entlang eines Süd-Nord-Schnittes im zentralen Roten Meer; 4) die Bedeutung des photochemischen Abbaus von gelöstem organischen Stickstoff im zentralen Roten Meer.

Erhebliche Mengen an nährstoffreichen Abwässern gelangen aus der Metropolregion Jeddah in die vorgelagerten oligotrophen Küstengewässer. Die täglichen Frachten an Gesamtstickstoff (TN) und Gesamtphosphor (TP) belaufen sich auf 6564 kg N und 2241 kg P mit einem Anteil von 83 % an anorganisch gelöstem Stickstoff bzw. 33 % an gelöstem Phosphat. Die Einträge machen sich küstennah in steilen Nährstoffgradienten bemerkbar, in denen die Konzentrationen von 2000 µM TN und 250 µM TP in den hypertrophen Küstenlagunen auf 6 µM TN und 0,4 µM TP im seewärtigen Küstenwasser absinken. Abwassereinträge aus dem Haupteinleiter, Al Khumra, führen dagegen zu einer großflächigen, jedoch moderaten Erhöhung der Nährstoffkonzentrationen im Oberflächenwasser, da die Einleitung über ein mehrdüsiges Diffuserrohrleitungssystem erfolgt. Im küstenferneren, oligotrophen

Wasser wird der Nährstoffpool durch organisch gelöste und partikuläre Verbindungen dominiert. Die Nitratgehalte sind weitgehend erschöpft, was auf eine rasche Umsetzung der anorganisch gelösten Stickstoffeinträge hinweist. Das N:P-Verhätnis wie auch der Vergleich der Nährstoffkonzentrationen mit Halbsättigungskonstanten der Nährstoffaufnahme deuten auf eine Stickstofflimitierung des Phytoplanktonwachstums hin.

Um die Auswirkungen der Nährstoffeinleitungen auf die Nährstoffausbreitung und die Phytoplanktonbiomasse im Küstenwasser von Jeddah zu untersuchen, wurde ein numerisches Modell auf Basis des Delft3D-Modellierungssystems entwickelt, welches an ein funktionales Modell des gesamten Roten Meeres gekoppelt war. Im Modell berücksichtigt wurden Umsatzprozesse durch Nitrifizierung, Stickstoff- und Phosphorremineralisierung, Phytoplanktonwachstum und –mortalität sowie Nährstoffaufnahme. Das Modell wurde mit Daten zweier Feldmessskampagnen kalibriert und validiert. Die gute Übereinstimmung von Feldmessungen und Modelldaten bestätigt die Leistungsfähigkeit des Modells zur Lösung künftiger Forschungs- und Managementaufgaben. Szenarienläufe mit erhöhten und reduzierten Nährstofffrachten ergaben, dass sich eine Änderung der Stickstoffeinträge stärker auf die Phytoplanktonbiomasse im Küstenwasser auswirkt als veränderte Phosphorfrachten. Eine 80 %ige Reduzierung der Stickstoffeinträge führte zu einem Rückgang der Nährstoff- und Chlorophyllkonzentrationen in der inneren Jeddahbucht um 57 %. Im Vergleich zum unverschmutzten Küstenwasser waren die Nährstoff- und Chlorophyllgehalte jedoch noch stark erhöht.

Die hydrographische Struktur entlang des Schnittes im zentralen Roten Meer entsprach den für das Gebiet typischen Winterverhältnissen mit einem Einstrom salzärmeren, warmen Oberflächenwasser aus dem Indischen Ozean durch die Meerenge von Bab-el-Mandeb. Kennzeichnend waren weiterhin die oligotrophen Stickstoff- und Phosphorkonzentrationen in der Deckschicht mit einem N:P-Verhältnis deutlich unter der Redfieldzahl. Die Nitrat- und Phosphatkonzentrationen

lagen in der durchmischten Oberflächenschicht meist unter der Nachweisgrenze, stiegen jedoch darunter rasch an. Ammonium war vollständig aufgezehrt. Die Nitritverteilung zeigte ein Maximum in 40 bis 80 m Tiefe, welches im Süden flacher und stärker ausgeprägt war. Die Chlorophyll-*a* Konzentrationen lagen im Oberflächenwasser unter 0,1 µg L^{-1} mit Ausnahme etwas höherer Konzentrationen (0,3 µg L^{-1}) an der nördlichsten Station. Direkt unterhalb der durchmischten Deckschicht wurde ein typisches Chlorophyllmaximum angetroffen, welches im nördlichsten Bereich Konzentrationen von 0,5 µg L^{-1} erreichte.

Der photochemische Abbau von gelöstem organischen Stickstoff bewegte sich im zentralen Roten Meer im Bereich von 1,0 bis 2,7 µmol N m^{-3} d^{-1} mit einem Durchschnittswert von 1,7 µmol N m^{-3} d^{-1}. Die für die gesamte euphotische Zone integrierte Photomineralisation belief sich auf 41.7 µmol N m^{-2} d^{-1}. Für die Versorgung der oligotrophen Deckschicht mit bioverfügbarem Stickstoff hat der photochemische Abbau von gelöstem organischen Stickstoff im Vergleich zu anderen anorganischen Stickstoffquellen (e.g. turbulente Diffusion aus tieferen Wasserschichten) nur eine untergeordnete Bedeutung.

ACKNOWLEDGEMENTS

Having pursued the doctorate at Kiel was a very rewarding experience.

I thank the DAAD for having supported me during most of the time I lived in Germany.

I thank the City of Kiel for having welcomed me and given me the opportunity to carry out my studies.

I thank CORELAB at the University of Kiel for having embraced me as its doctoral student. At CORELAB, I thank my Doktorvater Prof. Dr. R. Mayerle who was always joyful, helpful and eager to discuss scientific aspects. I also specially thank Dr. Hesse for his many hours of support, guidance, help, and for sharing the interest in my scientific questions. I also thank all my colleagues at CORELAB for the friendly time shared at the office, in the field campaigns, at lunch or some random pubs.

I thank the University of Jeddah and the Jeddah Transect Project for the support and fund of the research.

I thank the many great friends I had the opportunity to share lots of laughs, toasts, grills, and special moments that made my time in Germnay so awesome; you guys remain (and will) in my most appreciated memories.

I thank life for giving me all these experiences.

I dedicate this achievement to my son Santiago and my wife Piedad, who are now the strongest support.

CONTENTS

LIST OF FIGURES

LIST OF TABLES

1. INTRODUCTION

Coastal areas are among the most biodiverse and important ecosystems in the world due to their unique transition between terrestrial and deep pelagical waters, as well as the availability of substrate. However, an increasing number of these systems is exposed to high anthropogenic pressure. Populations in coastal zones are growing faster than in any other region on Earth (World Ocean Review, 2010). As a consequence, the adjacent waters are often subjected to a high load of pollutants entering the marine system through continental run-off, atmospheric deposition or from the direct discharge of domestic and industrial wastewater effluents.

Nutrient pollution is among the most prominent drivers in marine habitat degradation. Nitrogen and phosphorus enrichment of susceptible coastal areas can cause excessive increase in algal biomass, resulting in the destruction of sea grasses and coral reefs, reduction of water transparency and oxygen availability, reduced populations of fish and shellfish and, more general, a decline in biodiversity (Smith, 2006). In some seas (North Sea and Yellow Sea) the annual fluxes of nutrients (nitrogen and phosphorus) to their coasts have been increased anthropogenically by 10 to 15 fold (Howarth and Marino, 2006). Although eutrophication, as the main consequence of nutrient enrichment, has been largely researched and debated, it remains as one of foremost problems in coastal ecosystem protection and many questions are still to be answered (Schindler, 2006).

There is scientific consensus that nitrogen enrichment represents one of the major threats to the equilibrium of coastal ecosystems (Howarth and Marino, 2006). Nitrogen has been shown to be predominantly the limiting resource for primary production in most of the nutrient poor marine surface waters (Tyrrell and Law, 1997;

Corredor *et al.*, 1999; Tyrrell, 1999). Several paths and reactions bring nitrogen into and transform it in the euphotic and photosynthetically active layer of the ocean. Two different types of nitrogen sources have been traditionally defined (Dugdale and Goering, 1967): the so-called new nitrogen, which enriches the euphotic layer with exogenous nitrogen through upwelling and/or diffusion of nitrate (NO_3^-), continental run-off, dissolved N_2 fixation and/or atmospheric deposition (Eppley and Peterson, 1979); and the regenerated nitrogen, which is the product of recycling of the existing pool of organic nitrogen into inorganic nitrogen (mainly ammonium, NH_4^+). In oligotrophic marine waters (such as the oligotrophic subtropical gyres) production mostly relies on regenerated nitrogen (Yool *et al.*, 2007; Clark *et al.*, 2008; Painter, 2011).

Several studies point out to the role that photochemistry (the reaction of chemical compounds exposed to a band of radiation; Miller, 1983) has on the transformation and recycling of dissolved organic nitrogen (DON) and/or inorganic nitrogen (DIN) in open oceanic (Kitidis *et al.*, 2006), coastal regions (Bushaw *et al.*, 1996; Buffam and McGlathery, 2003) and river plume waters and estuaries (Morell and Corredor, 2001; Kitidis *et al.*, 2008). The production of NH_4^+ through photomineralization of DON has been shown to play an important role as a source of bioavailable nitrogen for N-limited planktonic communities, being comparable to other sources such as atmospheric deposition (Kitidis *et al.*, 2006; Stedmon *et al.*, 2007) or even periodically exceeding it (Vähätalo and Zepp, 2005). Furthermore, a high percentage of DON in the water is refractory (ibid.) but can be transformed by the photochemical process into biologically available nitrogen (Obernosterer and Benner, 2004), which would otherwise be out of reach for primary producers. In temperate pelagic areas the role of photomineralization should be largest in summer during periods of high irradiation, low DIN concentrations and N-limited primary production (Vähätalo and Zepp, 2005), but less important on a yearly basis. On the other hand, in tropical or

subtropical areas, such as the main part of the Red Sea, the photochemical process should have a permanent impact the whole year round.

1.1. The Red Sea and the Jeddah Metropolitan Area

The Red Sea is among the most oligotrophic environments with large areas dominated by species-rich coral reef communities hosting a high biodiversity. Since a steady natural freshwater runoff and a significant upwelling of nutrient rich deep water is missing (UNEP, 1985), coastal settlements may represent a major source of nutrient enrichment to this sensitive ecosystem.

Jeddah, located on the Red Sea coast, is the second largest city of Saudi Arabia and an important industrial centre. More than 900 factories are located in Jeddah, with food processing, mineral products, chemical and plastic production, metal industries, paper and textile manufacturing dominating the sector (Jeddah Chamber of Commerce and Industry, 2009). The Jeddah Metropolitan Area (JMA) has recently experienced a large population increase, from about 300,000 inhabitants in the early 1970's to over 3.4 mill. people in 2010. This population boom is expected to continue, with estimates of 5.7 mill. people living within the metropolitan area by the year 2029 (Jeddah Municipality, 2009). During the time of the present study only 45 % of the population were covered by sanitary sewerage networks, while the remaining population continues to rely on the use of septic tanks (ibid.). Existing wastewater treatment facilities are deficient and often work over their recommended capacities. As a consequence, a mixture of treated and raw wastewater is released into the oligotrophic coastal waters (Mudarris and Turki, 2006). Wastewater discharge constitutes a considerable threat to the sensitive marine ecosystem, dominated by species-rich coral reef communities. Previous studies have indicated a significant enhancement in nutrient levels (Shaik *et al.*, 1986; El-Rayis, 1998; El Sayed, 2002;

Al-Farawati *et al*., 2008; Basaham *et al.*, 2009; Al-Farawati, 2010), as well as in contaminants (Saad and Fahmy, 1996; Basaham, 1998; Turki, 2007) and faecal bacteria (Turki & Mudarris, 2008) in the Jeddah Bay. Such enhancements go along with direct and indirect eutrophication effects such as increases in phytoplankton biomass (Khomayis, 2002), degradation of mangrove stands (Mandura, 1997) and shifts in the benthic community structure (Al-Farraj *et al.*, 2012). These studies, however, were confined to discrete areas immediately adjacent to the outfalls and thus did not allow for a comprehensive appraisal of nutrient inputs and dispersion into the coastal water. In addition, in view of the rapid population growth, ongoing efforts have been made in the past few years to improve wastewater management within the city including the upscaling of existing and construction of new sewage treatment plants.

1.2. The Present Research

The general aim of this work was to evaluate the nutrient situation of both the coastal area off Jeddah and the oligotrophic marine waters of the central Red Sea by means of field campaigns, numerical modelling and *in-situ* experiments. To achieve these goals, the present research is divided into the following objectives:

1) assessment of the nutrient distribution (N, P) in the coastal waters off the Jeddah Metropolitan Area (JMA), 2) determination of the actual nutrient loads deriving from wastewater discharge into the coastal area of the JMA, 3) evaluation of the trophic status and potential nutrient limitation in the area, 4) application of a numerical model in order to simulate the fate of anthropogenic nutrient discharges and the effect of nutrient load reductions or enhancements in the coastal waters, 5) assessments of the gradients of dissolved nitrogen and phosphorus on a south-north transect along the oligotrophic central Red Sea, and 6) quantification of nitrogen transformation due to

photomineralization in the central Red Sea and to evaluate its environmental importance.

The study has been carried out within the framework of a large interdisciplinary project called “The Jeddah Transect”, which was funded by the King Abdulaziz University (KAU), Saudi Arabia. Leading institution on the German side were the Helmholtz Centre for Ocean Research (GEOMAR) in Kiel, on the Saudi Arabian side the KAU in Jeddah.

The objectives of the present work are developed in the following chapters. Chapter 2 presents a general description of the study area, including the Jeddah’s coastal environment and the Red Sea. Chapter 3 details the methods used in the sampling campaigns and experiments, laboratory analyses, model development, information acquisition, processing and calculations. Results are presented in Chapter 4. It includes a description of salinity and nutrient gradients in Jeddah’s coastal waters, evaluation of anthropogenic nutrient inputs deriving from the city and results of an assessment of the eutrophication of the coastal waters (section 4.1). In the following results of a numerical model for both the simulation of nutrient and chlorophyll-*a* distribution in the coastal area are presented, including results of model simulations of nutrient load reduction and enhancement scenarios (section 4.2). Section 4.3 deals with the distribution of physico-chemical parameters and nutrients in oligotrophic open sea waters on a transect from south to north along the central axis of the Red Sea. Finally, in section 4.4 experimental results of nitrogen photomineralization in the central Red Sea are given and photomineralization rates integrated for the entire euphotic zone are presented. Chapter 5 presents a general discussion of the results. Main conclusions and recommendations are written in Chapter 6.

2. STUDY AREA

2.1. The Red Sea

The Red Sea is a long, narrow basin separating the African from the Asiatic continent. The Sea extends from N-NW to S-SE between 30°N to 12°30'N almost in a straight line (Figure 2.1.). Its total length is about 1932 km and average breadth is ca. 280 km. The maximum breadth is only 306 km in the southern sector (paragraph taken literal from Morcos, 1970). At its northern end it forks to form the Gulfs of Suez and Aqaba while, in the south, it meets the Gulf of Aden and the Indian Ocean through Bab-el-Mandeb Strait (UNEP, 1985).

Most of the current knowledge of the physical oceanography of the Red Sea is based on a study presented by Morcos (1970). Very few comprehensive investigations regarding nutrients have been carried out throughout this large marine ecosystem, among which are those by Naqvi *et al.* (1986) and Grasshof (1969). In contrast to the central area, the north of the Red Sea, i.e. the Gulf of Aqaba, and the south, i.e. the Bab-el-Mandeb Strait, have been investigated more intensely.

2.1.1. Physical Characteristics

The area of the Red Sea is about 4.38×10^5 km^2, the average depth is ca. 491 m while the greatest depth is over 2500 m (Morcos, 1970). The real separation of the Red Sea from the Gulf of Aden is situated north of Bab-el-Mandab Strait, where the deepest channel is slightly greater than 100 m (Morcos, 1970). This strait acts as a shallow sill

which physically limits the influence of the Indian Ocean on the Red Sea (UNEP, 1985).

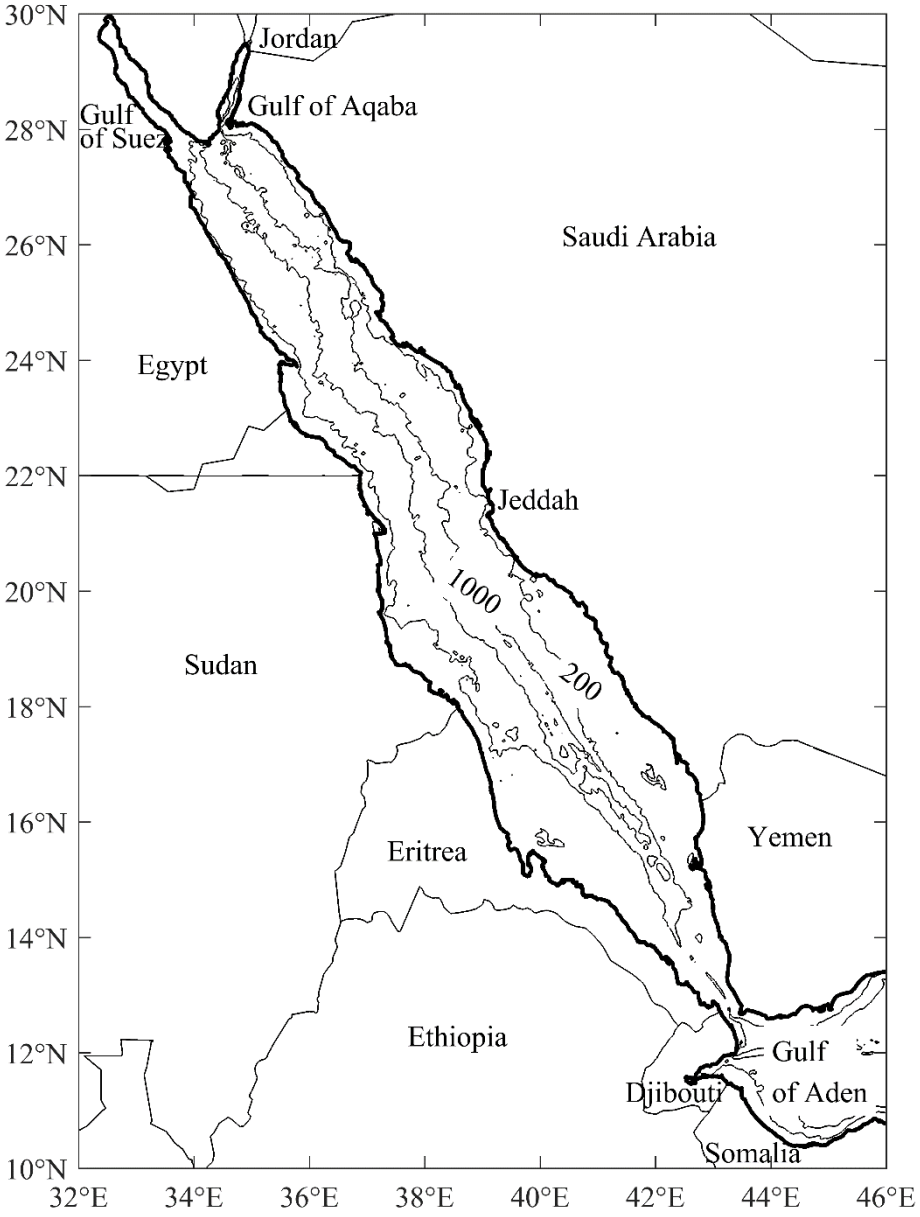

Figure 2.1. The Red Sea. Isolines of 200 m and 1000 m depth are shown. Northern Gulfs of Suez and Aqaba, southern Gulf of Aden and political boundaries are shown. Bathymetry data from ETOPO global relief model (Amante and Eakins, 2009). Own elaboration.

The Red Sea is surrounded by very arid areas leading to a yearly net evaporation rate of about 2.1 m yr^{-1} (Sofianos *et al.*, 2002). In general, the average precipitation is extremely small, ranging between ca. 0.15 and 0.50 m yr^{-1} (Sofianos *et al.*, 2002). Because most rainfall in the region falls in short showers and thunderstorms, flash floods are a widespread feature. They generally occur yearly at one location and are more frequent in the southern Red Sea than in the north (UNEP, 1985). The runoff is negligible since there are no major rivers discharging into the sea; the net evaporative loss is then made up for by inflow from the Bab-el-Mandeb Strait (Shaik *et al.*, 1986). The winds generally blow along the axis of the sea with three distinct regimes (Morcos, 1970): N-NW throughout the year in the area northwards of about 20°N; in the area southwards of about 20°N wind direction is also from N-NW but only in the period from May to September. From October to April winds generally change to S-SE; a third regime develops in the intermediate region between October and April when the N-NW winds from the northern region and the S-SE winds from the southern region meet. This latter area is characterized by relatively low-pressure calms.

Regarding the air temperatures, the south of the Red Sea is considered to be among the hottest regions of the world. The lowest temperatures are found in the northern part, though never below 5 °C.

The average spring tidal range is about 0.5 m, but decreases from both ends of the Red Sea towards the central area where, near Port Sudan and Jeddah, there is no appreciable semidiurnal tide (UNEP, 1985); in this region there is an amphidromic center (Morcos, 1970).

Both water temperature and salinity are the highest of the world for marine environments. Surface water temperatures change with the latitude throughout the year. The warmest surface water is found between the latitudes 16 N and 18 N with an annual average of 28.7 °C and reaching values as high as 31.9 °C in September

(Morcos, 1970). The minimum surface temperature averages 21.9 °C in January between 26 N and 28 N. The depth of the surface layer above the thermocline varies from 100 to 200 m. Below this layer, temperature decreases slowly to minimum values of about 21.6 °C at ~370 m from where it remains almost constant (UNEP, 1985).

The Red Sea salinity changes also with the latitude, from 36 PSU in the south, i.e. the Gulf of Aden, to highest values of 40.6 PSU in the north at depths of 300 m (Morcos, 1970). There is a slight shift in salinity from east to west, the salinity being slightly higher on the Egyptian side than on the Saudi-Arabian (ibid.). The changes along the year are small, of only some tenths of a salinity unit.

Shaik *et al.* (1986) reported Secchi disc readings in the central Red Sea as much as 32 m, suggesting a euphotic zone of >100 m.

2.1.2. Chemical Characteristics

The Red Sea is among the most oligotrophic marine environments, with vastly rich reef communities and a high biodiversity. The epipelagic zone from surface to 100 m depth is nutrient poor and there is low phytoplankton and zooplankton diversity (UNEP, 1985). Nitrate is more often depleted than phosphate (UNEP, 1997). Deep sea waters are also relatively oligotrophic and species poor (UNEP 1985).

Shaik *et al.* (1986) reported low and often undetectable ammonium, nitrite and soluble reactive phosphorus concentrations in the surface layer. They varied along the year, with higher values between February and April, and lesser between May and September. Nitrate supply to the upper layers, where it is almost completely depleted, is progressively less significant from south to north, due to diffusion from an underlying intermediate water mass richer in nutrients flowing from the Indian Ocean into the Red Sea (Poisson *et al.*, 1984). Nitrogen losses (based on nitrate) of the Red Sea through the Bab-el-Mandab Strait have been estimated to account for

6.2×10^{10} mol yr^{-1} due to an outflowing bottom current; the losses could be balanced by nitrogen fixation of coral reef communities (Bethoux, 1988) and *Trichodesmium* (Naqvi *et al.*, 1986). Nitrogen contributions into the Red Sea by rivers and rainwater are minimal (Morcos, 1970).

Shaik *et al.* (1986) reported bimodal seasonality in chlorophyll-*a* concentrations, with higher values from December to February and from June to September.

The concentration of oxygen is low because of the high temperature and salinity and the fact that photosynthetic production of oxygen is quite small (Poisson *et al.*, 1984). Three layers are distinct with respect to oxygen: the upper layer which is saturated or almost saturated with oxygen, a well developed intermediate oxygen minimum layer, and deep water layer with oxygen concentrations higher than in the intermediated layer (Poisson *et al.*, 1984).

2.2. The Coastal Environment of Jeddah

Jeddah is located on the Red Sea coast of Saudi Arabia in the Tihama coastal plain in front of the Sarawat mountains. The arid climate is characterised by high air temperatures with an average of 28.5°C over the last 15 years and a range from 13°C to up to 51°C. The wind regime is dominated by winds from N to NNW directions (Basaham *et al.*, 2009); average precipitation rate is as low as 54 mm y^{-1} (Ewea, 2010). Apart from a number of rarely flooded wadis, surface waters draining the hinterland of Jeddah are absent (Al-Farawati *et al.*, 2008). Jeddah Bay represents a natural harbour due to the shelter of coral reefs and exhibits a few semi-enclosed lagoons, some of which are located close to downtown Jeddah like Al Shabab and Arbaeen lagoon (Figure 2.2.). Both lagoons receive massive discharges of partly treated wastewaters. Another important wastewater outlet is the submerged Al

Khumra sewer pipe in the southern area. The sewer pipe discharges about 500 m off the coast in water depths between about 25 m and 50 m (Figure 2.2.).

Jeddah's coastal waters are characterised by high surface temperatures and salinities accounting for an annual average of 29 °C and 38.8 PSU in Jeddah Bay (Suleiman A. Aziz *et al.*, 2011). Towards the open sea the area exhibits steep bathymetric gradients which are part of the rift valley between Africa and the Arabian Peninsula. The 500 m isobath spreads close to the coast, often less than 1 n.m. away from the shore. As a result water depths larger than about 600 m are common in the area of investigation. An amphidromic point in the centre of the Red Sea is responsible for a minor tidal range usually smaller than 0.5 m. The tides in the coastal waters of Jeddah are typically mixed and predominantly semi-diurnal. Hence, water exchange of the bay is primarily wind-driven, but hindered by numerous coral reef barriers resulting in long residence times.

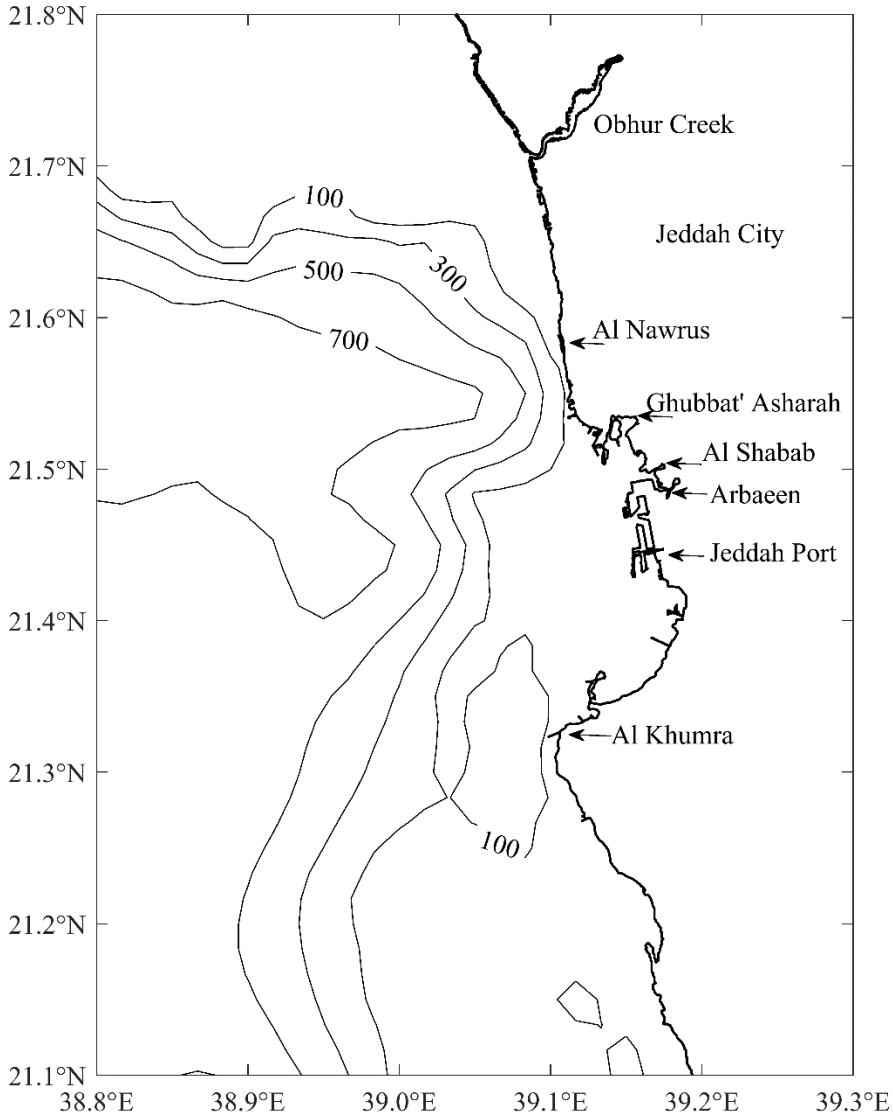

Figure 2.2. Jeddah's coastal area on the Red Sea with isobaths (m). Obhur Creek, Al Shabab and Arbaeen lagoons, the port and the location of main wastewater outfall Al Khumra are shown. Bathymetry data and line boundaries from the National Geophysical Data Center-National Oceanic and Atmospheric Administration (NGDC-NOOA) Own elaboration.

2.2.1. Freshwater Consumption and Wastewater Production in Jeddah

Wastewater budget estimations for Jeddah are presented in Table 2.1. Taking into account the mean daily freshwater production in 2009, and considering losses due to

leakage of water conduits as well as disposal on land and wastewater reuse, a total wastewater discharge in the order of 5.0×10^5 m^3 d^{-1} is estimated along the coast.

Main wastewater outlets at Al Khumra, Arbaeen and Al Shabab lagoons account for a total discharge of ~4.0×10^5 m^3 d^{-1}. From these values, it can be derived that 9.9×10^4 m^3 per day of wastewater is discharged by diffuse inputs and smaller outlets such as inside Ghubbat` Asharah lagoon or at Al Nawrus in the North.

Table 2.1. Daily wastewater budget and discharge of wastewater outlets.

Wastewater budget	**Volume** [10^3 m^3]	**Reference**
Freshwater production	777	SWCC, 2009
Loss through leakage (20 %)	155	Shawly, 2008
Freshwater consumption° = wastewater generation	622	Approximation
Disposal sewage lake (Wadi Al Asla)	50	Ewea, 2010
Reuse for irrigation and industry	70	Jeddah Municipality, 2009
Total wastewater discharge to coastal waters*	**502**	
Discharge wastewater outlets		
Al Khumra sewage pipe	300	Basaham *et al.*, 2009
Arbaeen lagoon	68	El-Rayis and Moammar, 1998
Al Shabab lagoon	35	El-Rayis and Moammar, 1998
Diffuse inputs & small wastewater outlets	99	Difference to total budget
Total discharge of wastewater outlets	**502**	

° calculated by subtracting loss through leakage from freshwater production.
* calculated by subtracting the disposal to sewage lake and reuse for irrigation and industry from wastewater generation.

3. MATERIALS AND METHODS

In this chapther a detailed description of sampling sites, sampling procedures, data acquisition, data analysis and calculations is given. Three sampling campaigns were carried out for the development of the present research. The first two campaigns aimed at studying the nutrient distribution and loads in the coastal waters of the Jeddah Metropolitan Area (JMA). They were carried out in April and October 2011. The purpose of the third sampling campaign was to assess the nutrient situation and photomineralization on a south-north transect along the central Red Sea. It was carried out in April 2012. Details of a numerical model developed for the Jeddah coastal area are also provided hereafter.

3.1. Field Measurements

The two measuring campaigns in the coastal waters of the JMA were conducted from aboard a 15 m motorboat in April and October 2011 and were supplemented by simultaneous land-based sampling along the coastline (Figure 3.1.). The aim of the first campaign was to get a comprehensive overview on local sources of nutrient inputs and on horizontal and vertical gradients in the coastal waters. It consisted of a spatial grid ranging from Obhur Creek in the north to Al Khumra south of Jeddah Bay, including a transect perpendicular to the coast starting at the inlet of Al Shabab and Arbaeen lagoons. Shipborne measurements during the second campaign were confined to this transect and to a small scale study in the vicinity of the Al Khumra

wastewater outlet in the South (see Figure 3.1.a). As for the land-based sampling, they were repeated in both April and October 2011.

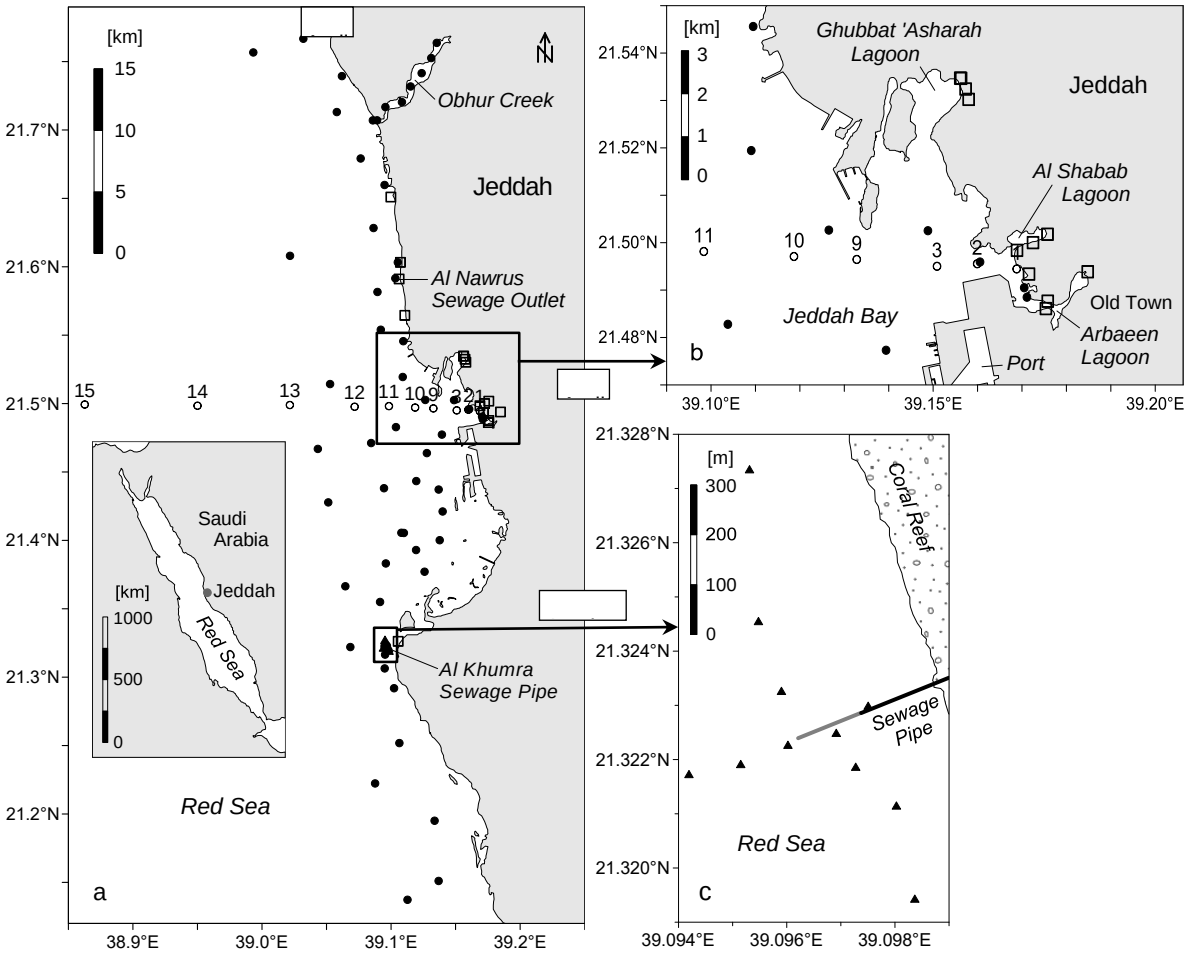

Figure 3.1. Sampling stations in April and October 2011 (a, b: black dots = shipborne survey in April; circles = shipborne survey in October; squares = land-based sampling in April and October; c: magnified view of Al Khumra study in October 2011).

Surface water samples were taken from aboard with a 5 L Niskin bottle (Hydro-Bios, Germany). Vertical hydrographic profiles up to a depth of 45 m were conducted with a CTD multiprobe (Sea and Sun Technology, Germany) The CTD was equipped with

a Clark cell for the assessment of dissolved oxygen levels (OxyGuard, Denmark) and a backscat fluorometer for phytoplankton chlorophyll-*a* measurements (Dr. Haardt, Germany) and calibrated against discrete measurements. Land-based sampling was performed with a telescopic sampler. Water temperature and salinity of land-based samples were determined by means of a portable temperature and conductivity meter (brand: WTW, Germany).

Results of these two sampling campaigns are presented in sections 4.1. and 4.2.

The third sampling campaign was carried out in the central waters of the Saudi Arabian Red Sea from south (16.5°N-40.9°E) to north (27.0°N-35.1°E) on-board the Dutch Research Vessel Pelagia. This campaign was part of a larger expedition within the framework of the joint project "The Jeddah Transect" held from 8th to 22nd April 2012. Samples from seven stations (Figure 3.2.) were collected at six different depths with a CTD-multiprobe-rosette system. The CTD system was equipped with 12-liters PVC bottles with Teflon-coated springs (OceanTest). At each station, vertical profiles of salinity, temperature, oxygen, chlorophyll-*a* and photosynthetically active radiation were taken with the CTD-multiprobe (Seabird Electronics). The CTD was assembled to a SBE43 dissolved oxygen sensor, a Chelsea Aquatracka MKIII fluorometer and a Satlantic logarithmic PAR sensor. During the entire expedition, global radiation was measured at the deck of the vessel. Besides, a hyperspectral UV-VIS radiometer (TriOs Ramses ACC-VIS) was used to measure radiation for a range of wavelengths from 275 and 720 nm. Measurements were done both in air and beneath sea surface down to a depth of ~50 m. Water samples and the in-situ data from the multiprobe were kindly provided by the joint project team.

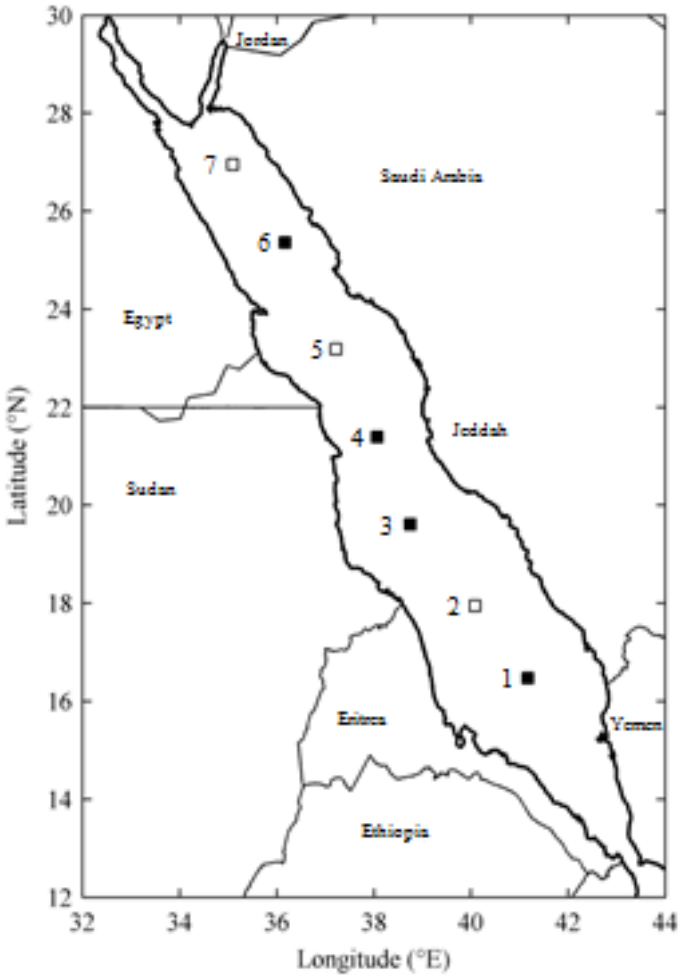

Figure 3.2. Map of the Red Sea. Stations are marked with black squares and numbered. Filled squares indicate stations where *in-situ* experiments were carried out.

3.2. Laboratory Analyses

Samples were analysed for total nitrogen (TN), total phosphorus (TP), ammonium (NH_4^+), nitrite (NO_2^-), nitrate (NO_3^-), urea (for the first two sampling campaigns), phosphate (PO_4^{3-}) and dissolved organic nitrogen (DON, for the third sampling campaign). Unfiltered subsamples for the analysis of TN and TP were stored in the laboratory at −10 °C in 200 ml acid-washed PE bottles until hot digestion to nitrate

with persulfate. Subsamples used for the determination of urea-N, NH_4^+, NO_2^-, NO_3^- and PO_4^{3-} were filtered directly after sampling through Rotilabo® syringe filters of 0.45 µm pore size, fixed with mercury chloride ($HgCl_2$) and stored in the dark at 4 °C in 250 ml acid-washed PE bottles prior to further analysis. Dissolved and particulate organic nitrogen (DON+PON), as well as dissolved and particulate phosphorus (DOP+PP) were calculated as the difference between total nutrient concentrations and dissolved inorganic fractions. Samples for DON analysis were filtered on board through Rotilabo® syringe filters of 0.45 µm pore size, immediately oxydised with persulfate in a pressure cooker and stored dark and cool in 50 mL brown glass bottles until further analysis in the laboratory. Nutrient concentrations were determined according to the colometric method as described by Grasshoff *et al.* (1999).

3.3. Photochemical Experiments

On the south-north transect along the central Red Sea, two replicate subsamples were taken from the water surface (0.5 m) at stations 1, 3, 4 and 6 (see Figure 3.2.). The samples were filtered through 0.2 µm membrane filters (Millipore), filled without headspace in pre-cleaned 0.5 L quartz glass bottles and exposed on deck to natural sunlight for approximately 8.5 h from morning to just before sunset in a running seawater incubator. A second subsample and a replicate were taken as blank. They were treated accordingly, but incubated in the dark in bottles wrapped with aluminium foil. DON concentrations were determined at the beginning and end of the incubations. After correction with the dark control, DON photomineralization rates were calculated from the difference of these concentrations.

3.4. Models' Set-up and Simulations of the Jeddah's Coastal Area

A description of the numerical model for simulation of flow and water quality in the Jeddah coastal waters is provided hereafter.

3.4.1. Hydrodynamic and Transport Model

A hydrodynamic model for the Jeddah near coastal waters was developed. The model is based on the Delft3D Modelling System (Delft Hydraulics). A radial grid centred in the Jeddah Bight is adopted on the horizointal plane (Figure 3.3.a). Altogether about 13,500 cells ranging from 60 m in the Jeddah Bight to 2300 m at the open sea boundary are used. Over the vertical 12 layers are considered (Figure 3.3.b). The model was set-up with the Z-model configuration in the vertical discretization, meaning that the layers' thicknesses are fixed, except for the top layer thickness, which is determined by the actual water level (Deltares, 2014). This configuration is recommended for aquatic systems that might have a strong stratification, which is the case for the central Red Sea. The vertical layers were set up to have the following thicknesses (from top to bottom): 18, 24, 33, 45, 61, 83, 113, 154, 209, 284, 386 and 530 m; the recommended variation-factor between consecutive layers should be within the range of 0.7 to 1.4 (ibid.), was maintained.

The radial grid of the Jeddah Model has a radius of about 120 km. Given that currents in the central Red Sea are very low and usually below 0.18 m/s (see Figure 3.4.a), [weekly modelled data for the years 1958 to 2008 from the Simple Ocean Data Assimilation reanalysis – SODA2.1.6. (National Center for Atmospheric Research Staff, 2016)] and averaging about 0.1 m s^{-1} (Madah *et al.*, 2015); the time step for the hydrodynamic and transport model was set to 5 min in order to preserve the Courant-Friedrichs-Lewy (CFL) condition.

Bathymetry data and line boundaries (Figure 3.4.b) were taken from the National Geophysical Data Center-National Oceanic and Atmospheric Administration (NGDC-NOOA). The flow model is run with water levels and meteorological data as external forcing. The water levels imposed at the open sea boundaries were taken from a larger scale model covering the entire Red Sea (for details, see Madah *et al.*, 2015). The latter is forced at the open sea boundary near the at Bab-el-Mandeb strait with 8 astronomical constituents (Q_1, O_1, P_1, K_1, N_2, M_2, S_2 and K_2) obtained from the global ocean tidal model TPXO 7.2).

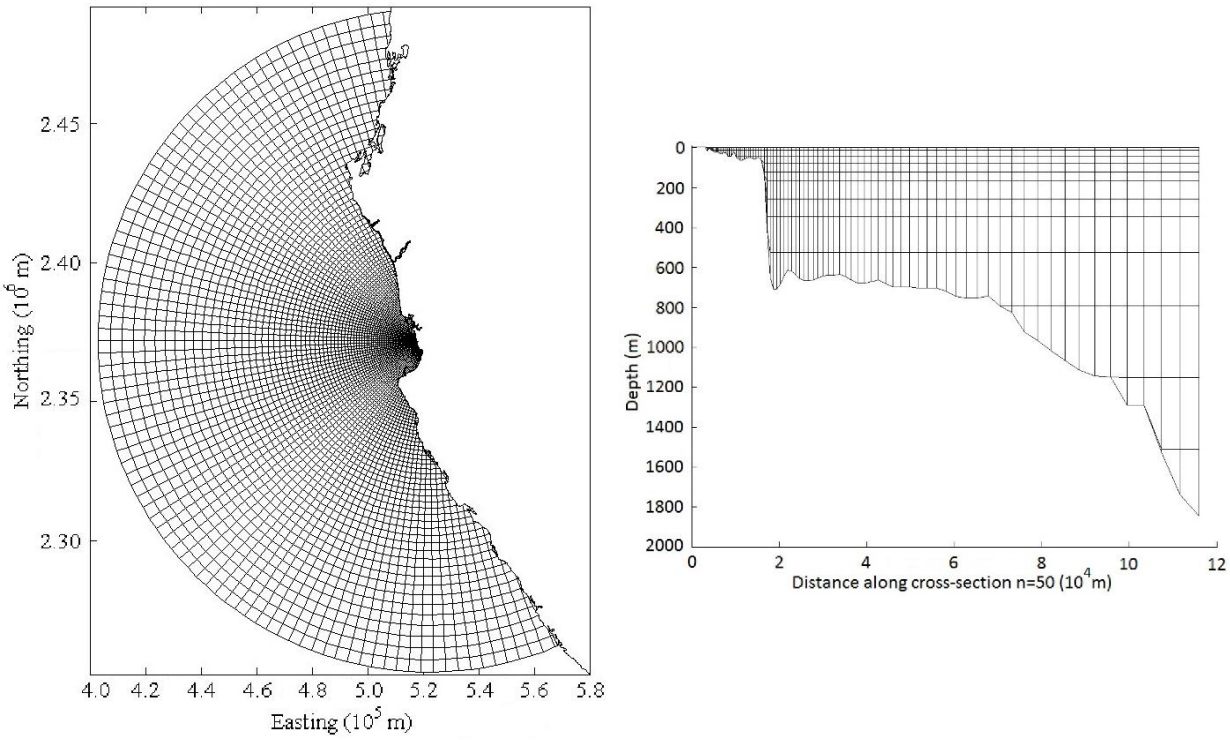

(a) (b)

Figure 3.3. Grid of the Jeddah Model (a) horizontal grid and (b) vertical grid.

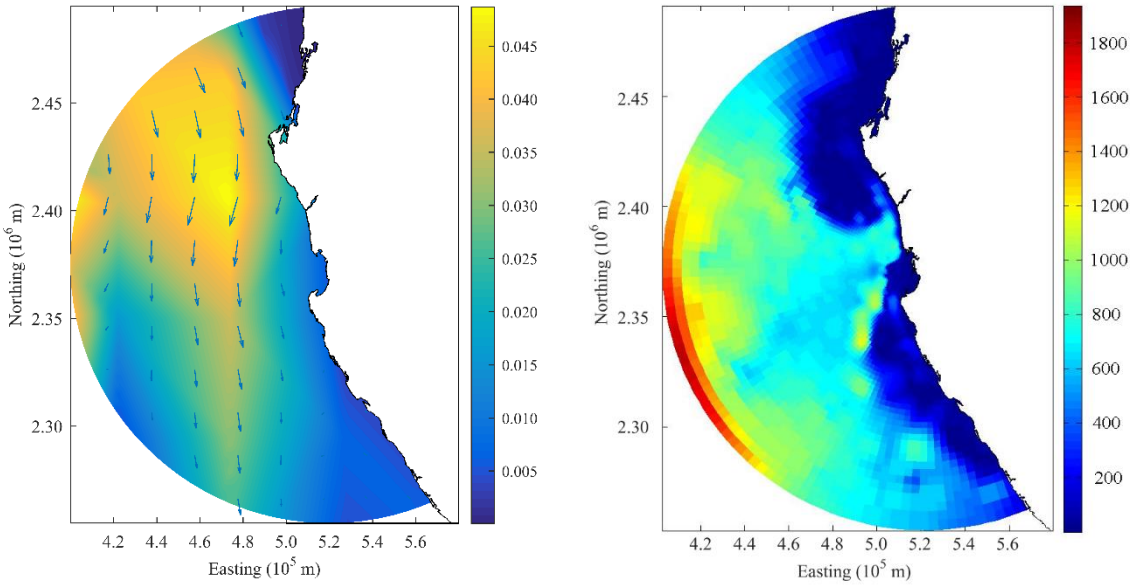

(a) (b)

Figure 3.4. Surface currents' magnitudes in the central Red Sea (a). The values (m s^{-1}) are the mean of weekly modelled data from SODA2.1.6. (National Center for Atmospheric Research Staff, 2016) interpolated into the hydrodynamic model grid. Current vectors are shown. Bathymetry (b) of the hydrodynamic model grid; values in m.

Temperature and salinity boundary conditions were set constant in time and their layered values at the open sea boundaries were taken from World Ocean Atlas (WOA09: temperature: Locarnini *et al.*, 2010; salinity: Antonov *et al.*, 2010). The meteorological data, including air temperature, relative humidity, wind direction and magnitude, as well as air pressure were taken from the Germany's National Meteorological Service (Deutsche Wetter Dienst, DWD). The flow model is run including the process' equations for temperature and salinity; initial values over the vertical for these parameters were taken from WOA09 (temperature: Locarnini *et al.*, 2010; salinity: Antonov *et al.*, 2010). Given that these realistic initial conditions were set in the model in order to remove initialization bias, the warming-up period for the model was defined as 1 month according to Hoad *et al.* (2010). The model was run for two years (2010 and 2011) with the corresponding meteorological forcing (air

temperature, relative humidity, wind direction and velocity magnitude, and air pressure), i.e. unsteady state; except for the waste water discharges which were kept constant due to unknown variability.

In order to account for waste water discharges along the coast, five main outlets were set at their corresponding locations (Figure 3.5.a) with the following discharges (Table 2.1.): a) Al Khumra sewage pipe, 3.0×10^5 m^3 d^{-1} (Basaham *et al.*, 2009); b) Arbaeen lagoon, 6.8×10^4 m^3 d^{-1}; c) Al Shabab lagoon, 6.8×10^4 m^3 d^{-1} (both data from El-Rayis & Moammar, 1998); d) An Nowras, 1.0×10^4 m^3 d^{-1}; and e) Ghubbat 'Asharah, 3.2×10^4 m^3 d^{-1} (Peña-García *et al.*, 2014).

The hydrodynamic and transport model was validated against salinity and temperature data from ARGO floats (ARGO) from the central Red Sea and against vertical salinity profiles taken at 8 stations in the inner Jeddah Bay in October 2011 (Figure 3.5.a).

3.4.1. Water Quality Model (WAQ)

A water quality module (Deltares, Delft Hydraulics, version 4.03, May 2011) was coupled to the results of the hydrodynamic transport model, i.e. to the outputs for advective transport and vertical dispersion. WAQ comprises process equations for ammonium, nitrate, phosphate, detrital nitrogen (DetN) and phosphorus (DetP), as well as microalgae (chl-*a*). In the calculation of these variables, the processes of nitrification, remineralization, net primary production, phytoplankton mortality, and nutrient uptake and release were taken into account.

Nutrient transformation due to nitrification and remineralization is accounted for according to the following equation (modified from Deltares, 2011):

$$R = K_1 \times [X] \qquad \text{Equation 3.1}$$

where R [gN m^{-3} d^{-1}] is the process' rate, K_1 [d^{-1}] is a first order rate for remineralization or nitrification corrected for ambient temperature and $[X]$ [g m^{-3}] is the current concentration of either NH_4^+, DetN or DetP.

Net primary production of algae is calculated according to (modified from Deltares, 2011):

$$NPP = \left\{\left[\left(PP_{Max} \times f_N \times f_{T,G} \times f_L\right) - \left(K_{MR} \times f_{T,M}\right)\right] \times \left(1 - K_{Rsp}\right)\right\} \times [Chl_a]$$

Equation 3.2

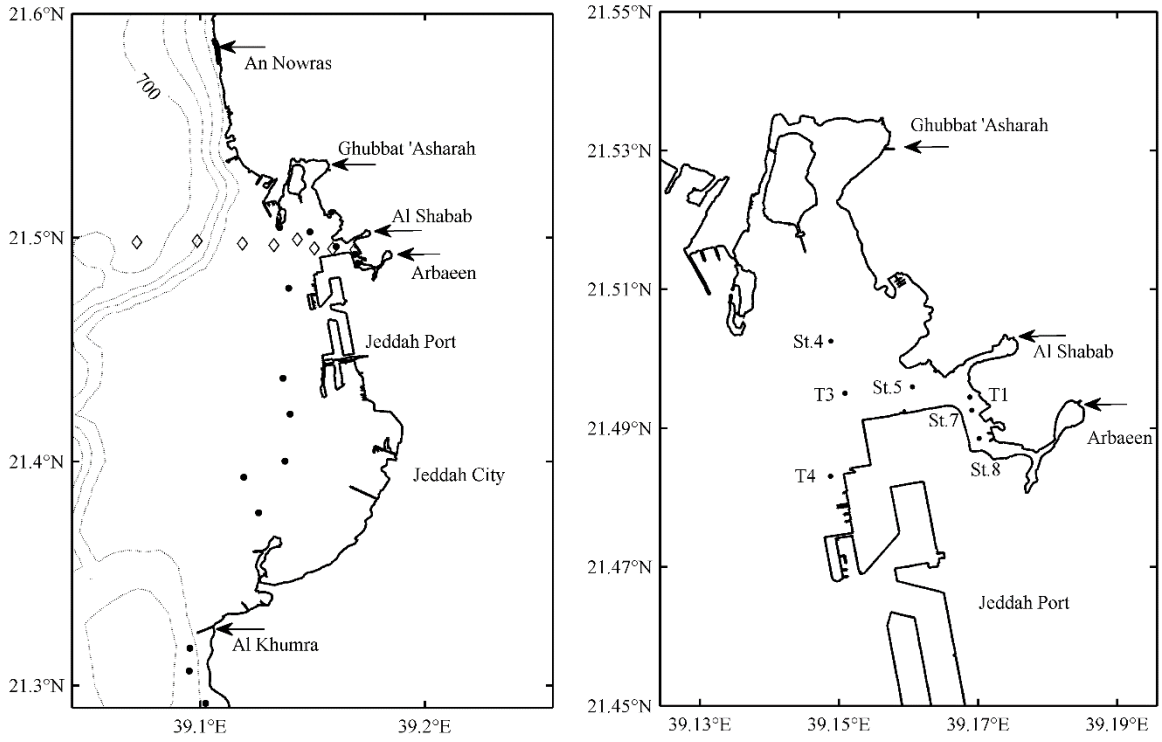

(a) (b)

Figure 3.5. Study area showing the five main waste water discharges (a, arrows), 8 stations for salinity validation (a, diamonds) and 13 stations sampled in April 2011 and used for calibration of the water quality model (a, black dots). Close up of the inner Jeddah Bay (b) showing 4 stations (T1, St.5, T3 and T4) sampled for model validation in October 2011 as well as locations used in the sensitivity analyses (St.8, St.7, St.5 and St.4).

where NPP [gC m^{-3} d^{-1}] is the net primary production rate of algae, PP_{Max} [d^{-1}] is the potential maximum primary production rate constant, $f_{T,G}$ [dimensionless] is a growth temperature function, f_L [dimensionless] is a light limitation function, K_{MR} [d^{-1}] is a constant of maintenance respiration, $f_{T,M}$ [dimensionless] is a mortality correcting function to ambient temperature, K_{Rsp} [dimensionless] is the growth respiration factor, and Chl_a [gC m^{-3}] is the algae biomass concentration. f_N [dimensionless] is a limiting function based on the availability of dissolved inorganic nutrients as follows:

$$f_N = \frac{[N]}{[N]+K_{half-sat}} \qquad \text{Equation 3.3}$$

where $[N]$ is the nutrient concentration [g m^{-3}] being either $[NH_4^+] + [NO_3^-/prf]$ or $[PO_4^{3-}]$; prf is a factor of preference for NH_4^+ over NO_3^- uptake. $K_{half-sat}$ [g m^{-3}] is the half saturation constant for dissolved nitrogen or phosphate.

Phytoplankton mortality is calculated as (modified from Deltares, 2011):

$$M = K_M \times f_{T,M} \times [Chl_a] \qquad \text{Equation 3.4}$$

where M [gC m^{-3} d^{-1}] is the mortality rate and K_M [d^{-1}] is the mortality rate constant.

Nutrient uptake by phytoplankton growth is calculated as (modified from Deltares, 2011):

$$N_{upt} = NPP \times CNP \times f \qquad \text{Equation 3.5}$$

where N_{upt} [g m^{-3} d^{-1}] is the nutrient uptake rate, CNP is the corresponding C:N:P ratio in phytoplankton biomass, and f [dimensionless] is a function for the relative amount of NH_4^+ or NO_3^- taken up on total dissolved inorganic nitrogen and equals 1 for phosphorus uptake.

Nutrient release by phytoplankton mortality is considered as (modified from Deltares, 2011)

$$N_{release} = M \times CNP \times f \quad \text{Equation 3.6.}$$

where $N_{release}$ [g m^{-3} d^{-1}] is the nutrient release rate, f defines the fraction of nutrients released as dissolved inorganic or organic nutrient (F(din/det)). In the present study, phytoplankton biomass was assessed as chlorophyll-*a*. Phytoplankton carbon had thus to be transformed into chlorophyll-*a* equivalents using a carbon-to-chlorophyll-*a* ratio of 99 g/g (Sathyendranath *et al.* 2009).

The water quality model was run with the same time step as the hydrodynamic model, i.e. 5 min. The warming up period accounted for 1 month. For model parameters not subjected to calibration, the default values listed in Table 3.1 were taken from Deltares (2011).

Table 3.1. Values of WAQ parameters not subjected to calibration (Deltares, 2011).

Parameter [unit]	**Value**
Growth temperature coefficient [dimensionless]	1.04
Mortality temperature coefficient [dimensionless]	1.07
Growth respiration factor [dimensionless]	0.15
Maintenance respiration [d^{-1}]	0.031
CNP [molar ratio]	106:16:1

Initial layered concentrations for NO_3^- and PO_4^{3-} were taken from World Ocean Atlas 2009 (WOA09; Garcia *et al*., 2010). For all the other parameters, offshore field data from the sampling campaign carried out in April 2011 were considered (Table 3.2.). DetN and DetP initial conditions were assumed to be 20 % the DON+PN and DOP+PP (see 3.2. Laboratory Analyses) concentrations, respectively. Vertical

hydrographic profiles from the sampling campaign in April 2011 (see 3.1. Field Measurements) were used for validation. Nutrient loads from the Jeddah Metropolitan Area as listed in Table 3.2 were calculated using the wastewater discharge rates (see 2.2.1. Freshwater Consumption and Wastewater Production in Jeddah) and estimates of wastewater nutrient concentrations (see 4.1.5. Nutrient Loads from the Jeddah Metropolitan Area) according to Peña-García *et al.* (2014).

Table 3.2. Initial nutrient concentrations and daily nutrient loads of wastewater discharges from the JMA into the Red Sea.

Parameter	**Initial Value [µM/µg L^{-1}]**	**Loads [kg d^{-1}]**				
		An Nowras	**Ghubbat 'Asharah**	**Al Shabab**	**Arbaeen**	**Al Khumra**
NH_4^+-N	0.58	40	129	141	274	1210
NO_3^--N	0.11*	68	218	240	465	2049
PO_4^{3-}-P	0.23*	15	47	52	101	446
DetN-N	0.86	55	176	192	357	1648
DetP-P	0.03	30	95	104	194	894
chl-*a*	0.29	-	-	-	-	-

* surface concentrations.

3.4.2. Sensitivity Analyses, Calibration and Validation of the Water Quality Module

WAQ sensitivity analyses: Sensitivity of modelled chlorophyll-*a* levels to different rates of model parameters listed in Table 3.3, corresponding to the equations of the five processes activated in the software was carried out. Mean, maximum and minimum rates were applied.

WAQ calibration: The water quality module was calibrated against field measurements of chlorophyll-*a*, NO_3^-, NH_4^+ and PO_4^{3-} concentrations carried out at highly polluted to pristine sites at 13 stations in April 2011 (Figure 3.5.a). The calibration procedure involved several simulations changing the most impactful process rates according to the results of the sensitivity analyses.

Validation of the WAQ: The calibrated WAQ model was validated using field data of dissolved inorganic nutrient and chlorophyll-*a* concentrations from 4 stations (T1, T3, T4 and St. 5) along a coastal nutrient gradient sampled in October 2011 (Figure 3.5.b). The performance of the calibrated model was evaluated by means of the mean relative error (MRE), mean absolute error (MAE), normalized mean absolute error (NMAE), root mean square error (RMSE), normalized root mean square error (NRMSE) and bias.

Table 3.3. Parameters used in the sensitivity analyses and model calibration.

Parameter/Rate	**Abbr.**	**Unit**	**Sensitivity Range**
Autolysis fraction dissolved inorganic nutrients/detrital organic nutrients	F(din/det)	(-)	0 - 1[a]
Half-Saturation Constant DIN[*]	Khalf-sat	mg N L^{-1}	$(1.4 - 59)\times10^{-3}$;[b]
Mineralization	K-min	d^{-1}	0.02[c] - 0.075[d]
Mortality	K-mort	d^{-1}	0.25 - 1.2[b]
Nitrification	K-nitrif	d^{-1}	0.02 - 2.00[e]
Potential Maximum Production	PPMax	d^{-1}	0.1 - 2.1[f]
NH_4^+ Preference over NO_3^-	NH4-pref	(-)	0 - 1[a]

[*] The value for the half saturation constant for phosphate changed proportionally according to the N:P Redfield ratio (7.2:1). [a] Deltares (2011). [b] Tyrrel (1999). [c] Koropitan *et al.* (2009). [d] Chen *et al.* (2011). [e] Yool *et al.* (2007). [f] Furnas (1990).

3.4.3. Scenarios

The validated model was applied to the simulation of a number of scenarios, covering either an 80% decrease or a 50% increase in mass loading rates of: a) all nitrogen species, b) all phosphorus species and c) both nutrient forms. A decrease of 80% was anticipated assuming an efficient upscaling of waste water treatment capacities in Jeddah including tertiary sewage treatment. The 50% increase in pollution was chosen according to the predicted population boost over the next two decades.

4. RESULTS

In this chapter, the main results of the investigations are summarized. The investigations were based on the results of the sampling campaigns carried out in April and October 2011 for the coastal waters of the Jeddah Metropolitan Area (JMA), and the central Red Sea carried out in April 2012 (see 3.1. Field Measurements).

4.1. Nutrient gradients and loads in the coastal Red Sea off Jeddah

In this sub-chapter, results of the investigations for the coastal waters of the JMA, based on the sampling campaigns of April and October 2011, are summarized. Emphasis is given to the analysis of nitrogen and phosphorus, their distribution and relative chemical species composition, their potential limitation of primary production, their loads from the JMA and, finally, eutrophication is assessed.

4.1.1. Salinity Distribution

Intense insolation and evaporation, together with low precipitation and the absence of riverine freshwater inputs in the area, lead to high water temperatures and to salinity values which exceeds oceanic levels. In April 2011, average surface temperatures of about 27.0 °C were observed, which are 3.7 K lower as compared to the temperature values of 30.7 °C measured in October 2011. Average surface temperatures and salinities at offshore sites proved to be insignificantly different from those prevailing

at a depth of 45 m, revealing only minor vertical gradients both in April and October 2011.

Figure 4.1 presents the salinity distribution in the coastal area of the Red Sea in front of the JMA for April and October 2011 (a), detailing the distribution of the Jeddah Bay (b) and the area of the Al Khumra outlet (c).

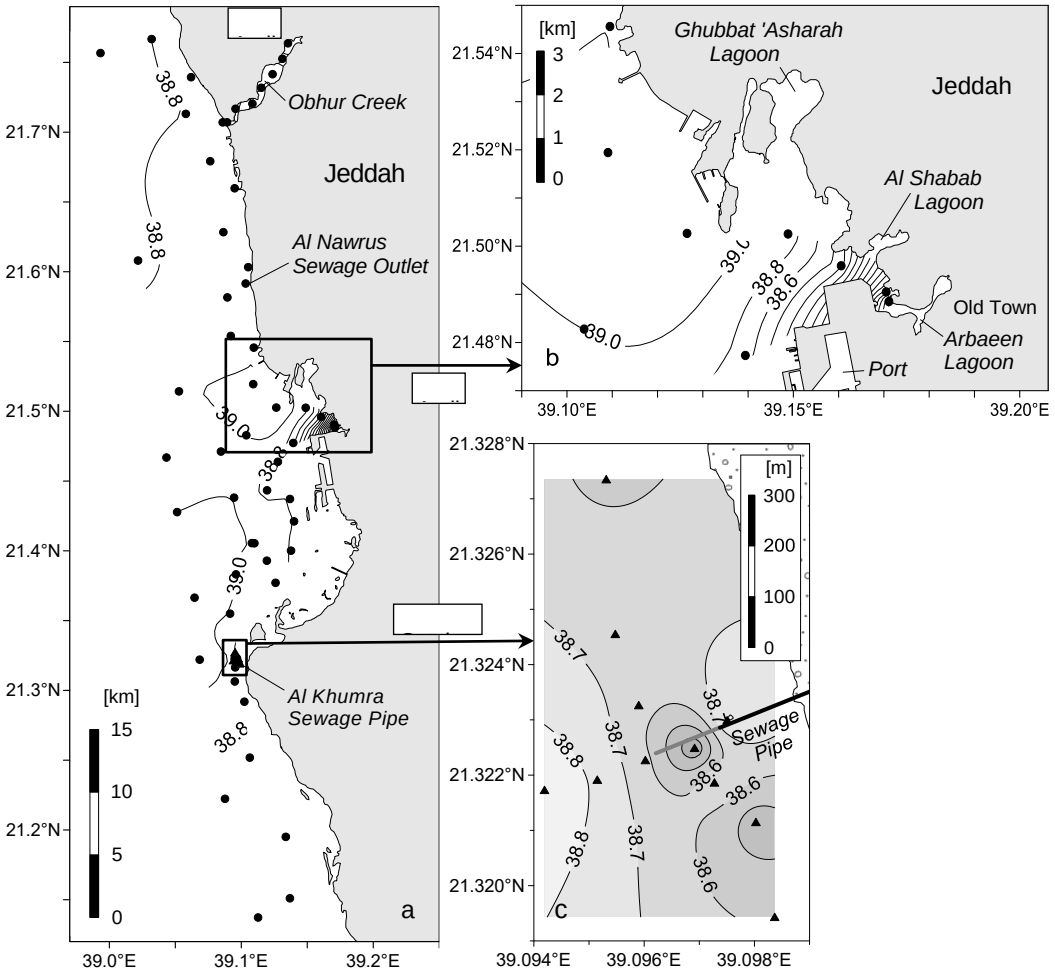

Figure 4.1. Salinity distribution (PSU) in the coastal waters of Jeddah in April 2011 (a), magnified view of Jeddah Bay (b) and gradients at Al Khumra outlet in October 2011 (c).

Horizontal surface patterns in offshore waters show uniform salinity levels of about 38.8 to 39.0 PSU in April 2011 (Figure 4.1.a) and 39.0 to 39.2 PSU in October 2011. As a result of wastewater discharge, a steep salinity gradient towards the mouth of the inner bay lagoons Al Shabab and Arbaeen resulted locally. Salinity values ranging from 38.8 to 35.2 PSU in April (Figure 4.1.b) and 39.0 to 35.5 PSU in October were observed. Inside the lagoons, salinity values in the surface water further decreased down to minimum values of 1 PSU in the direct vicinity of sewage outlets. This confirms that the two lagoons represent the main sources of urban freshwater input to the shallow inner bay area. By contrast, the small scale study conducted at Al Khumra in October 2011 yielded a confined decline in salinity of 0.7 PSU in the surface water overlying the serial diffuser system (Figure 4.1.c).

4.1.2. Hot Spots of Nutrient Inputs and Dispersion

Figure 4.2 and Figure 4.3 present the total nitrogen (TN) and total phosphorus (TP) distribution, respectively, in the coastal area of the Red Sea in front of the JMA for April and October 2011 (a), detailing the distribution of the Jeddah Bay (b) and the area of the Al Khumra outlet (c).

The land-based sampling revealed several hot spots of increased nutrient concentrations along Jeddah Bay (Figure 4.2 and Figure 4.3).

High levels of TN and TP prevailed inside the lagoons in front of the wastewater outlets in April, with peak values of 2045 µM TN inside Al Shabab lagoon and 308 µM TP inside Arbaeen lagoon. Moreover, high concentrations of both TN and TP were also measured at Ghubbat `Asharah lagoon in the northernmost part of the bay.

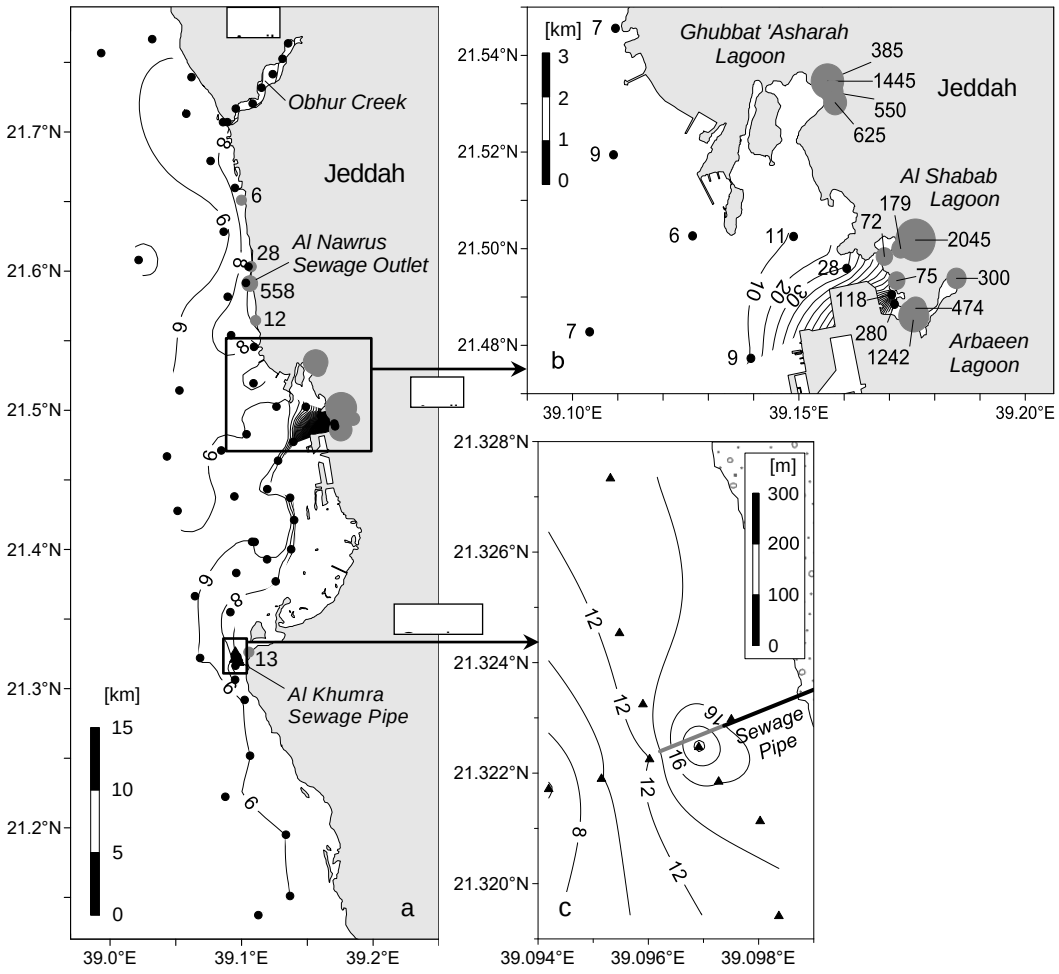

Figure 4.2. Total nitrogen (TN) concentrations [µM] at local sources of nutrient inputs (scaled grey dots) and in the coastal waters in April 2011 (a), magnified view of Jeddah Bay (b) and gradients at Al Khumra outlet in October 2011 (c).

Another, albeit less concentrated, hot spot of nutrient emissions is the Al Nawrus wastewater outlet situated outside Jeddah Bay on the northern corniche of Jeddah. The impact from this source, however, is restricted to the direct vicinity of the outlet which is subjected to recreational activities and touristic resorts.

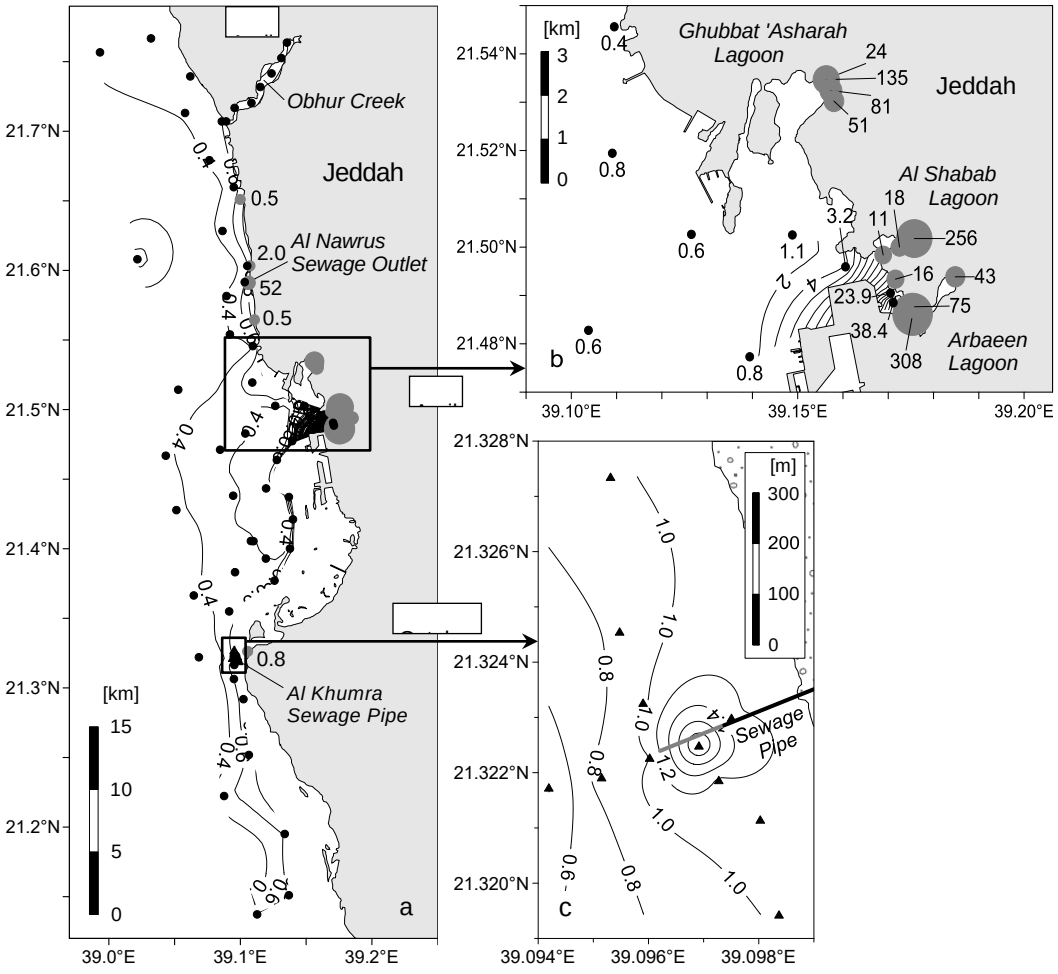

Figure 4.3. Total phosphorus (TP) concentrations [µM] at local sources of nutrient inputs (scaled grey dots) and in the coastal waters in April 2011 (a), magnified view of Jeddah Bay (b) and gradients at Al Khumra outlet in October 2011 (c).

In the inner bay, steep gradients are apparent north of the port where discharges from the lagoons interfuse. Within this mixing zone, TN and TP concentrations rapidly decrease from highly polluted to oligotrophic conditions within a span of 2 n.m. These sharp gradients are consistent with the reduced tidal flushing of the semi-enclosed lagoons in the inner bay area, and the prevalence of north-western winds. In keeping with the pattern of salinity, the nutrient distribution in open water was rather

homogenous, exhibiting concentrations typical for oligotrophic conditions of ~6 µM TN (Figure 4.2.) and ~0.4 µM TP (Figure 4.3.) during the surveys in April and October. Unfortunately, it was not possible to investigate the effect of nutrient emissions from the Ghubbat `Asharah lagoon on gradients inside the bay, due to restricted access. Nevertheless, nutrient concentrations 2 n.m. south of the Ghubbat `Asharah outlet appeared to be unaffected by these inputs.

Figure 4.4 presents the distribution of the inorganic species of nitrogen (ammonium, NH_4^+; nitrite, NO_2^-; nitrate NO_3^-) and phosphorus (phosphate, PO_4^{3-}) for the Jeddah Bay while Figure 4.5 for the Al Khumra outlet. Consistent with TN and TP, levels of dissolved inorganic nitrogen components and phosphate sharply decreased from the mouth of the lagoons to uniformly low concentrations in the coastal water (Figure 4.4.). This holds especially true for nitrate and ammonium, which were largely exhausted in the coastal water with nitrate levels occasionally below the detection limit. Compared to the steep gradients in dissolved inorganic nutrients, urea levels showed only a moderate increase from 0.2 to 0.5 µM in the pristine offshore water up to 6.0 µM in areas surrounding the wastewater outlets inside the lagoons.

Nutrient data from the westward transect conducted in October (see stations 1-15 in Figure 3.1.) revealed similar gradients as observed in April. However, maximum nutrient concentrations inside the lagoons were lower in October, concomitant with increased salinity. When compared to data collected in April, significantly lower levels of dissolved inorganic nitrogen and phosphate prevailed in the open coastal water, with both nitrate and ammonium levels often below the limit of detection. In contrast, offshore levels of TN and TP were consistent during both surveys.

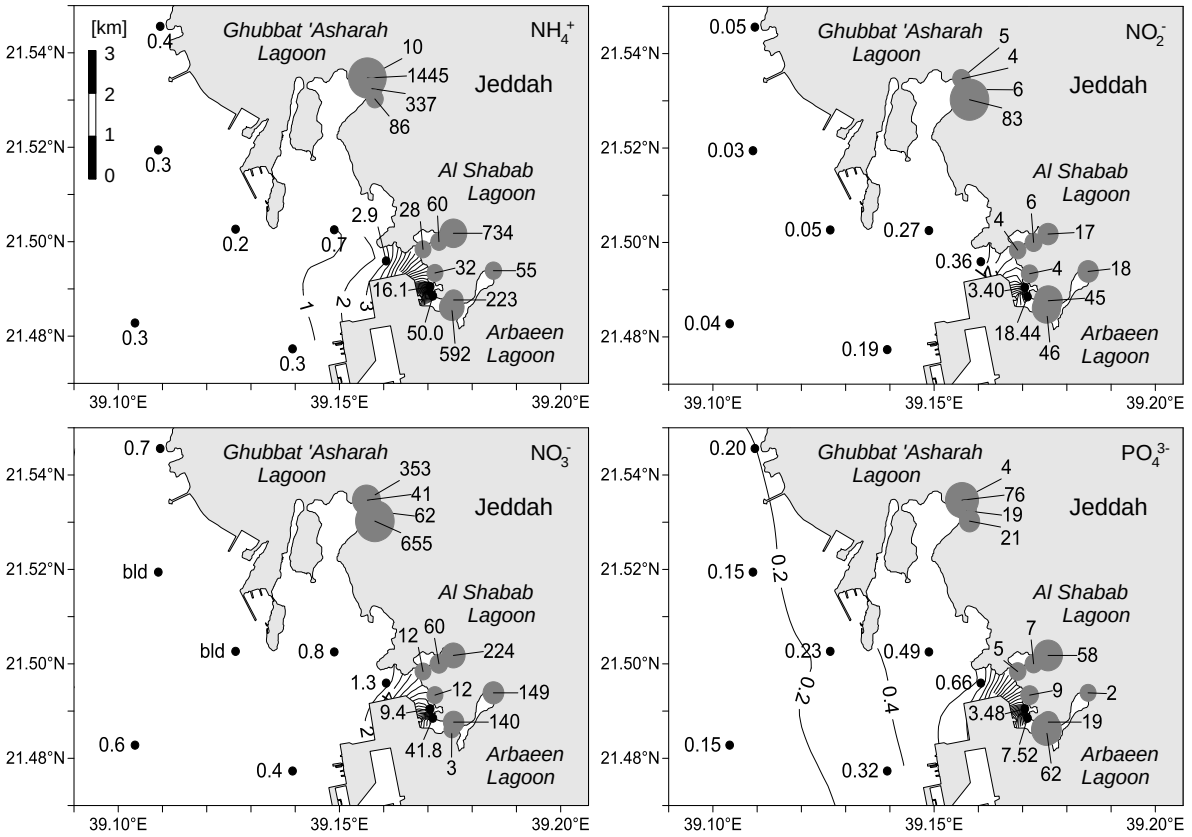

Figure 4.4. Ammonium (NH_4^+), nitrite (NO_2^-), nitrate (NO_3^-), and phosphate (PO_4^{3-}) concentrations [µM] at local sources of nutrient inputs (scaled grey dots) and dispersion of inorganic nutrients inside Jeddah Bay in April 2011 (bld = below limit of detection).

In contrast to the strong impact of wastewater discharge on nutrient levels in front of central Jeddah, nutrient enhancement in the surface water close to the Al Khumra sewage outlet in the south of Jeddah Bay turned out to be comparatively moderate with peak TN and TP values of 21 µM and 2.1 µM respectively (Figure 4.2.c and Figure 4.3.c). This represents an increase in TN by a factor of 4 and in TP by a factor of 5 when compared to the low concentrations in the outer coastal water. Nutrient levels rapidly decreased towards the offshore area down to background values, whereas elevated levels persisted in the nearshore water, north and south of the outlet.

Dissolved inorganic nitrogen and phosphate accounted for approximately half of TN and TP, with nitrate being the dominant inorganic species (Figure 4.5.).

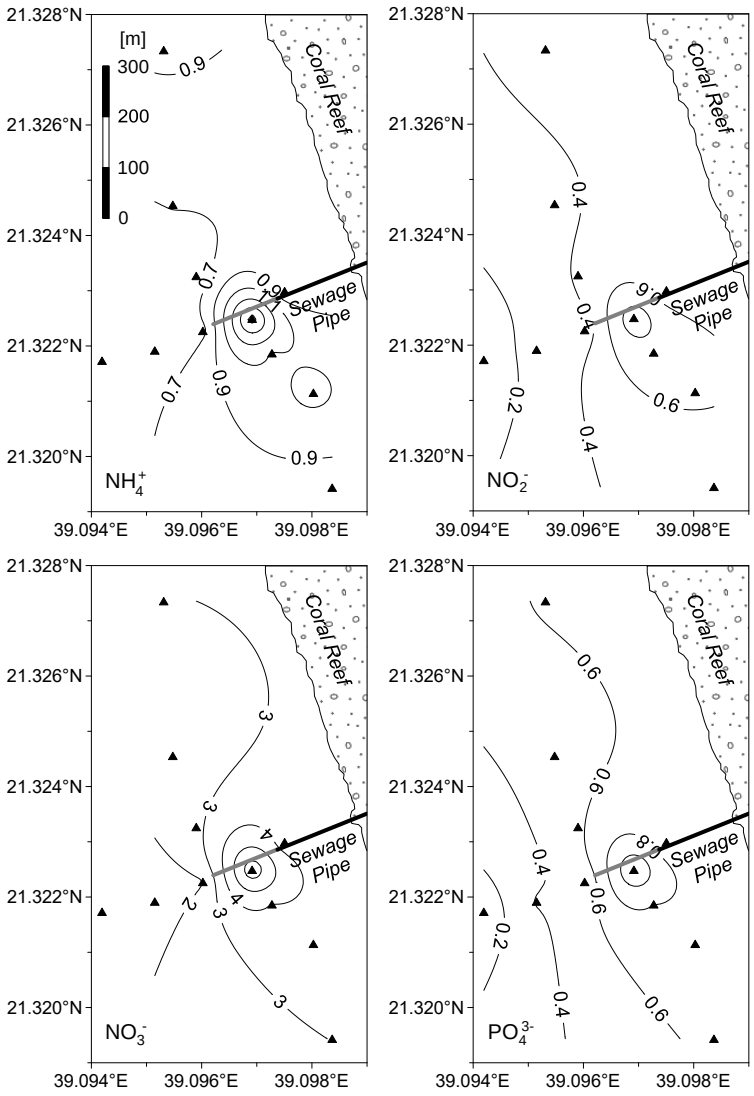

Figure 4.5. Ammonium (NH_4^+), nitrite (NO_2^-), nitrate (NO_3^-), and phosphorus (PO_4^{3-}) concentrations [µM] at Al Khumra outlet in October 2011.

4.1.3. Nutrient Composition

Figure 4.6 presents the nutrient composition for nitrogen and phosphorus at locations impacted with wastewater and locations of oligotrophic coastal waters. A comparison of the nutrient composition at sites of massive wastewater impact (arbitrary thresholds >50 µM TN and >3 µM TP corresponding to the Redfield ratio) with those of coastal water exhibiting oligotrophic conditions of <6 µM TN (Downing, 1997) and <0.8 µM TP (Håkanson *et al.*, 2007) reveals that wastewater-impacted sites are dominated by dissolved inorganic nitrogen compounds (Figure 4.6.).

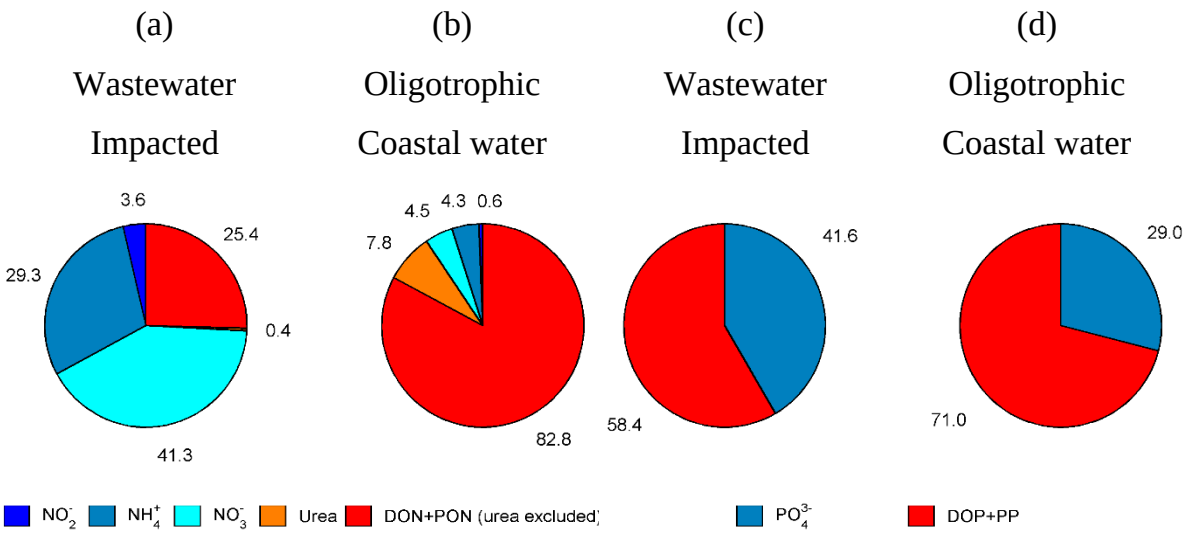

Figure 4.6. Molar partition of organic[1] (red/orange) and inorganic (blue) nitrogen (a, b) and phosphorus (c, d) compounds [%] at sites of massive wastewater pollution and in oligotrophic coastal waters.

On average, nitrate and ammonium account for 41.3 % and 29.3 % of the TN concentrations respectively. Although urea is a main end product of nitrogen

[1] Due to the method applied, an undefined amount of particulate inorganic phosphorus might be included.

metabolism in many vertebrates, it shares only a small portion of TN at the wastewater-impacted stations (0.4 %), likely due to intense biological hydrolysis in the sewerage system favored by high ambient temperatures.

In contrast to the situation in the wastewater impacted sites, dissolved organic and particulate nitrogen largely dominated the nitrogen pool in the oligotrophic coastal water (90.6 % of TN, including 7.8% of urea). With respect to phosphorus, the situation was slightly different. Dissolved organic and particulate fractions dominated at both sites, making up almost 60 % of total phosphorus in the polluted waters, but even 71 % of TP in the oligotrophic coastal water.

4.1.4. Potential Nutrient Limitation

During April and October 2011 campaigns, the mean molar DIN:PO_4^{3-} ratio at stations impacted by massive sewage inputs was approximately 17, thus exceeding the Redfield number. There was a significant, positive correlation ($r = 0.9$; $p = 0.001$) between DIN and PO_4^{3-} concentrations at polluted stations in April reflecting a rather balanced dissipation of these nutrient species. In the pristine offshore water, DIN:PO_4^{3-} ratios were always well below the Redfield ratio during both sampling campaigns (mean: 1.7), indicating potential nitrogen limitation of phytoplankton growth. It can thus be deduced that the nitrogen-rich wastewater inputs compensate for any nitrogen deficiency in the near coastal mixing zone inside the bay.

By sorting the TN:TP ratios of the oligotrophic coastal waters in ascending order, the relative cumulative frequency can be calculated. Figure 4.7 shows the results of the relative cumulative frequency compared to the ratio considered as N-deficient (TN:TP < 20; Guilford and Hecky, 2000), to the Redfield ratio (TN:TP = 16) and to the ratio considered as strongly N-limitant (TN:TP < 10; Downing, 1997). It resulted that 96 % of samples had N-deficiency (TN:TP < 20), 73 % of the samples were

below the Redfield ratio, and 30 % of the samples had strong N-limitation (TN:TP < 10).

Potential nutrient limitation, as deduced from the TN:TP ratios, does not allow for an appraisal of *in situ* nutrient limitation of primary production. Levels of nitrate, ammonium and inorganic phosphate in the study area were thus compared to half-saturation constants (Ks) of nanophytoplankton communities in oligotrophic waters, as adopted from Aumont and Bopp (2006) (K_S-NO_3^-: 0.26 µM; K_S-NH_4^+: 0.013 µM; K_S-PO_4^{3-}: 0.001 µM). From this comparison, nitrate was likely to limit primary production, both in April and October, in offshore coastal waters, whereas ammonium levels fell below the half-saturation constant only in October. In contrast to the deficiency in nitrogen, phosphorus was still available in sufficient concentrations in both April and October.

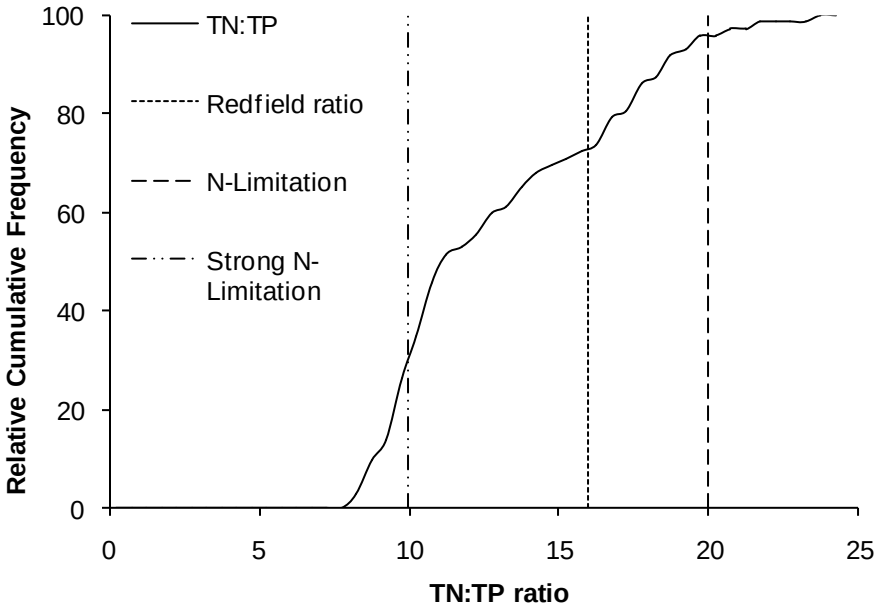

Figure 4.7. Relative cumulative frequency of TN:TP ratios in Jeddah oligotrophic waters. Redfield ratio and two ratios implying N-limitation are shown as vertical lines.

4.1.5. Nutrient Loads from the Jeddah Metropolitan Area

In order to obtain a quantitative estimate of average nutrient loads from wastewater inputs, *in situ* nutrient concentrations of all land-based samples were plotted against salinity, and extrapolated by linear regression to a salinity of 0 PSU, which yielded a significant inverse relationship ($p = 0.001$). Table 4.1 presents the resulted concentrations of the different nutrient species of nitrogen and phosphorus from the linear regression to salinity of 0 PSU. Mean TN and TP concentrations of 934 µM and 144 µM, respectively, were derived. Calculation of dissolved inorganic nitrogen fractions resulted in 776 µM DIN, comprised of 442 µM NO_3^-, 288 µM NH_4^+ and 46 µM NO_2^-. The phosphate input concentration accounted for 48 µM PO_4^{3-}.

Table 4.1. Estimates of coastal nutrient inputs from wastewater.

Concentrations [µM]		**Al Khumra**	**Arbaeen**	**Al Shabab**	**Diffuse & small inputs**	**Total**
		Average Discharge Q [103 m3 d-1]				
		300	68	35	99	502
		Mean Daily Nutrient Loads [kg d-1]				
TN-N	934	3923	889	458	1294	6564
TP-P	144	1339	304	156	442	2241
DIN-N	776	3259	739	381	1075	5454
NH_4^+-N	288	1210	274	141	399	2024
NO_2^--N	46	193	44	23	63	323
NO_3^--N	442	1856	421	217	612	3106
PO_4^{3-}-P	48	446	101	52	148	747

From multiplication of derived nutrient concentrations at a salinity of 0 PSU with reported average discharge data (Q), mean daily nutrient loads to coastal waters were derived. Loads of the different nutrient species for the three main wastewater outlets

and diffusive and small inputs are also presented in Table 4.1. In total, nitrogen and phosphorus loads amount to 6,564 kg d^{-1} TN-N and 2,241 kg d^{-1} TP-P, comprised of 83 % DIN-N and 33 % PO_4^{3-}-P. Therefore, Al Khumra represents the most important source of nutrient inputs in the study areas, in terms of both nitrogen and phosphorus. TN and TP loads from Al Khumra account for 3,923 kg d^{-1} TN-N and 1,339 kg d^{-1} TP-P, 60 % of total, and include 3,259 kg d^{-1} of DIN-N and 446 kg d^{-1} of PO_4^{3-}-P. Arbaeen and Al Shabab lagoons together account for a daily nutrient input of 1347 kg d^{-1} TN and 460 kg d^{-1} TP, including 1,120 kg d^{-1} DIN-N and 153 kg d^{-1} PO_4^{3-}-P.

4.1.6. Eutrophication Assessment

An eutrophication assessment of coastal waters was performed based on the deviation of *in situ* nutrient concentrations in comparison to background levels, as outlined in the European Water Framework Directive (European Parliament and Council, 2000). According to the common procedure followed by OSPAR (2003) a 50 % enhancement above natural background levels has been used as an acceptable threshold value with respect to anthropogenic nutrient enrichment**.** Considering the sensitivity of the Red Sea's coral reef ecosystem, the more stringent criterion of 25 % above salinity-related background values has been applied in the present assessment, as proposed by the Danish contracting party (ibid.).

Natural background values were derived from the nutrient concentrations in the oligotrophic offshore waters as stated by Andersen *et al.* (2004) at a salinity of ~39. These values account for 6 µM TN and 0.4 µM TP, thus resulting in thresholds of 7.5 µM TN and 0.5 µM TP, respectively.

TN and TP concentrations exceeded threshold levels at local sites in front of the Al Shabab and Arbaeen lagoons, at Obhur Creek, in areas close to the shoreline north of the bay, and at Al Khumra (Figure 4.8.). Ghubbat `Asharah lagoon and the inner

southern bay had to be excluded from the assessment due to insufficient data. According to the applied assessment criteria, designated problem areas as defined by undesirable nutrient enrichment are comparatively narrow and close to coastal line, even at Al Khumra wastewater outlet.

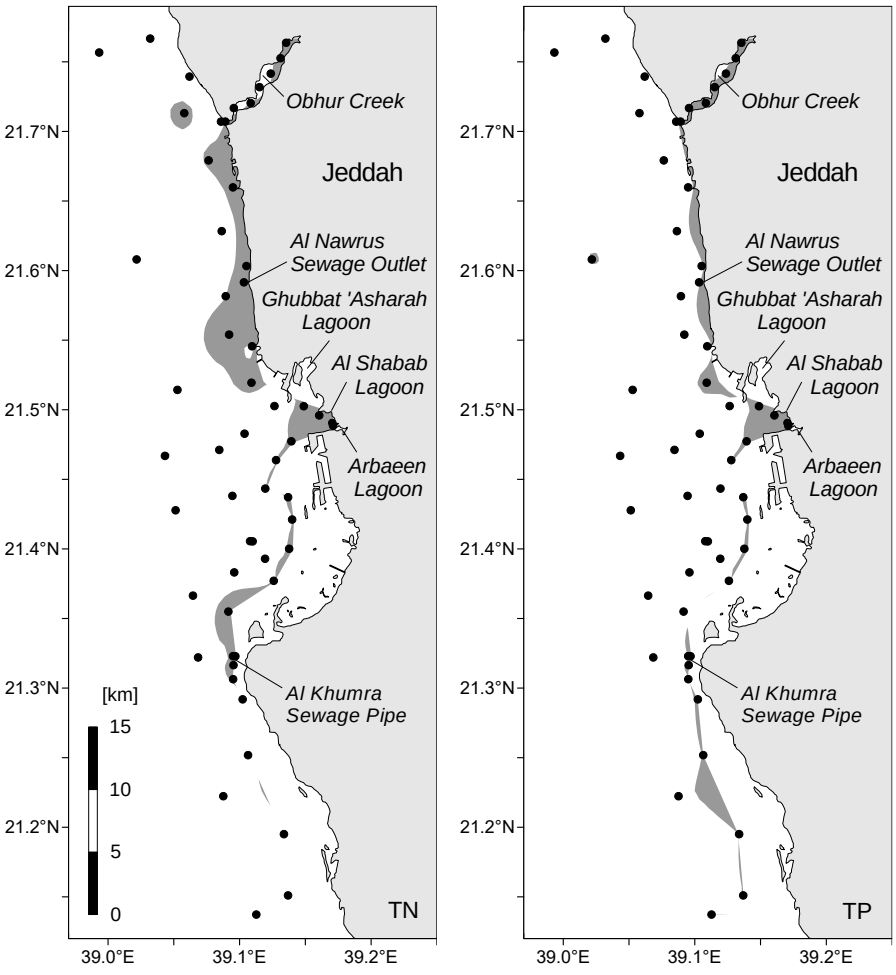

Figure 4.8. Areas with total nitrogen (TN) and phosphorus (TP) concentrations 25 % above average offshore background level (6 µM TN, 0.4 µM TP) in April 2011 (eutrophication problem areas indicated by dark grey colour; black dots = assessed area).

4.1.7. Eutrophication Effects

The highly eutrophied Arbaeen and Al Shabab lagoons are subject to enhanced phytoplankton biomass production, as can be deduced from strongly elevated chlorophyll-*a* levels. Surface chlorophyll-*a* concentrations at the mouth of the lagoons amounted to 19.7 µg L^{-1} and 5.8 µg L^{-1} in April and October 2011, respectively. Similar to nutrient gradients, the chlorophyll-*a* concentration rapidly decreased towards the open bay to levels of <0.5 µg L^{-1} in both seasons. Vertical chlorophyll-*a* profiles reveal a rapid decrease in concentrations from the surface to less than 2 µg L^{-1} at a depth of 3 m, consistent with reduced light penetration and a pronounced pycnocline 2.0 m below the surface.

There was a significant, positive correlation ($p = 0.001$) between TN and TP concentrations and chlorophyll-*a* levels with a slope of 1.31 and 1.58, respectively. TN and TP accounted for ~71 % and ~72 % of the variance in chlorophyll-*a* concentrations. Moreover, significant, positive correlations of both DIN and PO_4^{3-} concentrations with chlorophyll-*a* levels ($p = 0.001$) indicate a strong response of phytoplankton biomass to nutrient enrichment.

Whereas oxygen saturation in the open coastal water uniformly accounted for ~100 %, equaling 6.6 mg L^{-1} O_2, a pronounced oxygen oversaturation of >150 %, or 9.7 mg L^{-1} O_2, prevailed in the surface waters directly in front of the lagoons. This is consistent with the intense phytoplankton development observed. In contrast, water within 3 m of the sea floor contained an oxygen saturation of only 30 %, or a concentration of 1.9 mg L^{-1} O_2. This hypoxic level is inadequate to cover the oxygen demand of many invertebrate species and higher forms of life.

4.2. Modelling the Distribution of Nutrients and Chlorophyll-*a* in the Coastal Waters off Jeddah

The present sub-chapter deals with the results obtained from the application of a transport and water quality model developed for the coastal waters of the Jeddah Metropolitan Area (see 3.4. Models' Set-up and Simulations of the Jeddah's Coastal Area). The model was developed to simulate the distribution of dissolved inorganic nutrients (DIN, DIP) and of phytoplankton biomass (as chlorophyll-*a* equivalents) as a result of anthropogenic nutrient input deriving from wastewater discharges. Simulations include scenarios assuming a 50% increase and a 80% reduction of wastewater nutrient loads from the city of Jeddah.

4.2.1. Hydrodynamic and Transport Model Validations: Temperature and Salinity

Figure 4.9 presents the comparison between ARGO and CTD measurements of temperature and salinity, and results of the hydrodynamic model for years 2010 and 2011. ARGO data for the central Red Sea are from 56 vertical profiles measured every 5 days starting on 14th April 2010. The temperature and salinity measurements are reported every 10 m and are plotted in Figure 4.9 as discrete colour-scaled points for the different dates of measurement. Model results are plotted as continuous lines with the same colour scale. The figure reveals that the hydrodynamic and transport model reliably reproduces well the annual variation in surface temperature (Figure 4.9.a) in the central Red Sea, reaching maxima (up to 32 °C) in the upper layer from July to October both in 2010 and 2011.

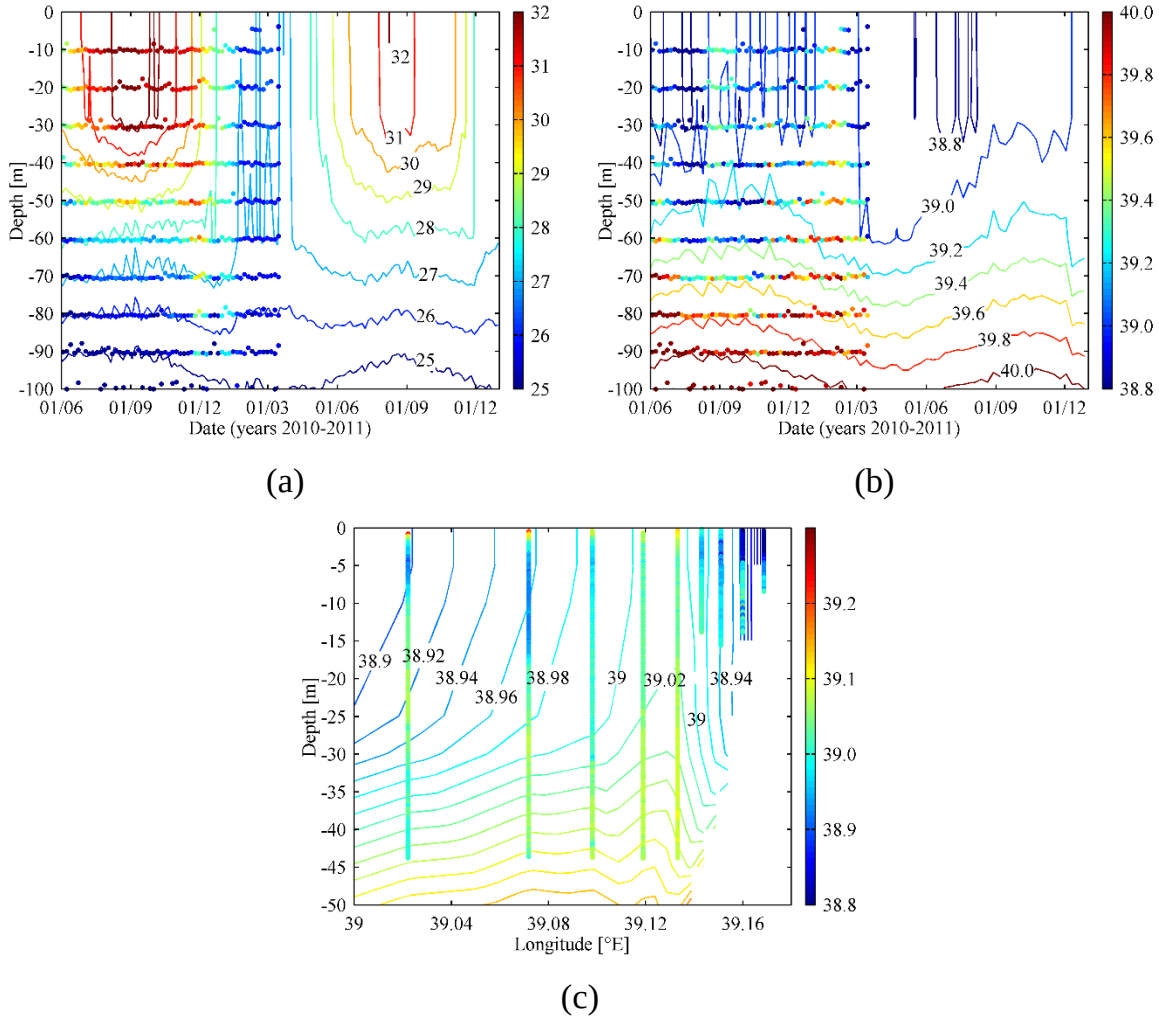

Figure 4.9. Comparison of model results for temperature (a) and salinity (b) with data from ARGO measurements in the central Red Sea and for salinity with CTD profiles in the inner Jeddah Bay (c). Points represent either ARGO or CTD measurements coloured according to the same scale as the isolines (model results).

The model also predicts the seasonal mixing (down to 80 m depth) observed in the ARGO measurements between December and April. During this period, the temperature values measured in the upper layer are quite uniform in the order of 26-27 °C. The comparison between model results and ARGO measurements results in a mean squared error (MSE) of 0.88°C (number of pair of data compared, n=544). The MSE was calculated as the average squared difference between ARGO data at

their date and depth and model results for the same date and depth. It should be noted that the MSE analysis was done from a fixed observation point in the model (located at 21.5°N-38.5°E). This model observation point is located around the ARGO floats' positions, which drifted between each measurement averaging at 21°N-38°E, although being all confined to a small area of the central Red Sea.

With respect to the salinity distribution, the model reproduces quite accurately the seasonal variation as observed in the ARGO data with slightly higher surface values of salinity during the hot season (August-October, Figure 4.9.b). The comparison between model and ARGO salinity data resulted in a MSE of 0.11 (n=544). Similarly, the salinity gradients observed in October 2011 on a transect from the inner bight near the lagoons towards the open waters beyond the coral reef barrier are well reproduced by the hydrodynamic model, including the slightly elevated salinity values at the free surface. This phenomenon might imply an upwelling between the longitudes 39.12 °E and 39.14 °E at a latitude of 21.5 °N (Figure 4.9.c). Based on these measurements the MSE value resulted equal to 0.17 (n=1397). There is a lack of data for the years 2010 and 2011, which did not allow for model comparisons. Nevertheless, the well-reproduced patterns of temperature and salinity both in space and time, as well as the dispersion pattern in the surroundings of the lagoons towards open waters, confirms the adequacy of the hydrodynamic model in predicting with reasonable accuracy.

4.2.2. Sensitivity Analyses of the Water Quality Module

The impact of maximum and minimum rates of the process parameters on chlorophyll-*a* (chl-*a*) concentrations addressed in the sensitivity analysis of the model (Table 3.3.) was evaluated at four stations within a gradient from high to low waste water influence. The location of the stations selected for the analyses is shown in Figure 3.5 (stations 8, 7, 5 and 4).

Figure 4.10 shows the resulting chlorophyll-*a* concentrations when running the water quality module with average values for the model parameters, except for one parameter, which is run with its maximum or minimum. It can be seen that the parameters that showed major effects on chlorophyll-*a* levels were the fraction of dissolved inorganic to organic nutrients released upon phytoplankton mortality (F(din/det)), the mortality constant (K-mort) and the maximum primary production (PPMax, Figure 4.10).

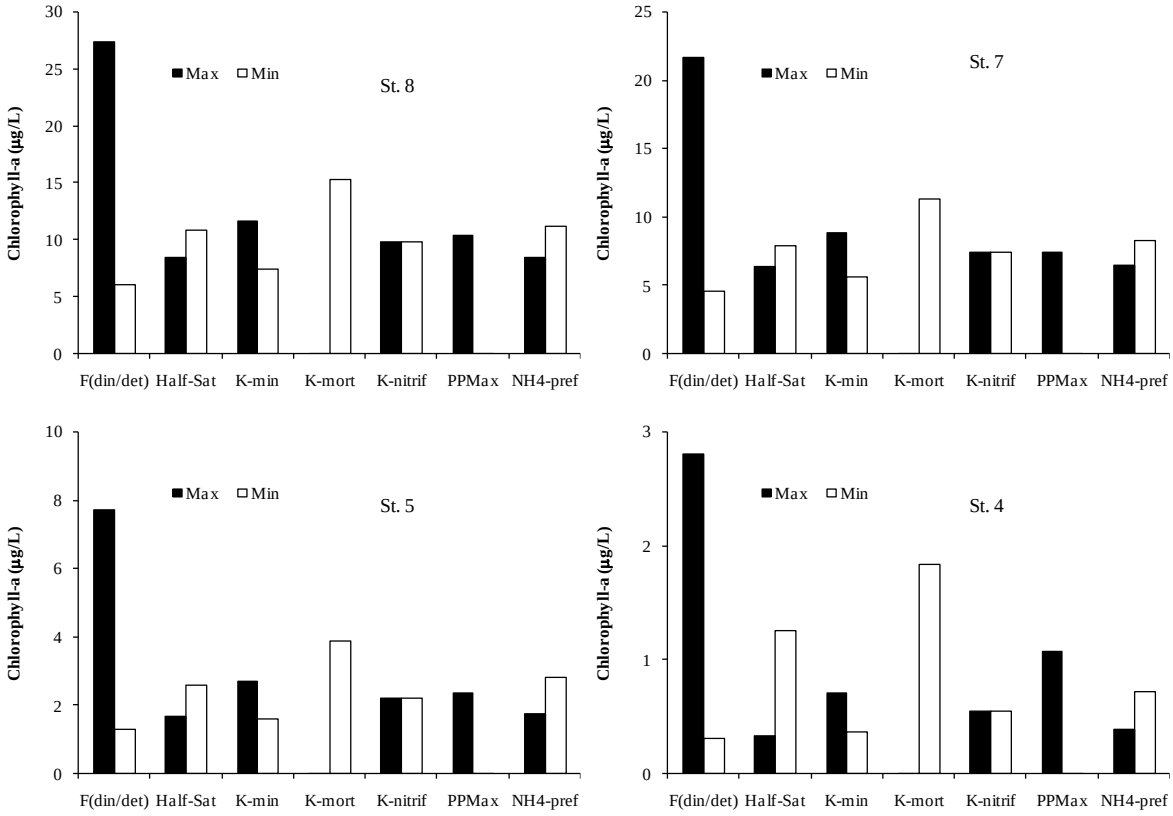

Figure 4.10. Chlorophyll-*a* concentrations in stations 8, 7, 5 and 4 resulting from simulations with maximum and minimum values for each of seven model parameters while keeping the others in the mean value (sensitivity analyses).

By contrast changes of the half saturation constant for both DIN and PO_4^{3-} uptake (Half-Sat), the mineralization (K-min) and preferential uptake of ammonium (NH4-pref) were of minor importance. On the other hand differences in the nitrification rate (K-nitrif) had almost no effect on the computed chlorophyll-*a* levels. The identification of PPMax as a decisive parameter is in agreement with other modelling studies on phytoplankton bloom formation and eutrophication (Lopes *et al.*, 2008; del Barrio Fernández *et al.*, 2012). Although the four sites exhibit very different levels of pollution from very high to low nutrient enrichment and phytoplankton biomass, the relative influence of each of the parameters on the model output was almost the same. It can thus be concluded that the parameter values can be kept constant instead of modifying them according to the specific trophic state in the area.

4.2.3. Chlorophyll-*a* and Nutrient Calibration

Results from the calibration of the water quality model against field data at 13 stations collected in April 2011 are shown in Table 4.2. A list of the values reported in other modelling studies is also listed in the table. Although this is not intended to be a rigorous review of the parameter values usually adopted in similar model investigations, it turned out that the calibrated values of the potential maximum primary production and of the half saturation constant for DIN and PO_4^{3-} are below the ranges adopted in recent model studies whereas the rates for mineralization and for the phytoplankton mortality constant are higher. The calibrated value of the nitrification rate falls within the range reported by other authors. This suggests that for the coastal area near Jeddah the biomass recycling parameters (K-mort and K-min) are of higher importance than in other areas.

Table 4.2. Calibrated rates and parameters of the water quality module used in this study along with ranges adopted in other models studies.

Parameter/Rate	**Calibrated**	**Unit**	**Values adopted in other models**
Autolysis fraction dissolved inorganic/detritus	0.2/0.8	(-)	--
Half-Saturation Constant DIN	5×10^{-3}	mg N L^{-1}	1×10^{-2} [a] - 5×10^{-2} [b]
Half-Saturation Constant PO_4^{3-}	6.9×10^{-4}	mg P L^{-1}	1×10^{-3} [a] - 2×10^{-1} [b]
Mineralization	0.08	d^{-1}	0.02[c] - 0.075[d]
Mortality	0.2	d^{-1}	0.02[e] - 0.10[f]
Nitrification	0.1	d^{-1}	0.04[c] - 0.14[d]
Potential Maximum Production	0.4	d^{-1}	1.5[g] - 4.2[b]
NH_4^+ Preference over NO_3^-	0.2	(-)	--

[a] Park *et al.* (2005). [b] Lopes *et al.* (2010). [c] Koropitan *et al.* (2009). [d] Chen *et al.* (2011). [e] Lopes *et al.* (2008). [f] Chau and Jin (2002). [g] del Barrio Fernández *et al.* (2012).

Table 4.3 presents the corresponding error values for the model calibration in terms of the mean relative error (MRE), mean absolute error (MAE), normalized mean absolute error (NMAE), root mean square error (RMSE), normalized root mean square error (NRMSE) and bias. The field data used in the calculation covered a large trophic gradient. At stations 8 and 7 (Figure 3.5.b) concentrations typical for extremely polluted waters were measured (mean values chl-*a*: 8.86 µg chl-*a* L^{-1}; NH_4^+: 0.46 mg N L^{-1}; PO_4^{3-}: 0.17 mg P L^{-1}), while at the other stations the concentrations were typical for oligotrophic conditions (mean values chl-*a*: 0.6 µg chl-*a* L^{-1}; NH_4^+: 9×10^{-3} mg N L^{-1}; PO_4^{3-}: 6×10^{-3} mg P L^{-1}).

The MRE value resulted rather high. However, considering that the actual waste water and nutrient discharges into Jeddah Bay are highly variable and estimates for mean

nutrient loads had to be applied, the model output reflects a reasonable approximation to the field observations in the highly polluted as well the oligotrophic environments.

Table 4.3. Calculated errors between measurements at 13 stations and model results for the calibration period (April 2011).

Variable	MRE (%)	MAE ([x])[a]	NMAE (%)	RMSE ([x])[a]	NRMSE (%)	Bias ([x])[a]
Chlorophyll-*a*	35.37	0.262(0.164)	2.52	0.412(0.222)	3.97	0.049
NH_4^+	49.13	0.063(0.003)	9.07	0.175(0.009)	25.02	−0.063
PO_4^{3-}	38.06	0.011(0.003)	5.01	0.021(0.003)	9.18	−0.001

[a] Values in x units of concentration, [mg chl-*a* L^{-1}] for chlorophyll-*a*; [mg N L^{-1}] for NH_4^+; [mg P L^{-1}] for PO_4^{3-}. Values in brackets are calculated excluding stations 8 and 7.

Furthermore, since at the non-polluted stations the concentrations were very low, a minor numerical difference between model data and measurements results in a large MRE, although this does not represent a major deviation from the prevailing field conditions. Accordingly, the moderate MAE and RMSE show that in terms of absolute concentrations deviations between model data and measurements are rather low. No errors were calculated for NO_3^- since at many sampling stations concentrations were below the detection limit. The percentage of both normalized errors for chl-*a* and phosphate simulations reveals a good agreement between model and measurements, whereas for ammonium the errors were quite high. When excluding the hypernutrified stations 8 and 7, however, the errors for NH_4^+ simulation considerably decrease. It should be mentioned that, as the amount of raw waste water from a fish processing factory in the near vicinity was unknown, this discharge could not be taken into account in the model predictions.

The Figure 4.11 shows the surface measured chlorophyll-*a* concentrations versus the modelled results of the calibration process at stations situated within the pollution gradient (for location of stations see Figure 3.5.b). It can be seen that the model reproduces well the spatial pattern exhibiting high chlorophyll-*a* concentrations at the entrance of the city lagoons (stations 8 and 7), and decreasing further offshore.

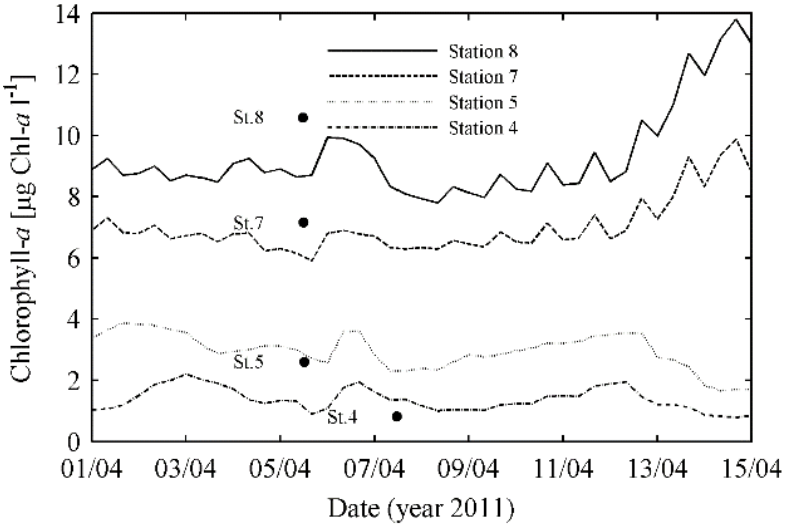

Figure 4.11. Model calibration for chlorophyll-*a* at four selected stations in the inner Jeddah Bight from 1st to 15th of April 2011 at stations 4, 5, 7 and 8.

4.2.4. Validation

Field measurements of chlorophyll-*a* concentrations used in the model validation were available from the sampling campaign carried out in October 2011 at the stations T1, 5, T3 and T4 located in the inner Jeddah Bay. The location of the stations is shown in Figure 3.5.b. In comparison to the period used for calibration (April 2011), the sampling campaign carried out in October 2011 showed higher surface water temperature values, given that the regular extremely warm summer had just passed.

Figure 4.12 shows the chlorophyll-*a* results of the WAQ model for the period of validation compared with field data. As can be traced from this comparison of field observations and model data (Figure 4.12.) and from the low values of MRE, MAE and Bias (Table 4.4.) the model reproduced rather well the chlorophyll-*a* levels observed in the area.

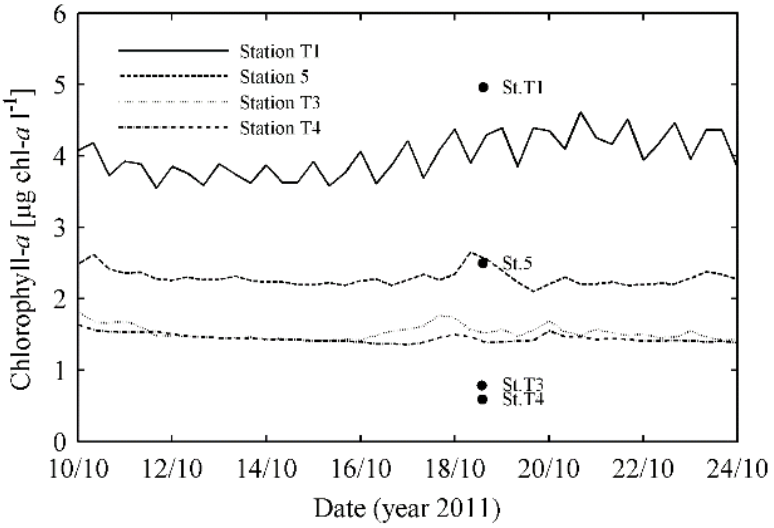

Figure 4.12. Results of model validation: Comparison of model results for chlorophyll-a with field measurements (black dots) in the Jeddah inner bight for October 2011.

The model slightly overestimates the concentrations at the more pristine stations T3 and T4. However, the rapid decrease in chlorophyll-*a* levels towards the outer bay is accurately reflected in the simulations. Considering the simulation of the nutrient distribution, the model reproduced the trend of higher concentrations at the near-shore stations towards oligotrophic levels offshore, albeit underestimating the phosphate concentration at the most polluted station T1.

As in the calibration period, the MRE value for NH_4^+ resulted quite high. However, as already mentioned, due to the low concentrations the absolute differences between model data and measurements (MAE: 0.008 mg N L^{-1}) do not constitute a major

deviation from the NH_4^+ levels observed. The percentage of the normalized errors is low for all of the three modelled variables, although much lower for chlorophyll-*a*.

Table 4.4. Model performance for the validation period from 10th to 24th October 2011.

Variable	MRE (%)	MAE ([x])[a]	NMAE (%)	RMSE ([x])[a]	NRMSE (%)	Bias ([x])[a]
Chlorophyll-*a*	16.73	0.270	6.19	0.402	9.21	−0.108
NH_4^+	200.10	0.008	27.52	0.010	35.00	0.008
PO_4^{3-}	65.70	0.033	19.59	0.054	31.63	−0.020

[a] Values in x units of concentration, [mg chl-*a* L^{-1}] for chlorophyll-*a*; [mg N L^{-1}] and NH_4^+; [mg P L^{-1}] PO_4^{3-}.

Figure 4.13 shows the chlorophyll-*a* results of the WAQ model versus the measurements carried out in April and October 2011 at all stations used for calibration and validation. The plot of measured chlorophyll-*a* concentrations against model data reveals the fidelity of the developed model. Model results reflecting both oligotrophic (lower left corner) and hypertrophic conditions (upper right corner) are shown in the plot.

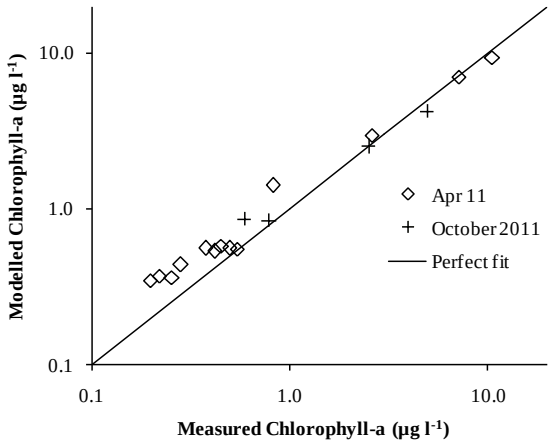

Figure 4.13. Model versus measured chlorophyll-*a* concentrations at all stations. Both axes are in logarithmical scale.

Figure 4.14 displays the average spatial distribution of chlorophyll-*a*, DIN, DIP and the DIN:DIP ratio as simulated by the model for the situation between 1st and 14th April 2011.

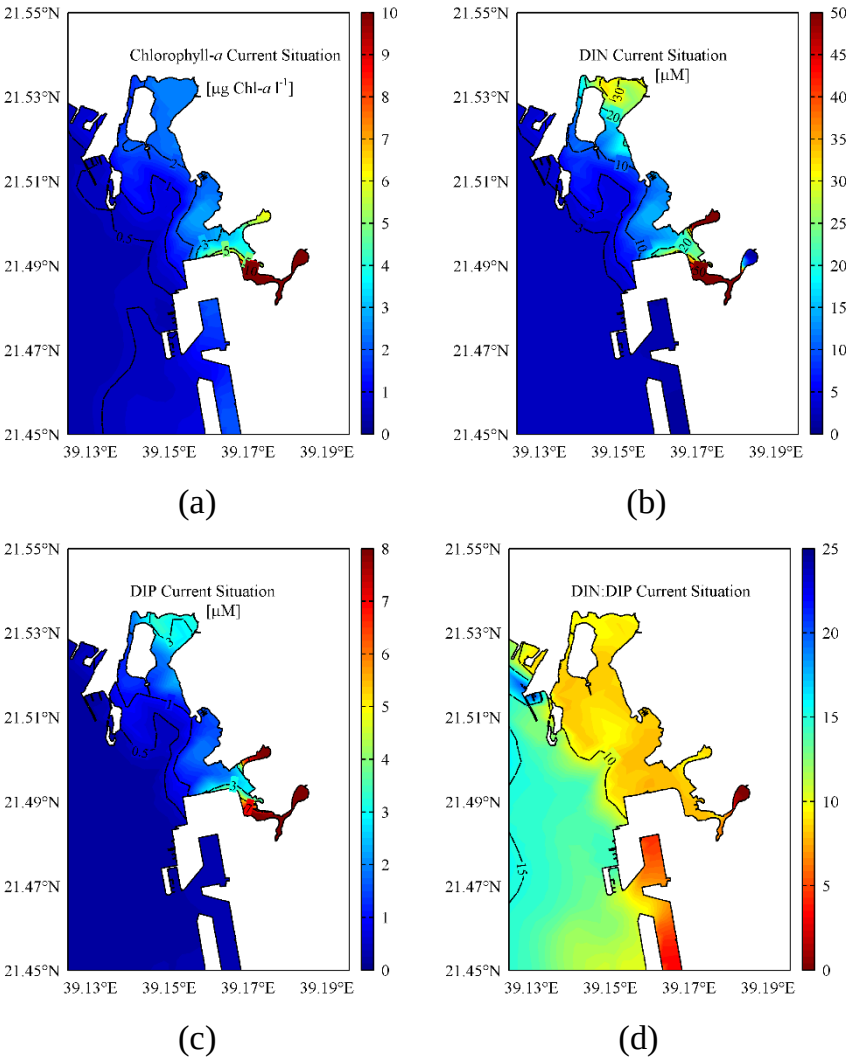

Figure 4.14. Simulated distribution of chlorophyll-*a* (a), DIN (b), DIP (c) and the DIN:DIP ratio (d) in April 2011 scenarios

The observed patterns with high phytoplankton biomass and nutrient concentrations in the inner Jeddah Bight, and especially in the lagoons, as well as the steep gradient towards oligotrophic conditions in the open sea water are well reproduced by the model. Furthermore, the model results reveal a low DIN:DIP ratio in the nearshore

area (see Figure 4.14.d). According to Peña-García *et al.* (2014), this indicates a potential nitrogen limitation. On the other hand, further offshore the DIN:DIP ratio resulted close to the Redfield number suggesting a more balanced nutrient supply.

Simulated scenarios assuming: a) a 50 % increase and b) a 80 % reduction of waste water nutrient loads were run over a period of 6 months and resulted in a significant effect on phytoplankton biomass levels in the inner Jeddah Bight. Figure 4.15 shows the chlorophyll-*a* concentrations in station T1 resulting from increases and reductions in nitrogen and phosphorus loads, whereas Figure 4.16 shows the surface chlorophyll-*a* pattern at the Jeddah Bight resulting from the scenarios.

The 50% increase of P loads resulted in an enhancement of chlorophyll-*a* concentrations in the adjacent coastal water ranging between 43 % and 66 % (average 54 %) when compared to the current situation in April 2011.

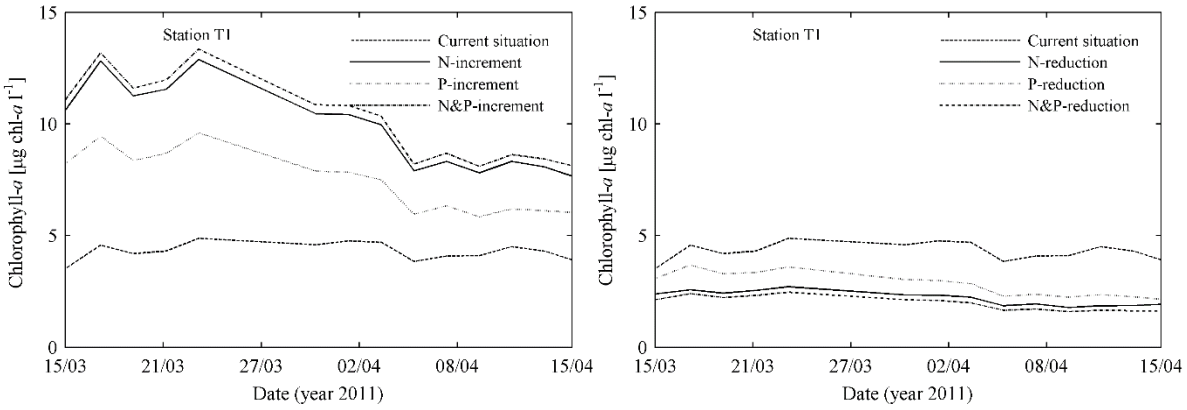

(a) (b)

Figure 4.15. Changes in concentrations of chlorophyll-*a* at station T1 as a result of (a) a 50 % increase in N and/or P loads and (b) an 80 % reduction.

A similar increase in N loads caused an even higher biomass increment, accounting for increases of 93 % to 119 % (average 105 %) for the same period.

A simultaneous 50 % increase of both N and P loads resulted in a chlorophyll-*a* enhancement only slightly higher than that resulting from an increase of N alone.

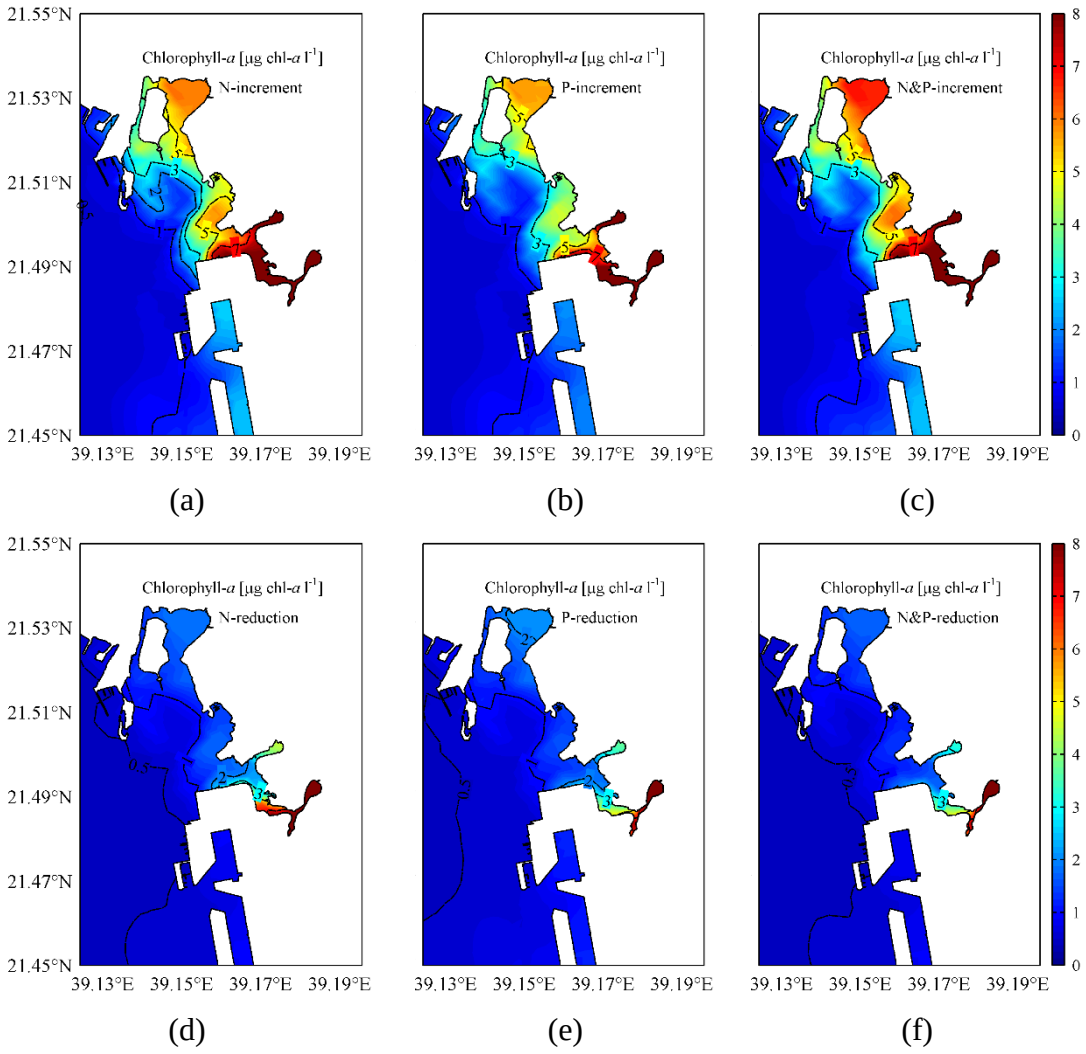

Figure 4.16. Simulated pattern of surface chlorophyll-*a* concentrations as a result of increased (a-c) or decreased (d-f) nutrient loads. Snapshot for mid April 2011.

In contrast to the results of the enhancement scenario, an 80% reduction of waste water nutrient loads had a less pronounced effect on the phytoplankton biomass concentrations in the adjacent coastal area. In all the reduction scenarios, the steep

gradient in phytoplankton biomass from the inner lagoons towards the open Jeddah Bight persists. When P loads were reduced by 80 %, chlorophyll-*a* concentrations in the inner bight decreased by 43 % in average (range 38-47 %) when compared to the situation during the period of measurements in April 2011. Corresponding N reduction resulted in a percentage decrease of mean chlorophyll-*a* levels accounting for 57 % (range 54-61 %). When both N and P loads were reduced simultaneously, the resulting chlorophyll-*a* concentrations were only slightly lower than those resulting from N reduction alone. Altogether the previous results thus suggest that phytoplankton growth in the Jeddah Bight is more sensitive to changes in nitrogen supply than to those of phosphorus.

4.3. Hydrographic Patterns and Nutrient Gradients along a South-North Transect in the Central Red Sea

Complementary to the study of nutrient gradients in the polluted coastal waters of Jeddah, the nutrient distribution in the oligotrophic waters of the central Red Sea was studied. In the following section, results from the investigations along a south-north transect on the central axis of the Red Sea conducted in April 2012 with RV Pelagia are described in detail (see 3.1. Field Measurements). Physico-chemical data from CTD-measurements (T, S, Chl-*a*, O_2) were kindly provided by the research team of the "Jeddah Transect" project.

4.3.1. Temperature and Salinity

The observations showed that in the Red Sea, salinity increases northwards with a surface gradient of ~3 PSU from less than ca. 38 PSU at 16.5 °N to about 40.5 PSU at 27 °N. In the latter location, salinity showed a rather uniform vertical distribution

increasing by less than 0.1 PSU in the upper 350 m layer (Figure 4.17.). On the contrary, in the south the effect of the Indian Ocean inflow through the Bab-el-Mandeb strait creates a much steeper vertical salinity increment of 1.5 PSU over a 10 m distance near 60 m depth.

It was found that the temperature in the southern Red Sea reached very high values at the free surface (~28 °C). There is also a steep vertical temperature gradient (Figure 4.17.), dropping 5.3 K in the upper 150 m. Surface horizontal gradients of 2.4 K were observed between the southern and northern Red Sea. As for salinity the vertical temperature distribution in the northern area is more uniform; the observations indicate that the water temperature decreased by only 1.4 K in the upper 350 m layer.

From the measurements it can be concluded that the mixed layer depth (MLD; calculated according to Kara *et al.*, 2000) was quite shallow (16 m < MLD < 45 m; Figure 4.17.). This result is in agreement with an analysis of profiles for the central longitudinal axis of the Red Sea from 1960 to 1993 (data from Hydrobase 3 database; Curry, 2013). These datasets, however, show that the MLD in the north was generally deeper (mean: 57 m) and even comprised several deep mixing events down to 180 m during winter. The MLDs near the other stations were shallower (in the order of 30-40 m depth) and thus in keeping with the situation of the present survey. An analysis of the data from two ARGO floats (ARGO data, own analysis) drifting near the station 2 resulted also in MLDs of ca. 38 m in the years 2010-2013 with events of deeper mixing (up to 110 m) in January and February.

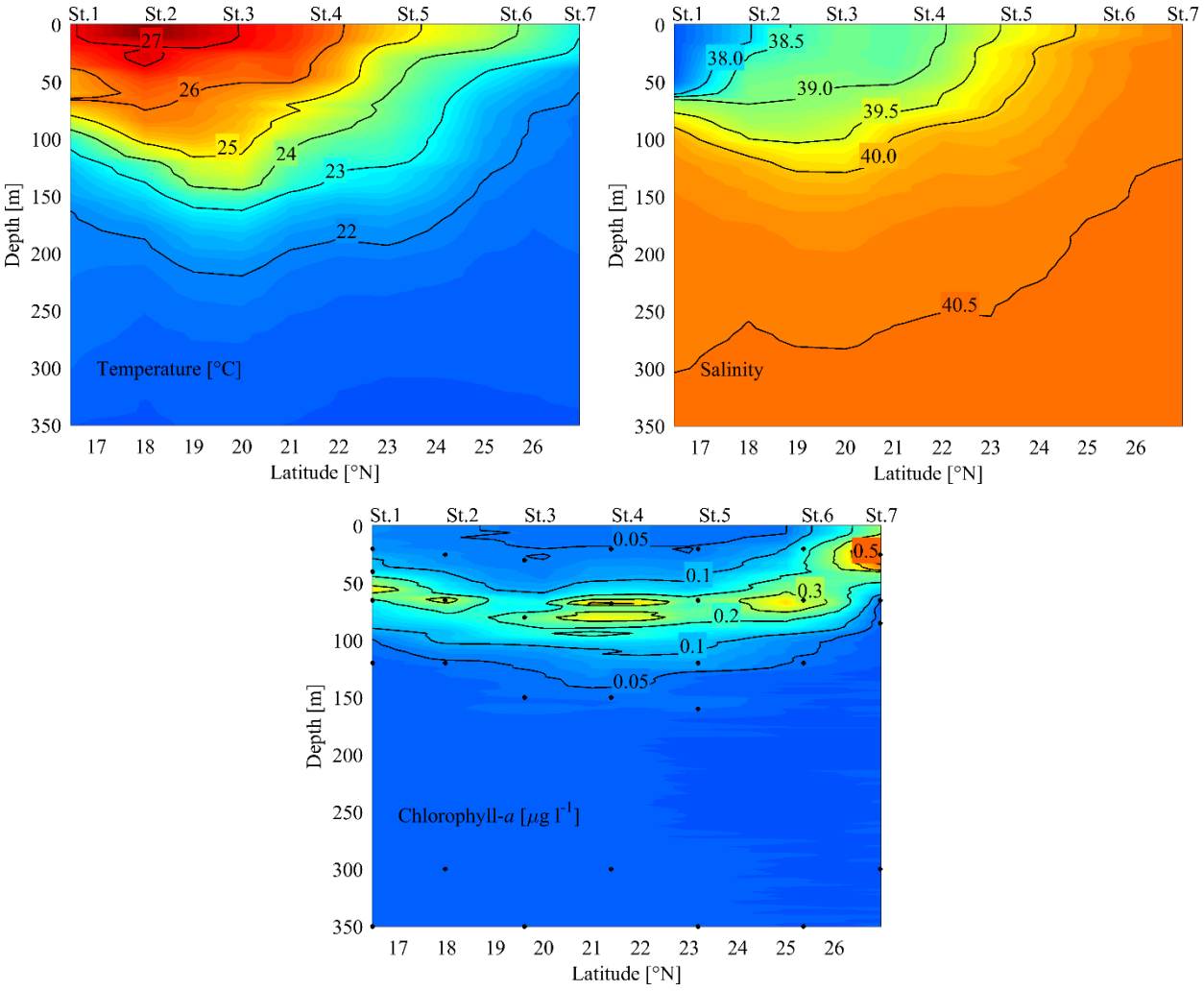

Figure 4.17. Distribution of a) water temperature, b) salinity and c) chlorophyll-*a* on a transect along the central Red Sea. The dashed line in the figure displaying the water temperature shows the calculated mixed layer depth determined from density variation according to Kara *et al*. (2000) with a $\Delta T = 0.8$ K. Black dots in the chlorophyll-*a* figure denote the depths at which samples were taken down to 350 m.

4.3.2. Chlorophyll and Oxygen

The Red Sea is characterized by chlorophyll-*a* concentrations typical to oligotrophic environments. Surface concentrations resulted very low, with lowest concentration levels below 0.05 µg L^{-1} in the central area of the Red Sea and highest values of ca.

0.3-0.5 µg L^{-1} in the northern parts (Figure 4.17.). The lower 0.05 µg L^{-1} isoline is deepest in the central area (144 m) and shallowest in the north (66 m). A pronounced deep chlorophyll maximum (DCM), with concentrations ranging from 0.3-0.5 µg L^{-1}, was observed. Its location changed along the central axis (Table 4.5.), being shallower in the north (19 m) and deeper in the central Red Sea (65-81 m). These depths were shallower than the limit of the euphotic zone (here defined as equal to the depth of 0.1 % surface PAR light, Table 4.5.). Table 4.5 shows characteristics such as the bottom depth of the mixed layer, the depth of the chlorophyll maxima, the depth of the euphotic zone, the upper and lower depths of the 120 and 60 µmol kg^{-1} oxygen concentration isolines, the depth of the nitrite maxima, and the nitrate gradient at the bottom of the euphotic zone, for the seven sampling stations along the central Red Sea.

From the surface down to a depth of ~60 m the observed dissolved oxygen concentration (Figure 4.18) resulted rather constant (250 µmol kg^{-1} south and central, and 260 µmol kg^{-1} in the north). In the south there was a steep vertical gradient starting at about 60 m. This major gradient was concomitant with the salinity gradient and it is characterized by a decrease in oxygen levels down to <120 µmol kg^{-1}. In the central area of the Red Sea the oxygen gradient was deeper with the major oxycline located between 150 m and 200 m. By contrast, in the north the vertical decrease in oxygen was much less pronounced and the gradient much smoother. As a result, the 120 µmol kg^{-1} isoline gets deeper further to the northern stations. There was a distinct oxygen minimum zone (OMZ; Figure 4.18., Table 4.5.) at a depth between ca. 250 m and 600 m with hypoxic values down to 40 µmol kg^{-1} (station 3). Besides, there were no suboxic areas (<10 µmol kg^{-1}) as found in the neighbouring Arabian Sea (Stramma *et al.*, 2008). The <60 µmol kg^{-1} region is narrower in the south and wider in the central Red Sea. By contrast, at the northernmost stations, oxygen levels in the OMZ only dropped to 90 µmol kg^{-1}.

Table 4.5. Location of sampling stations with main hydrographic characteristics.

Parameter	**St. 1**[†]	**St. 2**	**St. 3**[†]	**St. 4**[†]	**St. 5**	**St. 6**[†]	**St. 7**
Latitude [°N]	16.5	18.0	19.6	21.5	23.2	25.3	26.9
Longitude [°E]	40.9	40.1	38.8	38.0	37.3	36.2	35.1
MLD [m]	38	16	32	47	19	21	38
DCM [m]	53	61	81	65	72	64	19
Euphotic zone [m]	108	113	162	110	140	110	129
Upper OMZ_{120} [m]	155	149	205	173	246	310	335
Upper OMZ_{60} [m]	319	245	286	247	282	393[*]	444[*]
Lower OMZ_{60} [m]	391	424	485	462	494	581[*]	521[*]
Lower OMZ_{120} [m]	-	-	1089	1111	1047	1015	775
NO_2^--M [m]	40	65	80	-	65	-	65
$\Delta NO_3^-/\Delta z$ [µmol m^{-4}]	262.4	69.6	60.1	98.7	53.0	177.7	24.9

[†] Stations where photomineralization experiments were carried out. MLD: mixed layer depth. DCM: deep chlorophyll maximum. OMZ_{120} and OMZ_{60}: depth of the 120 and 60 µmol kg^{-1} isolines in the oxygen minimum zone, except data with the asterisk mark [*], where the shown depth is for the 90 µmol kg^{-1} isoline. NO_2^--M [m]: depth of nitrite maximum. $\Delta NO_3^-/\Delta z$: nitrate gradient at the bottom of the euphotic zone.

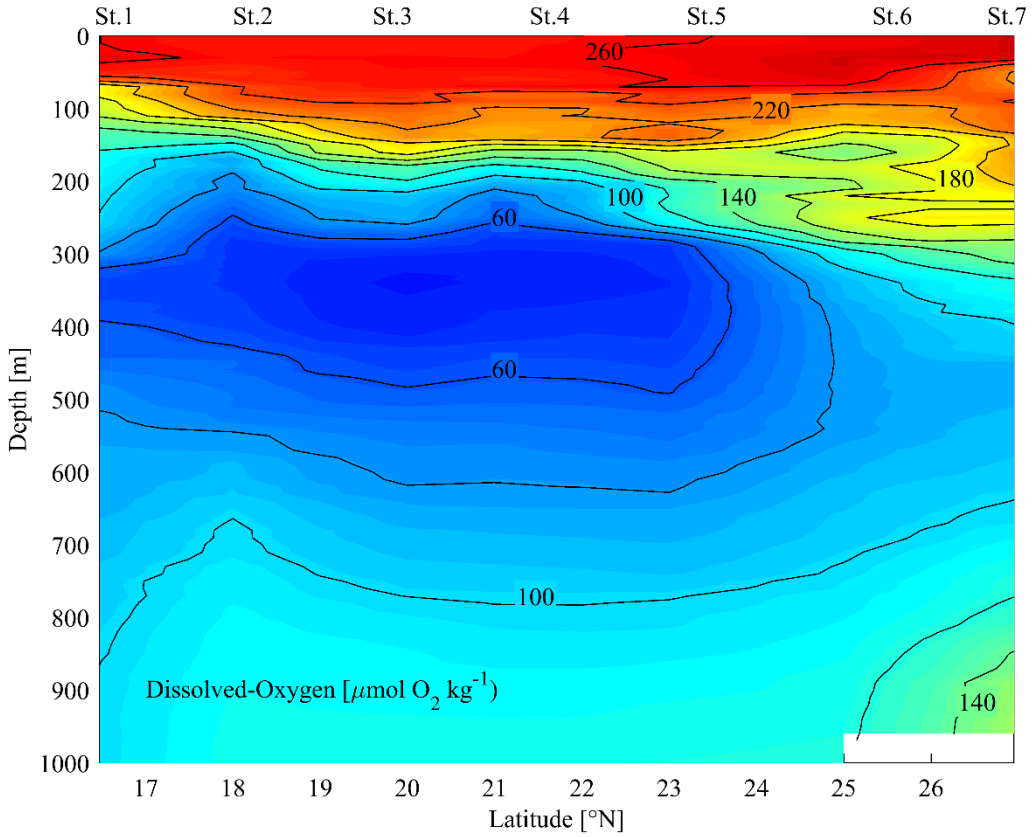

Figure 4.18. Dissolved oxygen distribution along the central Red Sea.

4.3.3. Nutrient Distribution

In the transect along the central Red Sea, chemical species of nitrogen (i.e. total nitrogen, dissolved organic nitrogen, ammonium, nitrite and nitrate) and of phosphorus (i.e. total phosphorus, dissolved organic phosphorus and phosphate) were measured from surface down to 350 m depth.

Ammonium was depleted in the central Red Sea. Only in the surface waters in the south (station 1) it was present in very low concentrations (0.25 µM). Nitrite levels in the upper 350 m were very low throughout the transect (average: 0.07 µM, *n*=29). A nitrite maximum (NO_2^--M) was observed at most stations at a depth of 40 m to 80 m being shallower in the south and deeper in the central Red Sea (Figure 4.19. and Table

4.5.). Concentrations of the NO_2^--M were higher in the south, attaining 0.5 µM at the southernmost station 1, and much lower values in the north. In general, the increase of NO_2^- concentrations in the NO_2^--M was low when compared to that of the adjacent Arabian Sea, where NO_2^- concentrations reach ~3 µM (Newell *et al.*, 2011). Nitrate levels in the surface water (Figure 4.19.) were very low being below the detection limit at stations 1, 4-6. At stations 2 and 3 surface concentrations of NO_3^- accounted only in average for about 0.47 µM. NO_3^- levels increased considerably below the DCM throughout the transect, reaching in the south more than 15 µM at a depth of 250 m.

PO_4^{3-} concentrations were also low in the surface water (Figure 4.19.). The distribution of PO_4^{3-} was similar to that observed for NO_3^- with surface values below the detection limit in the north at stations 5-7 and a pronounced increase below the euphotic zone up to levels of 1 µM at a depth of 350 m.

DIN:DIP and NO_3^-:DIP ratios in the surface layer were very low. Average values of ~8:1 and ~6:1 resulted respectively, suggesting N limitation. In the DCM the DIN:DIP ratios increased due to low PO_4^{3-} concentrations. Below the DCM DIN:DIP ratios increased up to an average of ~24:1.

In keeping with the low NO_3^-:DIP ratios, the NO_3^- deficit (defined as $\Delta N = (16 \times [PO_4^{3-}]) - [NO_3^-]$) (Tyrrell and Lucas, 2002) was positive in surface waters except at station 2 (Figure 4.20.). In general the observed average values resulted rather low (~1 µM) as compared to results from upwelling systems where denitrification occurs such as off Benguela (ibid.) and on the Peru-Chile shelf (Hall *et al.*, 1996).

In the waters directly below the chlorophyll maximum, average ΔN accounted for −1.6 µM. In deep waters around the OMZ (300-350 m), average ΔN decreased even to −4 µM suggesting a low importance of denitrification. In deep waters, ΔN was positive (1.8 µM) only where the apparent oxygen utilization (AOU, defined as the

difference between the measured oxygen concentrations and the potential equilibrium saturation concentration) was highest (175 µmol O_2 kg^{-1}, Figure 4.20.), which occurred around 20 °N latitude and 350 m depth. This might imply denitrification at this location.

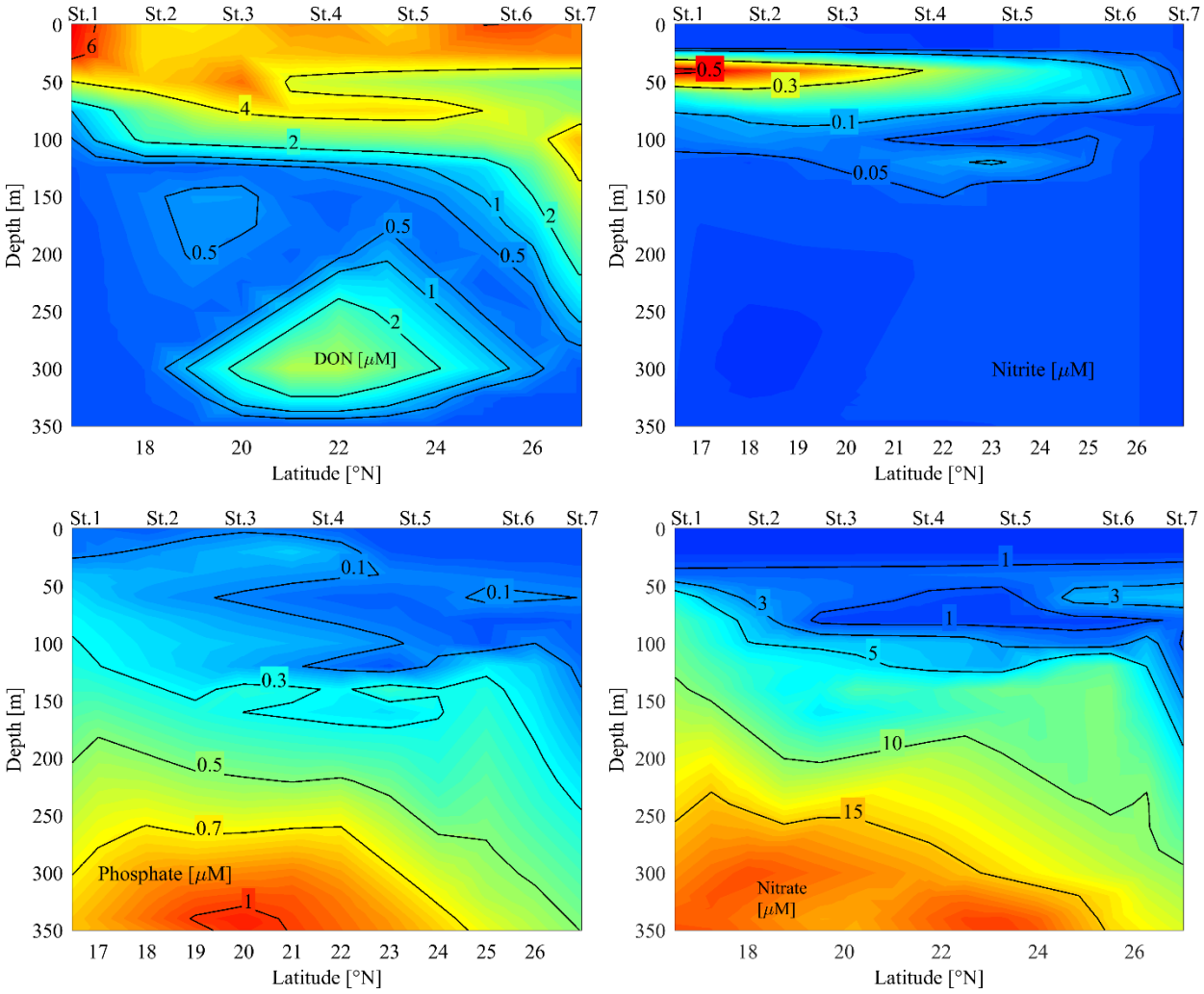

Figure 4.19. Spatial distribution of nitrogen and phosphate species (µM) along the central Red Sea.

Opposite to the distribution of dissolved inorganic nitrogen, DON concentrations were highest in surface waters, reaching 6 µM in the south and with a tendency to

decrease northwards (Figure 4.19.). The observed values resulted in the range of values reported for global oceans (Letscher *et al.*, 2013) and constituted the largest pool of dissolved nitrogen in the upper mixed layer. The fact that highest DON concentrations prevail in the south near Bab-el-Mandeb strait is consistent with data from the adjacent Arabian Sea. It has been suggested that there is a source of DON correlated with monsoon-driven upwelling (ibid.).

DON concentrations decreased to levels of 0.5 µM in deep waters below the euphotic zone. A patch of elevated concentrations was found in deep waters around the OMZ (Figure 4.19.), which was concomitant with elevated levels of apparent oxygen utilization (AOU, Figure 4.20.).

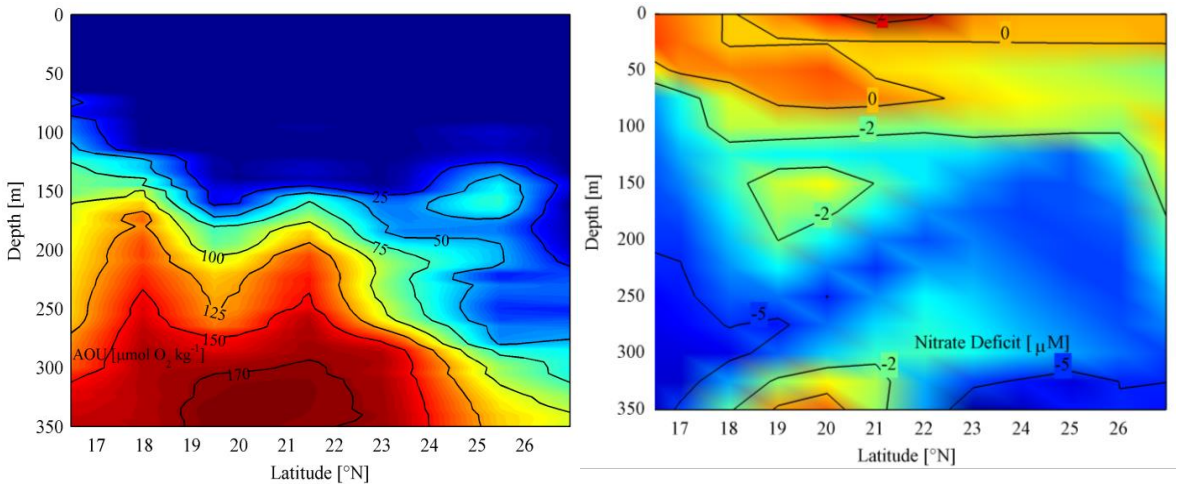

Figure 4.20. Apparent Oxygen Utilization (left) and Nitrate Deficit (right) in the central Red Sea.

4.4. Photomineralization of Nitrogen in the Red Sea

On the transect along the central Red Sea photomineralization experiments were carried out with surface water samples from stations 1, 3, 4 and 6. The location of the stations is shown in Figure 3.2.

4.4.1. Photomineralization of Dissolved Organic Nitrogen

According to the observations, changes in DON due to photomineralization (PM) resulted higher at stations 1 and 3 and lower at the northern stations 4 and 6 (Table 4.6.). After 8.5 hours of incubation photomineralization of DON accounted for 1.55 µmol m^{-3} on an average of the four stations and ranged between 0.95 and 2.44 µmol m^{-3}.

To scale the experimental results of ~8.5 h to the full daylight period, the following equation was used:

$$PM_{Daylight} = PM_{Exp} \times \frac{1 - cos[f^{-1}\pi(t_s - t_r)]}{cos[f^{-1}\pi(t_1 - t_r)] - cos[f^{-1}\pi(t_2 - t_r)]}$$

Equation 4.1

where $PM_{Daylight}$ is the photomineralization rate [µmol m^{-3} d^{-1}; results shown in Table 4.6.], PM_{Exp} is the photomineralized DON in the experiment [µmol m^{-3}], f is the fraction of photoperiod [d] , t_r and t_s represent time of sunrise and sunset [d], respectively; and t_1 and t_2 represent the time when experiments started and finished, respectively. $PM_{Daylight}$ resulted in just slightly higher values than the experimental results (Table 4.6.). Table 4.6 presents the results of the photomineralization experiments and its associated rates calculated for the daylight hours and the euphotic zone.

Table 4.6. Experimental results of DON photomineralization (PM) and calculated rates for the daylight period in surface waters of the Red Sea. The depth integrated rates of photomineralization for the euphotic zone are also presented.

Station	PM rates			
	Experimental [µmol m^{-3}]	**Daylight [µmol m^{-3} d^{-1}]**	**Specific [10^{-4} d^{-1}]**	**Depth Integrated [µmol m^{-2} d^{-1}]**
1	2.435	2.730	4.0	29.7
3	1.589	1.787	4.1	37.5
4	0.952	1.005	1.8	38.8
6	1.211	1.330	2.1	60.9

4.4.2. Photomineralization in the Euphotic Zone

The photomineralization rates obtained for surface waters were used to calculate the total photomineralization in the euphotic zone during the daylight according to the following equation was adopted (modified from that of Vähätalo and Zepp, 2005 and Vähätalo *et al.*, 2000):

$$PM_{Total} = \int_{\lambda_{280}}^{\lambda_{700}} \int_{surf}^{Z_{euph}} \int_{t_r}^{t_s} I_{(\lambda,t,surf)} e^{-k_{(\lambda)}Z} c_{\phi} e^{-d_{\phi}\lambda} k_{(DOM,\lambda)} \lambda (hcN_A)^{-1} 10^{-3} dt\, dZ\, d\lambda$$

Equation 4.2.

where, PM_{Total} [µmol m^{-2} d^{-1}] is the total photomineralization rate in the euphotic zone during an entire day for the range 280-700 nm represented by λ_{280} and λ_{700}. In the equation $surf$ represents surface and Z_{euph} [m] is the depth of the euphotic zone, t_r and t_s [d] represent the time of sunrise and sunset, respectively; $I_{(\lambda,t,surf)}$ [W m^{-2} nm^{-1}] is the measured daylight irradiance at the surface for each integer

wavelength λ [nm] at distinct times during the day, $k_{(\lambda)}$ [m^{-1}] is the total extinction coefficient for each integer wavelength, Z [m] is the depth, c_ϕ [µmol DON mineralized/µmol photons absorbed] and d_ϕ [dimensionless] are the coefficients defining the spectrum quantum yield for DON photomineralization (ϕ_λ, *see below*), $k_{(DOM,\lambda)}$ [m^{-1}] is the light extinction coefficient due to dissolved organic matter at each integer wavelength, h is the Planck's constant (equal to 6.626×10^{-34} W s^{-2}), c is the speed of light in vacuum (equal to 2.998×10^{8} m s^{-1}), and N_A is Avogadro's constant (equal to 6.022×10^{23} mol^{-1}).

$k_{(DOM,\lambda)}$ was calculated by a linear regression of the following equation:

$$I_{(\lambda,Z)} = I_{(\lambda,surf)} \times e^{-\{k_{(W,S,T,\lambda)}+(k_{(chl-a,\lambda)}\times[Chl-a])+k_{(NAP,\lambda)}+B_\lambda+k_{(DOM,\lambda)}\}Z}$$

Equation 4.3.

where $I_{(\lambda,Z)}$ is the measured irradiance [W m^{-2} nm^{-1}] for each integer wavelength at different depths, while $I_{(\lambda,surf)}$ is the irradiance for the surface; $k_{(W,S,T,\lambda)}$ [m^{-1}] is the light extinction coefficient of pure water at each integer wavelength (Boivin *et al.*, 1986; Buiteveld *et al.*, 1994; Pope and Fry, 1997) corrected for salinity (Röttgers *et al.*, 2014) and temperature (ibid.); $k_{(chl-a,\lambda)}$ [m^{-1} (µg L^{-1})$^{-1}$] is the specific light extinction coefficient due to chlorophyll-*a* (Prieur and Sathyendranath, 1981) concentration [Chl-*a*; µg L^{-1}], $k_{(NAP,\lambda)}$ [m^{-1}] is the light extinction coefficient due to non-algal particles (Bricaud *et al.*, 1998), and B_λ [m^{-1}] is the total backscattering coefficient (Morel and Maritorena, 2001).

The variation in $k_{(\lambda)}$ and $k_{(DOM,\lambda)}$ for the four stations where experiments were carried out are shown in Figure 4.21. and Figure 4.22., respectively. It can be seen that the resulting $k_{(\lambda)}$ values are smaller in the northern stations St.4 and St.6 since water is much clearer in this region of the Red Sea. On the other hand, $k_{(DOM,\lambda)}$ values in the range 600-700 nm are close to zero. This is consistent to the results reported by

Vähätalo *et al.* (2000) for a lake and Vähätalo and Zepp (2005) for the Baltic Sea. The reason is that almost the total light absorption in the dissolved phase is due to water molecules. In the range 300-400 nm, however, $k_{(DOM,\lambda)}$ represented in average 74% of the $k_{(\lambda)}$.

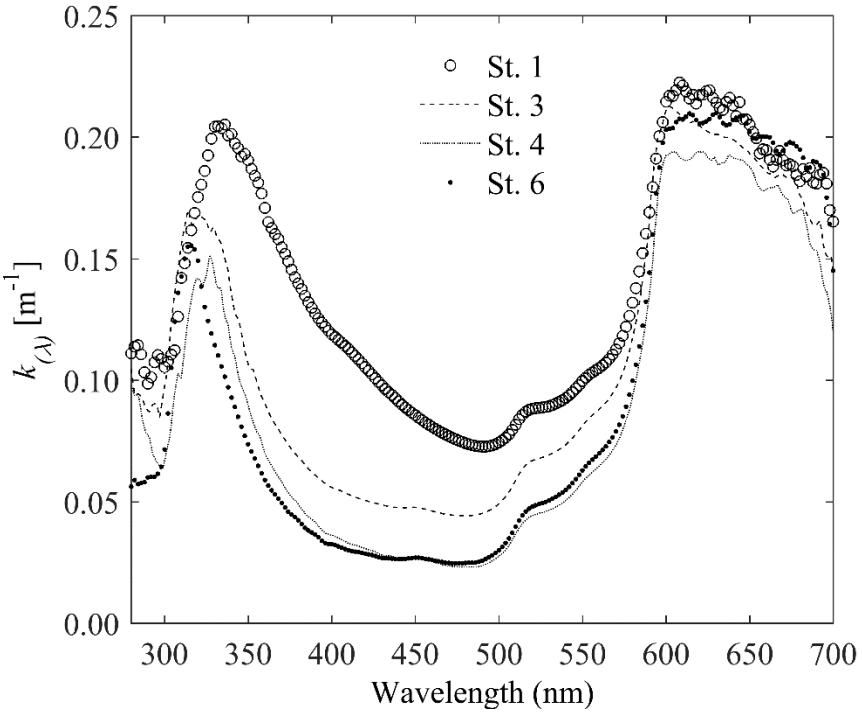

Figure 4.21. Total light extinction coefficients at each wavelength in the range 280-700 nm.

The ranges of $k_{(DOM,370)}$ and $k_{(DOM,442)}$ for the Red Sea resulted between 0.0379-0.1439 m^{-1} and 0.0011-0.0664 m^{-1}, respectively. These values are in agreement and well within the ranges published by Röttgers and Doerffer (2007) for the Atlantic Ocean (0.027-0.1440 m^{-1} at 370 nm and −0.005-0.048 m^{-1} at 442 nm). The calculation of $k_{(DOM,\lambda)}$ using Equation 4.3 was done using vertical profiles of irradiance, salinity, temperature and chlorophyll-*a* rather than measuring the extinction coefficient directly with a spectrophotometer. Taking into account the

depth-integrated light absorption at different depths due to changes within the water column of salinity, temperature and chlorophyll-*a*, a better estimate of depth-integrated light absorption due to dissolved organic matter can be achieved.

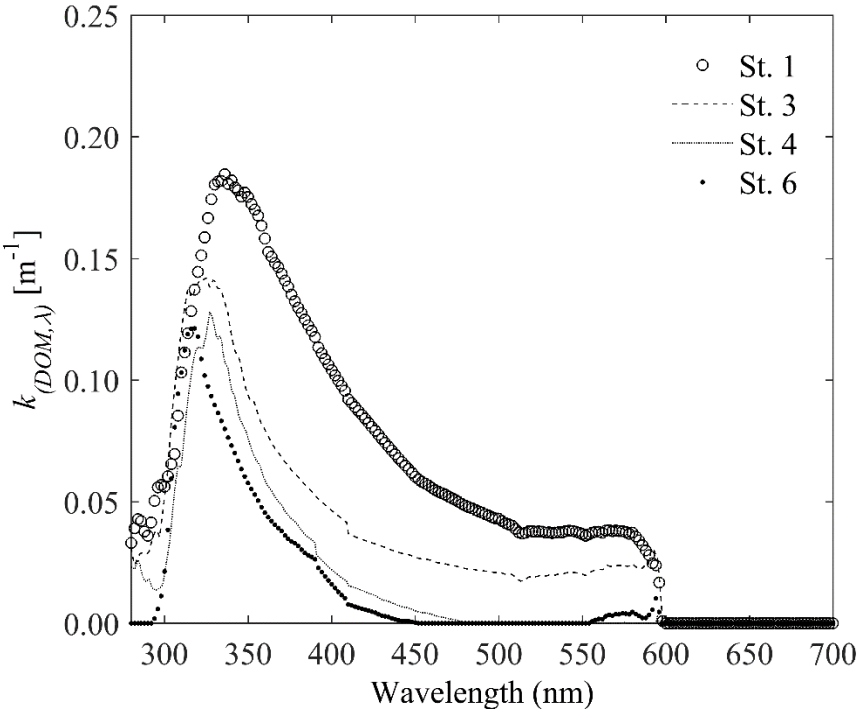

Figure 4.22. Light extinction coefficient due to dissolved organic matter at each wavelength in the range 280-700 nm.

In order to calculate the spectrum quantum yield ($\phi_\lambda = c_\phi \times e^{-d_\phi \lambda}$) for DON photomineralization, Equation 4.2 was equated to the photomineralization experimental result. In this case the upper depth integration limit was changed to 0.055 m (radius of quartz experimental bottle) and the time integration limits were changed to the initial and final times of the experiments. The coefficients were calculated by optimizing the equation using the Matlab function fminsearch (The MathWorks) and the modified fminsearchbnd function to ensure positive coefficients. It can be seen that ϕ_λ decreases as λ increases (Vähätalo and Zepp, 2005), indicating

that shorter wavelengths yield larger mineralization rates. According to the results (see Figure 4.23) the average values of quantum yield parameters c_ϕ and d_ϕ are 4.534 nmol DON mineralized/µmol photons and 0.016, respectively, for the four experimental stations.

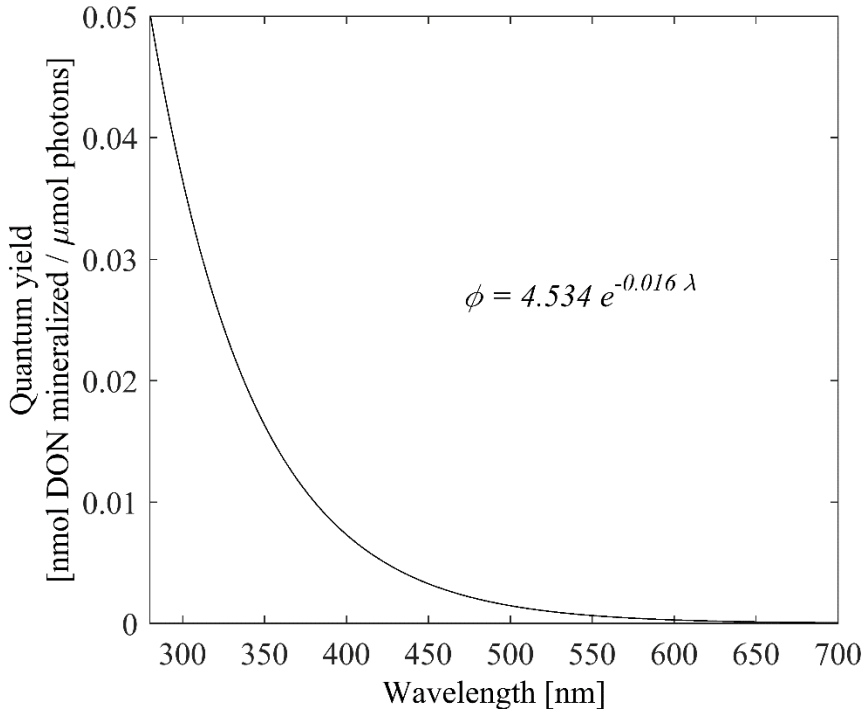

Figure 4.23. Average spectrum quantum yield at each wavelength in the range 280-700 nm

The UV-B (280-315 nm) range was responsible for only 2% of the total DON photodegradation, while the UV-A range (315-400 nm) accounted for 44%. In the whole euphotic zone, the median wavelength inducing DON photomineralization resulted in the range 402-412 nm (Figure 4.24.). This indicates that UV was responsible for half the photomineralization, while the other half was due to the visible range (400-700 nm).

DON photomineralization integrated for the euphotic zone accounted in average for 41.7 µmol m^{-2} d^{-1} . Daily turnover of DON due to photomineralization was rather slow at all four stations; it averaged 0.03% and ranged between 0.018% and 0.041% (Table 4.6.). DON turnover was lower in the north (stations 4 and 6). The present results show that DON in the euphotic zone of the Red Sea can be completely replaced by photomineralization within an average lapse of time of 33 d.

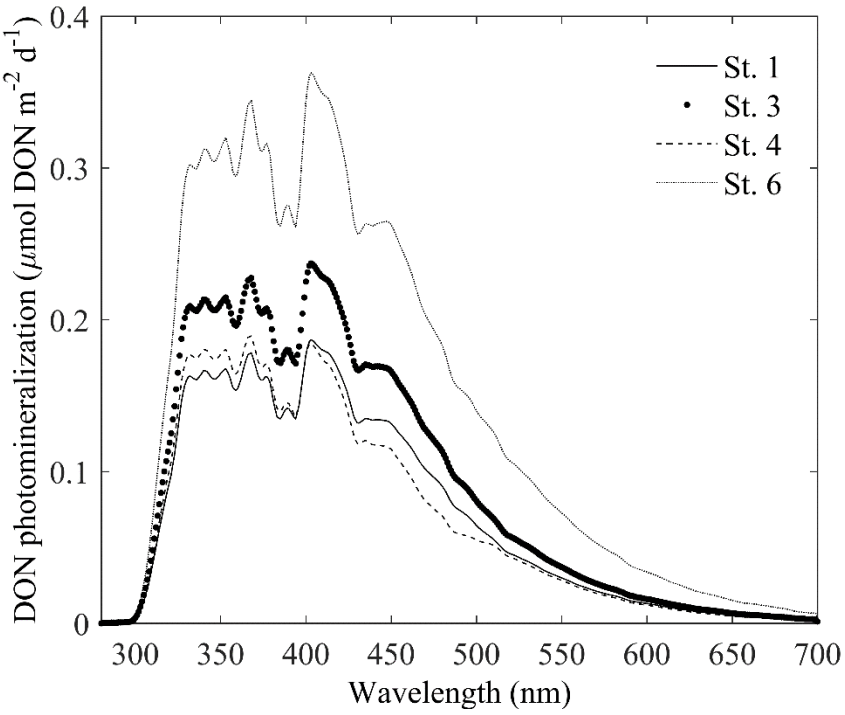

Figure 4.24. DON photomineralization in the euphotic zone at each wavelength in the range 280-700 nm.

5. GENERAL DISCUSSION

5.1. Nutrient Loads and Dispersion in the Jeddah Bight

In this chapter, the anthropogenic nutrient inputs into the Jeddah Bight are compared to previous studies and analyzed in the context of other nitrogen sources such as inflow from the Indian Ocean, nitrogen fixation and estimated inputs from other metropolitan areas (numeral 5.1.1). Also, the nutrients distribution in the coastal area are discussed and its different trophic status are analyzed (numeral 5.1.2). Finally, the potential nutrient limitation in the Jeddah Bight is discussed given several nitrogen to phosphorus ratios (numeral 5.1.3).

5.1.1. Anthropogenic Nutrient Inputs

The Red Sea with its coral reefs, seagrass beds and mangroves, is among the most pristine water bodies in the world. Its oligotrophic ecosystem is particularly sensitive to nutrient pollution. Because of the absence of any permanent riverine inputs, the discharge of wastewater may, apart from atmospheric deposition, constitute a major source of anthropogenic nutrient inputs to the area and may contribute quite significantly to the overall nutrient budget of the Red Sea. The Jeddah Metropolitan Area is the main point source of wastewater to the Red Sea. Bethoux (1988) stated that 8.7×10^8 kg of dissolved inorganic N and 1.2×10^7 kg of dissolved inorganic P are lost annually from the Red Sea to the Indian Ocean via the Bab el Mandab strait. Anthropogenic nutrient discharges, as reported in this study, would then account for 0.3 % of the nitrogen loss and 6.7 % of phosphorus loss. According to the current

results, nutrient emissions from Jeddah resulted by a factor of 6 greater than the rate of annual nitrogen fixation by *Trichodesmium* in the Red Sea as estimated by Bethoux (ibid.) at ~3.6×10^5 kg yr^{-1} N.

In this study, the nutrient loads on the Jeddah coastal waters (Table 4.1) were estimated from wastewater outflows (Table 2.1) and nutrient concentrations at salinity of 0 PSU (Table 4.1). If the nutrient loads estimations were based on the mean per capita nutrient emissions rates of 12 g N d^{-1} and 2 g P d^{-1} N, as proposed by Baker *et al*. (2007) and the Jeddah population of 3.4 million inhabitants during the time of the investigations, the loads resulting in this study (Table 4.1) would account for about 16 % and 33 % of human N and P emissions. This percentage can largely be explained by the fact that ~24 % of the municipal sewage water is deposited in the desert reservoir Wadi Al Asla, or used for irrigation and industrial purposes, and that an unknown fraction of this sewage undergoes full or partial treatment. Depending on the efficiency of the treatment process this could account for an additional nutrient reduction of about up to 50 to 80 %. It should also be considered that sewage emissions from Jeddah constitute a mixture of domestic and industrial wastewater. This is particularly true for the main outfall at Al Khumra which drains the industrial area in the South of the city. This may, apart from downstream denitrification, help explaining the high proportion of phosphorus relative to nitrogen in the load calculations, especially when considering that phosphate-containing industrial detergents are still in use.

When comparing the estimates for nutrient discharges from Jeddah as estimated in this study with those for the year 1989 carried out by El-Rayis (1998), both TN and TP loads have increased by a factor of 5. It should be noted, however, that Jeddah's total population at those times was estimated at 1.6 mill. inhabitants, making up to less than 50 % of the current experiments (Shawly, 2008). A field survey conducted in 1997 by El Sayed (2002) estimated the total daily wastewater nutrient fluxes from the lagoons to be in the order of 2×10^3 kg N and 800 kg P. Despite of the increase in

Jeddah's population to ~2.1 mill. inhabitants, these values are considerably higher than the flux estimates of 1.35×10^3 kg N d^{-1} and 460 kg P d^{-1} estimated in the present study for a population of 3.4 mill. This discrepancy may reflect the efforts made over the past 5 years to improve wastewater treatment in the city, involving the up-scaling and upgrading of existing treatment stations, such as Al Khumra in the south. Besides the construction of a new sewage treatment plant near the international airport (Jeddah Municipality, 2009) further contributed to the reduction in wastewater from Jeddah. As a result of these efforts, the daily wastewater treatment capacity has increased from ~2.25×10^5 m^3 in 2001, to ~3.4×10^5 m^3 in 2006 (Shawly, 2008).

Apart from Jeddah, major sites of pollution to the Red Sea are the industrial areas in the Gulf of Aqaba and Suez, the densely populated port cities Jizan, Yanbu, Port Sudan, Al Hudaydah, and the tourism industry on the Egyptian Red Sea coast with its center in Hurghada. The total population of the 13 largest coastal cities with more than 50000 inhabitants along the Red Sea coast currently accounts for ~9 mill. inhabitants. This corresponds to an average annual growth of about 3 %, when compared to the coastal population in 1997 (Hinrichsen, 1998). Assuming similar conditions for these cities in sewage management and associated *per capita* nutrient discharges as observed in Jeddah, total sewage discharge to the Red Sea may account for a nutrient input of 6.4×10^6 kg yr^{-1} N and 2.2×10^6 kg yr^{-1} P. This constitutes a tremendous environmental stress to the coastal area and could lead to the disrupt of the natural reef communities.

5.1.2. Coastal Nutrient Patterns and Eutrophication Effects

The dispersion of anthropogenic nutrient loads from Jeddah is limited to a small coastal strip in front of the city. Dilution with the nutrient-poor coastal water of the Red Sea is substantial enough to produce steep and stable gradients of the nutrient plumes in front of the largely stagnant water body inside the city lagoons. The nutrient

concentrations had a negative linear relationship with salinity, meaning that the higher the concentration the lower the salinity and vice versa. This negative linear relationship with salinity indicates a largely conservative behaviour of both nitrogen and phosphorus components. El-Rayis (1998) found similar nutrient levels and relationships in the surface water inside and in front of the lagoons. However, nitrate as well as nitrite levels, and their percentage share on total dissolved nitrogen reported are far lower than those observed in the present study. This may be the result of more recent modifications in the quality of the sewage water, involving more efficient aeration during the treatment process, as well as the installation of aerators in front of the outlets. Nevertheless, the high share of ammonium in total nitrogen concentrations at wastewater-impacted sites indicates the prevalence of domestic wastewater lacking any substantial secondary and tertiary treatment (Mizerkowski *et al.*, 2012).

As a consequence of nutrient discharge, which is limited to a distance of few kilometres from the coastline, the trophic status of the area changes from hypertrophic inside the lagoons, through eutrophic in the transition zone adjacent to the inlets, to oligotrophic conditions in the outer coastal water. The hypertrophic character of the lagoons, as evidenced by TN and TP levels similar to those reported for raw sewage water (Metcalf and Eddy, 1991), are associated with intense phytoplankton bloom formation and a sharp oxycline. Since oxygen saturation in the adjacent coastal waters was at equilibrium with the air, the pronounced hyperoxia in the surface water is likely to be caused by vigorous photosynthesis, rather than by physical processes. In contrast, the oxygen deficiency in the deeper waters suggests intense microbial degradation of organic matter deriving from wastewater inputs and primary production. Oxygen oversaturation has previously been observed in the surface layer of the Al Shabab lagoon (El Sayed, 2002), whereas anoxic conditions associated with H_2S formation prevail in the stagnant, high salinity bottom water of both lagoons (El-Rayis and Moammar, 1998) resulting in noxious degasing into the atmosphere. Despite the predominance of dilution processes, it can be assumed that the steep

decrease in nutrient levels within small distances from the wastewater sources is not merely a result of dilution, but also related to the role of the lagoons as a natural nutrient stripper. The processes within the lagoons involve intense nutrient uptake and precipitation associated with massive anoxic sludge accumulation (Magram, 2009) and denitrification as a sink for dissolved inorganic nitrogen. In the nutrient-enriched surface water of the plume in front of the lagoons, observed chlorophyll-*a* levels were still about 20 to 40 times higher than the annual average of 0.05 µg L^{-1} prevailing in the more pristine coastal waters north of Jeddah (Al-Harbi and Khomayis, 2005), while oxygen saturation accounted for 120 % at the surface and 80 % near the sea floor. Considering the elevated nutrient and phytoplankton biomass levels, and the concomitant oxygen oversaturation at the surface, this intermediate zone can thus be classified as eutrophic (Hughes *et al.*, 2011). Although nutrient emissions from the Ghubbat `Asharah lagoon (in Jeddah city, see Figure 2.2) could not be studied in detail, it can be suggested from the high nutrient levels at the wastewater outfalls discharging into this lagoon that this area is also affected by serious nutrient enhancement and concomitant eutrophication effects.

Compared to central Jeddah, environmental impacts deriving from the main sewage outlet at Al Khumra, which accounts for ca. 60 % of the TN and TP loads from the city of Jeddah, are less obvious from surface nutrient patterns. This is most probably partly related to the improved design of the outfall, consisting of a submerged multiport diffuser pipe dispersing the wastewater over a distance of 150 m from a water depth of 25-50 m. These findings are consistent with those previously stated by Al-Farawati (2010) which concluded that the positioning of the effluent at the edge of the fringing reef facilitates dilution of the discharged sewage, but concomitantly enhances the spread of pollutants over larger areas. In a model simulation of the plume dispersion, Al-Ghamdi (2010) found that, due to strong cross-flowing currents and high-exit momentum, sewage concentrations at Al Khumra rapidly drop by a factor of 10^3 within a distance of about 190 m downstream of the exit. According to the

author, this corresponds to the distance where the submerged plume touches the water surface, which may explain the comparatively moderate enhancement of nutrient concentrations in the surface layer as observed in this study. However, even though the situation initially appears less dramatic than in the shallow semi-enclosed lagoons, given the large amount of sewage discharged at Al Khumra, it can be assumed that deleterious effects occur on a greater spatial scale. Impacts are likely to occur especially in the nearshore benthic realm constantly exposed to elevated nutrient levels, where threshold concentrations for macroalgae overgrowth of coral reef communities are in the range of ~1 µM DIN and 0.1 µM PO_4^{3-} (Lapointe, 1997). Changes in the macrozoobenthic community structure around the outfall have recently been reported by Al-Farraj *et al.* (2012) and attributed to enhanced organic enrichment associated with oxygen deficiency.

Risk *et al.* (2009) tracked the record of sewage discharge from Jeddah using $\delta^{15}N$ records from black corals as a proxy. The water quality pattern obtained in their study is largely similar to the present nutrient distribution, with some deviation in the highly polluted area in front of the city lagoons. The latter may be explained by the fact that the coral near the city were dead. As a result in order to project isotopic trends inshore the authors were forced to use $\delta^{15}N$ values from macroalgae, normalized by correlation with coral isotopic data.

From numerous field studies it is well known that, in poorly flushed regions, strong and persistent nutrient enhancement, as observed in this study, results in a degradation of hermatypic coral reef communities. This is due to the combined cascading effects of accelerated phytoplankton and macroalgae proliferation, reduced light supply, enhanced sedimentation and the competitive advantage of filter-feeding and detritivorous invertebrates (see review by Fabricius, 2005). Excess nutrients may also lead to uncontrolled growth of zooxanthellae populations which disrupts the balance of nitrogen and carbon flux between host and algae, and results in reduced calcification (Marubini and Davies, 1996). Furthermore, elevated phosphate

concentrations (> 2 µM PO_4^{3-}) may directly act as an inhibitor of calcite crystal formation in coral (Kinsey and Davies, 1979). To be noticed that this level was largely exceeded inside and in front of the lagoons.

5.1.3. Potential Nutrient Limitation

While the high share of dissolved inorganic nutrients in total nutrient concentrations, as observed at the polluted nearshore sites in the near coastal waters of Jeddah, is typical for domestic wastewater (Metcalf and Eddy, 1991), the pronounced nutrient depletion and increased percentage of particulate and organic nitrogen and phosphorus in the oligotrophic coastal waters adjacent to the wastewater sources suggest a rapid transformation of dissolved inorganic nutrient compounds entering the coastal system. Considering the favorable year-round light and temperature conditions, the nutrient-starved primary producers provide an efficient sink for dissolved nutrient inputs. However, phytoplankton biomass can hardly account for the predominance of organic nutrients in the offshore coastal waters, considering that chlorophyll-*a* levels did not exceed 0.1 µg L^{-1}. Applying a maximum conversion factor of 200 for C:Chl-*a* [g g^{-1}], as usually adopted for small sized picoplankton in oligotrophic regions (Wang *et al*., 2009), and Redfield ratios, phytoplankton biomass would account for less than 5 % of the particulate and organic nitrogen and phosphorus pools in the oligotrophic waters. It seems more likely that the higher share of particulate and organic nutrients in the open coastal water reflect either the increasing importance of residual, biologically refractory forms of N and P while dissolved inorganic nutrients are depleted, or is the result of DON and DOP release. The predominance of dissolved organic forms of N and P is a frequent phenomenon in oligotrophic surface waters of oceans (e.g. Jackson and Williams, 1985; Lucea *et al*., 2003), which has been attributed to high phytoplankton lysis rates, rather than exudation (Agustí and Duarte, 2000; Lucea *et al*., 2003).

An increasing dominance of DON and DOP on total nutrients from wastewater-polluted, nearshore sites towards pristine offshore waters has also been or observed in the Florida Keys (Lapointe and Clark, 1992). This trend was associated with a significant shift from high N:P ratios (>15) in the primarily P-limited areas nearshore, to low ratios (~6) in the more N-limited, open ocean waters (ibid.) and confirmed in the present study. The assessment of potential nutrient limitation, taking the Redfield ratio as an arbitrary measure, indicates that N-deficiency prevails in the more pristine offshore waters near Jeddah, whereas the wastewater-impacted, nearshore sites were close to the stoichiometric balance. On the other hand, the pronounced N-deficiency in the offshore waters is in contrast to studies stating that phosphorus availability is the limiting factor in most oligotrophic seas (TP <0.8 µM) (Downing, 1997; Guildford and Hecky, 2000; Smith, 2006). The present results are in agreement with those reported in the World Ocean Atlas 2009 (Garcia *et al.*, 2010), revealing that the central Red Sea has a typical NO_3^-:PO_4^{3-} ratio of 2.1:1. The region thus belongs to those areas characterized by low NO_3^-:PO_4^{3-} ratios (LNP areas) as a result of nitrate deficiency as pointed out by Tyrrell and Law (1997).

These ratios are far lower than the 20:1 and 21:1 ratios found respectively by Grasshoff in 1969 and Naqvi *et al.* in 1986, suggesting a deficiency in phosphate relative to nitrate in the Red Sea. This may hold true for the southern region of the Red Sea, which is heavily influenced by exchange with the Indian Ocean. Nevertheless, it does not reflect the situation in the open coastal waters of Jeddah, which exhibit a distinct nitrate deficit. For sea areas where nitrogen fixation plays a minor role, the nitrate deficit defined as $\Delta N = (16 \times [PO_4^{3-}]) - [NO_3^-]$ (Tyrrell and Lucas, 2002) is proposed to be an indicator of enhanced denitrification activity (occurring at a N:P ratio of −100:1, minus meaning nitrogen removal). In the present case, the average nitrate deficit in the oligotrophic coastal water accounted for 2.68 µM. It can thus be assumed that, in the coastal ecosystem of Jeddah, denitrification plays a substantial role, and that nitrogen fixation is of less importance

when compared to other areas of the Red Sea. Denitrification constitutes an important nitrogen sink in the oxygen minimum zone (OMZ) of the oceans (Naqvi *et al*., 2006) and it is also likely to occur in the OMZ of the Red Sea at depths of 300 to 400 m below the free surface.

From the correlations of nutrient concentrations with chlorophyll-*a*, one cannot deduce which nutrient is likely to control algal growth. The slope for the yield of chlorophyll-*a* per unit of TP resulted higher than that reported for N-limited systems (Smith, 2006), but lower than for P-limited ones. The correlation coefficients of nitrogen and phosphorus with chlorophyll-*a* were similar for both total and dissolved inorganic fractions. It can thus be argued that both nitrogen or phosphorus reduction could be taken as management options aiming at mitigating existing eutrophication effects.

Söderström (1996) stated that ambient DIN:PO_4^{3-} ratios must be compared with ratios of the nutrient half saturation constants for nitrogen and phosphorus uptake (K_S-N:K_S-P) before assessing whether N or P controls phytoplankton growth. Since the molar K_S-N:K_S-P ratio may have values $\geq$ 4.4:1 (ibid.), an equivalent DIN:PO_4^{3-} ratio in the ambient water may represent neutrality between N and P for algal growth. In the present case, for those oligotrophic stations were all inorganic chemical species of nitrogen were measurable, the DIN:PO_4^{3-} ratio was 3.8:1 and hence below this minimum threshold, indicating potential nitrogen limitation. Similarly, the comparison of absolute DIN and PO_4^{3-} levels in the open coastal waters with half-saturation constants reported for nanophytoplankton populations under extreme oligotrophic conditions provides strong evidence that nitrogen availability controls phytoplankton growth in the offshore area. The K_S values from Aumont and Bopp (2006) applied in the present case (see section 4.1.4.) are at the lower limit of the broad range of half-saturation constants reported in literature. Nonetheless, inorganic phosphate in Jeddah offshore waters was still available in non-limiting quantities when compared to more conservative appraisals of half-saturation constants, as those

reported by Tyrrel (1999; K-PO_4^{3-}: 0.05 µM), while nitrate levels were primarily below the limit of detection. Nitrogen limitation, as a result of nitrate depletion, has also been observed in the upper mixed layer of the Gulf of Aqaba in the northern Red Sea in late summer and fall (Badran *et al.*, 2005) and held responsible for the subsequent proliferation of N-fixing cyanobacteria populations (Gordon *et al.*, 1994).

5.2. The Impact of Nutrient Load Reduction on Phytoplankton Biomass in the Coastal Waters off Jeddah

The reduction of anthropogenic nutrient loads may be an effective measure to mitigate eutrophication phenomena (Cugier *et al.*, 2005, Greening and Janicki, 2006). However, due to complex interactions and associated time-lags, regime and baseline shifts, in most cases the response of the system in terms of phytoplankton biomass to variations in nutrient loadings is not linear (Duarte *et al.*, 2009; Kemp *et al.*, 2009).

For reasons of simplicity, the water quality model applied to study the response of phytoplankton biomass to nutrient load variation in the Jeddah coastal waters focuses on the water column and does not consider nutrient or carbon sinks such as denitrification and settling. The results from the scenario simulations thus rather represent worst case assumptions for phytoplankton biomass formation. They imply a high sensitivity of the phytoplankton community in Jeddah Bay to changes in the anthropogenic nutrient inputs. Since river nutrient discharges or freshwater sources, other than waste water, are absent in the region, it can be assumed that the bulk of the high phytoplankton standing stock in the inner Jeddah Bay is sustained by waste water nutrient loads only. Open sea loadings, likewise, can hardly provide a basis for the development of coastal phytoplankton blooms since nutrient concentrations in the open coastal waters were typical for oligotrophic conditions, not exceeding 6 µM TN and 0.4 µM TP.

Weak tidal currents of less than 5 cm s^{-1} and the adequate light conditions throughout the year are supposed to be important factors triggering the pronounced increase of phytoplankton biomass in the 50% nutrient load enhancement scenario. By contrast, the comparatively moderate response of phytoplankton biomass to an 80% nutrient load reduction indicates that even under these conditions nutrient supply is still sufficient to sustain an intense phytoplankton growth. The low flushing rates and hence poor dilution associated with rapid on-site recycling of nutrients stimulated by high water temperatures favour the retention of nutrients in a confined area, thus keeping them available for algal growth. The importance of hydrodynamics and especially residence time for the response of phytoplankton biomass to nutrient load reduction has been illustrated in a number of field studies and model simulations (Bricker *et al*., 2008; Lucas *et al*., 2009; García *et al.*, 2010).

The susceptibility of the Jeddah coastal waters to nutrient enrichment is thus supposed to be much higher than to nutrient reduction. Figure 5.1.a-c presents the DIN:DIP ratios resulting from the nutrients reduction scenarios (see 3.4.3). The higher impact of nitrogen load variations on chlorophyll-*a* levels compared to those of phosphorus suggests that nitrogen is the main limiting nutrient in the area. This is in keeping with findings from Badran *et al.* (2005) for the northern Red Sea. It thus appears that a reduction of nitrogen loads alone would be an efficient measure to mitigate eutrophication effects in the coastal ecosystem of Jeddah. The resulting shift in N:P-ratios (Figure 5.1.a), however, may promote the formation of diazotrophic cyanobacteria blooms during conditions of concurrent nitrogen limitation and phosphorus excess in the open bay waters (Paerl, 2008).

Since the technical and economical effort required for removing a significant portion of phosphorus from waste water is much lower than for eliminating nitrogen, a simultaneous substantial reduction of P should thus be considered for a more effective control of coastal eutrophication phenomena (Figure 5.1.b). The dual reduction of

both N and P loads results in a more balanced pattern of DIN/DIP-ratios close to the Redfield number (Figure 5.1.c).

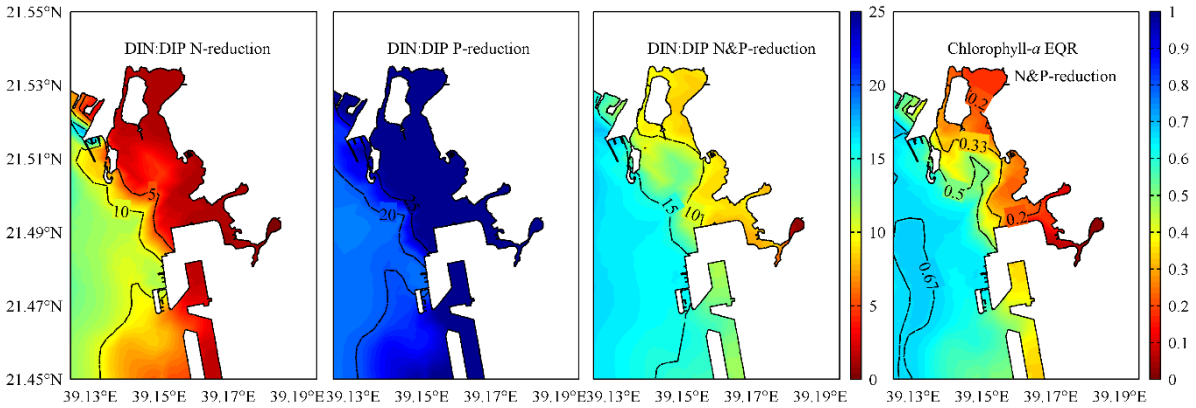

Figure 5.1. Distribution of the surface DIN:DIP ratio as result of an 80% nutrient reduction scenario (a-c). The ecological quality ratio for chlorophyll-*a* is shown in the right panel (d).

However, the simulations reveal that even a major mitigation effort as a dual reduction of urban nutrient loads by 80% would not be sufficient to change the water quality of the inner Jeddah Bight towards a good ecological state. Figure 5.1.d displays results of model simulations of the ecological quality ratio (EQR) for chlorophyll-*a* resulting from an 80% reduction in both N and P. EQR is defined as the relation between a reference condition value and the observed value (Andersen *et al.*, 2004). In the present case, it is based on a reference value of 0.3 µg chl-*a* L^{-1} which was the mean concentration in the offshore pristine Red Sea water. According to the results, only in a confined area in the offshore water an EQR value of 0.67 is reached. This represents 50% increase with respect to the background conditions and hence the boundary between good and moderate conditions according to OSPAR (2003).

In order to successfully implement efficient measures to mitigate nutrient pollution of the Jeddah Bay area, it would be a prerequisite to first mitigate anthropogenic nutrient

inputs to the lagoons and to redirect wastewater to sewage works equipped with tertiary treatment, such as the new treatment facilities which have recently been put into operation in Jeddah. Besides, as much as possible, treated water should be re-used for industrial processing and irrigation purposes.

Instead of dumping the remaining treated waste water into the sheltered and poorly flushed coastal reef area, it should be directed through extended multiport diffuser pipes across the narrow shelf towards the deep outer water body which offers a higher potential of cross cutting currents to allow for rapid mixing and dilution. However, a gradual return of the coastal ecosystem to its past ecological state upon nutrient load reduction cannot be expected even under conditions of zero emission. This is because the original coral reef communities with their unique food web interactions and biogeochemical cycles flourishing in near vicinity of the city about 60 years ago (Risk *et al*., 2009) are invariably degraded.

5.3. Hydrographic Patterns and Nutrients in the Central Red Sea

In this chapter , the hydrographic patterns of temperature, salinity, dissolved oxygen, chlorophyll-*a* and chemical species of nitrogen and phosphorus are discussed for the central Red Sea.

5.3.1. Temperature, Salinity and Dissolved Oxygen

The surface distribution pattern of temperature and salinity along the south-north transect in the central Red Sea as described in section 4.3.1. is well in keeping with the current understanding of the Red Sea's hydrography (e.g. Fenton *et al.*, 2000; Acker *et al.*, 2008): The less saline and warmer surface water in the south reflects the intrusion of water from the Arabian Sea and the Gulf of Aden during the period of the

campaign (end of winter season). This surface inflow at the transect is characterized by a general downward slope of temperature and salinity isolines in the upper 400 m from north to south, and a surface gradient in temperature and salinity of 6 K and 2.5 PSU, respectively. As confirmed by from ARGO data and model results (see 4.2.1) the winter mixing deepens the thermocline below a 100 m depth in the central area, which is in keeping with previous observations (i.e. Quadfasel and Baudner, 1993).

The oxygen minimum zone results from the enhanced decomposition of sinking particulate organic matter associated with increased oxygen consumption. The steeper oxycline and the more pronounced oxygen depletion in the south of the central Red Sea, which, in the present case, cumulates in hypoxic concentrations of ~40 µmol O_2 kg^{-1}, have also been described by Fenton *et al.* (2000). This pattern (Figure 4.18.) might be due to elevated mean chlorophyll concentrations in the surface layer, as a response to the nutrient-rich water intrusion from the Indian Ocean through the Bab-el-Mandab strait (Acker *et al.*, 2008). There should thus be a higher amount of sinking particulate organic matter and consequently, increased oxygen consumption in the south when compared to the situation in the north of the Red Sea, where the effect of the Indian Ocean intrusion is of minor relevance.

5.3.2. Chlorophyll-*a* and Nutrients

Surface chlorophyll-*a* concentrations observed along the central axis of the Red Sea were typical for oligotrophic conditions, ranging from <0.05 µg L^{-1} in most cases to 0.20 µg L^{-1} near the Gulf of Aqaba. This situation is in agreement with the chlorophyll pattern derived from satellite data as reported by Acker *et al.* (2008). It has, however, been argued that due to an excess of chromophoric dissolved organic matter (CDOM; Brewin *et al.*, 2015) the values reported by Acker *et al.* (ibid.) might overestimate chlorophyll concentrations.

Deep Chlorophyll Maximum (DCM) at the nutricline as observed in the present study is a common feature in many tropical seas. It is generally due to nutrient limitation of phytoplankton growth in the surface water above the DCM and light limitation in the lower layers. Raitsos *et al.* (2013) described a distinct DCM in the central Red sea with concentrations of ~0.5 µg L^{-1} located below the mixed layer at a depth of 60 m to 80 m. Calbet *et al.* (2015) reported a clear, though modest, deep chlorophyll maximum in the Red Sea, which is in keeping with results of this study.

In the present case, the DCM was found primarily below the mixed layer at a mean depth of 1.33 % of surface irradiance (range: 0.98-1.81%). Except for the northernmost station 7, where DCM was found within the upper mixed layer at a depth of ~20 m corresponding to 17% of surface irradiance. This shallow chlorophyll maximum may be due to the presence of a cyclonic eddy occurring in winter and spring in the northern central Red Sea around 27°N. This eddy causes a supply of nutrients (predominantly nitrate, see Figure 4.19) from the deep water to the mixed layer (Raitsos *et al.* 2013).

Similarly, the patchy distribution of chlorophyll in the DCM with maxima at 27°N, 25°N, 20-22°N, 18°N and 16°N may coincide with the edges of gyres and eddies present in the Red Sea (Zahn *et al.*, 2014; Wafar *et al.*, 2016). A similar patchiness in the phytoplankton biomass distribution of the Red Sea has also been reported by Qurban *et al.* (2014).

The very low nutrient concentrations in the surface waters of the central Red Sea are in line with the absence of major nutrient inputs through continental runoff and in agreement with previous observations (e.g. Calbet *et al.*, 2015). The main nutrient source to the mixed layer of the central Red Sea is through horizontal transport from the Arabian Sea/Gulf of Aden and the turbulent intrusion of nitrogen and phosphorus from deeper water layers. Ammonium depletion and nitrate deficit in the upper mixed layer is in keeping with reports suggesting nitrogen limitation of phytoplankton growth in the Red Sea (Badran *et al.*, 2005; Qurban *et al.*, 2014).

As commonly found in tropical marine waters (Lomas and Lipschultz, 2006), the primary nitrite maximum (PNM), the nitracline and the deep chlorophyll maximum are located more or less at the same depth, i.e. about 50 m in the south and north, and ca. 70 m in the centre of the Red Sea (see Figure 4.17.). The presence and maintenance of a nitrite maximum in tropical waters have been suggested to result from enhanced nitrite excretion by phytoplankton as a consequence of incomplete nitrate reduction. This incomplete nitrate reduction is due to light limitation and/or to a decoupling of the first step of microbial nitrification from the second step, decoupling that occurs as a consequence of selective light inhibition of the photosensitive microbes performing the step of nitrite oxidation (Mackey *et al.*, 2011). Meeder *et al.* (2012) suggest that neither differential photoinhibition of nitrifying bacteria nor excretion of light-stressed phytoplankton are responsible for establishing the PNM in the northern Red Sea during the strongly stratified conditions in summer. They suggest that the summer PNM would rather be due to a segregation of the different transformation processes involved because of the different rate constants of ammonification, ammonium oxidation and nitrite oxidation in conjunction with the temporal process of the downward flux of particulate organic matter from the DCM. The present results (Figure 4.17.) seem to fit in with this model. The nitracline, i.e. enhancement of nitrate concentrations, appears to be slightly deeper than the PNM which, in turn, seems to be slightly deeper than the DCM. Unfortunately, the vertical resolution of nutrient measurements in this study does not allow to be entirely certain about the exact depth at which PNM and nitracline are located relative to the DCM. If the PNM and the DCM were located very close to each other, one might instead conclude that nitrite excretion by light-limited phytoplankton would be the reason for maintaining the PNM. This latter process is actually held responsible for the formation of the PNM in the Red Sea during winter (Meeder *et al.*, 2012).

5.4. The Importance of Photomineralization of Dissolved Organic Nitrogen in the Central Red Sea

In view of the area of the Red Sea of about 4.38×10^{11} m^2, and taking an average PM_{Total} of 39.2 µmol N m^{-2} d^{-1}, photomineralization in this large marine environment represents a transformation of nitrogen up to approximately 1.7×10^7 mol N d^{-1}. On an annual basis, this rate (8.8×10^7 kg N yr^{-1}) is one order of magnitude smaller than the annual loss of dissolved inorganic N from the Red Sea to the Indian Ocean via the Bab-el-Mandeb strait in the order of 8.7×10^8 kg N yr^{-1} (as reported by Bethoux (1988). However, DON transformation by photomineralization exceeds by two orders of magnitude the annual nitrogen fixation by *Trichodesmium* in the Red Sea estimated at about 3.6×10^5 kg N yr^{-1} (ibid.). The DIN supply by photomineralization as calculated in the present study also outbalances both the total inorganic nitrogen load of ~2.0×10^6 kg DIN yr^{-1} from the Jeddah Metropolitan Area (see section 4.1.5.) and the estimates of total nitrogen input from sewage discharge into the Red Sea of about 6.4×10^6 kg N yr^{-1} as reported above. Qurban *et al.* (2014) calculated the diffusive mass flux of nitrate into the euphotic zone from deeper water layers in the northern Red Sea on the basis of nitrate uptake rates and estimated the fluxes to be in the range 0.03 to 0.23 mmol N m^{-2} s^{-1}. Assuming these values to be the same for the entire Red Sea, the annual nitrate flux would range from 5.8×10^{12} to 4.5×10^{13} kg N yr^{-1}. These rates are five and six orders of magnitude higher than the estimates of potential inorganic nitrogen supply due to DON photomineralization. Furthermore it indicates that the diffusive nitrate flux would be the process enriching the euphotic zone with the highest amount of assimilable nitrogen. However, due to the fact that Qurban *et al.* (2014) estimated the diffusive mass flux of nitrate without including nitrification in the euphotic layer as a source of nitrate for uptake, the nitrate flux may be overestimated. Qurban *et al.* (2014) also estimated an averaged surface ammonium uptake in the northern Red Sea of 9 µmol m^{-3} h^{-1}. Assuming a period of

12 h for phytoplankton ammonium uptake during daylight, this would result in a daily uptake rate of 108 µmol m^{-3} d^{-1}. If one assumes that a large portion of photomineralized DON ends up as NH_4^+ (Bronk *et al.*, 2007; Bushaw *et al.*, 1996), DON photomineralization in the surface water (1.71 µmol m^{-3} d^{-1} on an average of 4 stations) can supply ~1.6% of the ammonium requirements. Considering these results, one can infer that photomineralization is a process bringing only moderate amounts of bioavailable nitrogen to the strongly N-limited environment prevailing in the Red Sea.

6. CONCLUSIONS AND RECOMMENDATIONS

6.1. Conclusions

The hydrochemical structure as assessed on a South to North transect along the central axis of the Red Sea is in line with findings of previous studies confirming the oligotrophic character of the environment.

Hydrographic data reflect the intrusion of warm and less saline water from the Arabian Sea. Other predominant features were a pronounced deep chlorophyll-*a* maximum situated above the bottom of the euphotic zone and a nitrite maximum at about the same depth. A distinct deep oxygen minimum zone occurred at a depth of 250 to 600 m.

The comparison of stoichiometric nitrogen to phosphorus ratios and half saturation constants for phytoplankton growth suggests a strong nitrogen limitation in the central Red Sea and the offshore coastal waters.

Estimates of photomineralization integrated to the euphotic zone averaged ca. 42 µmol N m^{-2} d^{-1}. Compared to other processes such as diffusive nitrogen input from deep layers, photomineralization is thus considered to bring only moderate amounts of bioavailable nitrogen tot the N-limited surface waters of the Red Sea.

Annual nutrient input from waste water discharge of the Jeddah Metropolitan Area was estimated to about 2396 tons of nitrogen and 818 tons of phosphorus, resulting in steep gradients towards the offshore water. However, eutrophication problem areas are confined to a small stripe near the coast.

The developed hydrodynamic model reliably reproduces the annual variation of surface temperature in the central Red Sea. Likewise, the model reproduces quite accurately the seasonal salinity variation in the surface waters.

The developed numerical water quality model for the coastal waters of Jeddah reflected with fidelity both oligotrophic and hypertrophic conditions in the area.

Scenario runs with varying nutrient inputs from waste water discharge indicate that changes in nitrogen loads have a more pronounced effect on coastal phytoplankton biomass than those of phosphorus. An 80% reduction of nitrogen load, however, only resulted in a 50% decrease of phytoplankton biomass within the following 6 months after reduction.

6.2. Recommendations

In order to mitigate impacts of waste water discharge from Jeddah into the Red Sea, existing treatment facilities have to be upscaled to tertiary treatment. The overall capacity of waste water treatment should be enhanced by a sound sewerage network and the construction of new plants.

The treated waste water should be directed through extended multiport diffuser pipes across the narrow shelf towards deeper offshore waters exhibiting cross cutting currents.

The effect of the measures taken should be controlled by a thorough monitoring system in the coastal waters and the lagoons.

Numerical models will help in decision making and should be applied to identify the magnitude and character of mitigation measures as well as the critical monitoring strategy in time and space.

In parallel to nutrient reduction, there should be a restoration program for the near coastal area. Sludge in the city lagoons should be dug out and deposited on land. Dead corals reefs may be progressively restored by planting new nursery-grown corals on old or artificial reef materials.

The experiments and calculation of photomineralization in the present study are a first and rather simple approach. Further studies are needed to clarify the role of this process for nitrogen supply in the oligotrophic surface waters of the Red Sea.

7. REFERENCES

Acker, J., G. Leptoukh, S. Shen, T. Zhu, and S. Kempler, 2008. Remotely-sensed chlorophyll-*a* observations of the northern Red Sea indicate seasonal variability and influence of coastal reefs. J. Mar. Syst. 69: 191–204.

Agustí, S. and C. M. Duarte, 2000. Strong seasonality in phytoplankton cell lysis in the NW Mediterranean littoral. Limnol. Oceanogr. 45 (4): 940-947.

Al-Farraj, S., A. El- Gendy, S. Al Kahtani and M. El- Hedeny, 2012. The Impact of Sewage Pollution on Polychaetes of Al Khumrah, South of Jeddah, Saudi Arabia. Research Journal of Environmental Sciences, 6: 77-87. DOI: 10.3923/rjes.2012.77.87.

Al-Farawati, R., 2010. Environmental conditions of the coastal waters of Southern Corinche, Jeddah, Eastern Red Sea: Physico-chemical approach. Aust. J. Basic Applied Sci., 4: 3324-3337.

Al-Farawati, R., A. Al-Maradni and R. G. Niaz, 2008. Chemical characteristics (nutrients, fecal sterols and polyaromatic hydrocarbons) on the surface waters for Sharm Obhur, Jeddah, eastern coast of the Red Sea. JKAU: Mar. Sci., 19:95-119.

Al-Ghamdi, A.S., 2010. Simulation of Jeddah multi-port sea outfall. J. Coast. Conserv., 14:63-69.

Al-Harbi, S. M. and H. S. Khomayis, 2005. Seasonal variation of chlorophyll-*a* and micro-nutrients in Obhur Creek, Red Sea. JKAU: Mar Sci. 16, 91-104.

Amante, C. and B.W. Eakins, 2009. ETOPO1 1 Arc-Minute Global Relief Model: Procedures, Data Sources and Analysis. NOAA Technical Memorandum NESDIS NGDC-24. National Geophysical Data Center, NOAA. doi:10.7289/V5C8276M [access date].

Andersen, J. H., D. J. Conley, and S. Hedal, 2004. Palaeoecology, reference conditions and classification of ecological status: the EU Water Framework Directive in practice. Marine Pollution Bulletin, 49: 283-290.

Antonov, J. I., D. Seidov, T. P. Boyer, R. A. Locarnini, A. V. Mishonov, H. E. Garcia, O. K. Baranova, M. M. Zweng & D. R. Johnson, 2010. World Ocean Atlas 2009, Volume 2: Salinity. S. Levitus, Ed. NOAA Atlas NESDIS 69, U.S. Government Printing Office, Washington, D.C., 184 pp.

ARGO. “These data were collected and made freely available by the International Argo Program and the national programs that contribute to it. (http://www.argo.ucsd.edu, http://argo.jcommops.org). The Argo Program is part of the Global Ocean Observing System.”.

Aumont, O. and L. Bopp, 2006. Globalizing results from ocean in situ iron fertilization studies, Global Biogeochem. Cycles: 20, GB2017, doi:10.1029/2005GB002591

Badran, M. I., M. Rasheed, R. Manasrah and T. Al-Najjar, 2005. Nutrient flux fuels the summer primary productivity in the oligotrophic waters in the Gulf of Aqaba, Red Sea. Oceanologia 47 (1): 47-60.

Baker, L. A., P. M. Hartzheim, S. E. Hobbie, J. Y. King and K. C. Nelson, 2007. Effect of consumption choices on fluxes of carbon, nitrogen and phosphorus through households. Urban Ecosyst 10:97-117; DOI 10.1007/s11252-006-0014-3.

Basaham, A. S., 1998. Distribution and behaviour of some heavy metals in the surface sediments of Al-Arbaeen lagoon, Jeddah, Red Sea coast. J. KAU.: Earth Sci., 10:59-71.

Basaham, A. S., A. E. Rifaat, M. H. El-Mamoney and M. A. El Sayed, 2009. Re-evaluation of the impact of sewage disposal on coastal sediments of the southern Corniche, Jeddah, Saudi Arabia. J. KAU: Mar. Sci. 20:109-126.

Bethoux, J. P., 1988. Red Sea geochemical budgets and exchanges with the Indian Ocean. Marine Chemistry, 24:83-92.

Boivin, L. P., W. F. Davidson, R. S. Storey, D. Sinclair and E.D. Earle, 1986. Determination of the attenuation coefficients of visible andultraviolet radiation in heavy water. Appl. Opt. 25: 877-882.

Brewin, R. J. W., D. E. Raitsos, G. Dall'Olmo, N. Zarokanellos, T. Jackson, M.-F. Racault, E. S. Boss, S. Sathyendranath, B. H. Jones and I. Hoteit, 2015. Regional ocean-colour chlorophyll algorithms for the Red Sea. Remote Sensing of Environment 165: 64–85.

Bricaud, A., A. Morel, M. Babin, K. Allali and H. Claustre, 1998. Variations of light absorption by suspended particles with chlorophyll a concentration in oceanic (case 1) waters: Analysis and implications for bio-optical models. J. Geophys. Res. 103: 31033-31044.

Bricker, S. B., B. Longstaff, W. Dennison, A. Jones, K. Boicourt, C. Wicks and J. Woerner, 2008. Effects of nutrient enrichment in the nation’s estuaries: A decade of change. Harmful Algae, 8: 21-32.

Bronk, D. A., J. H. See, P. Bradley and L. Killberg, 2007. DON as a source of bioavailable nitrogen for phytoplankton. Biogeosciences, 4, 283–296.

Buffam, I. and K. J. McGlathery, 2003. Effect of ultraviolet light on dissolved nitrogen transformation in coastal lagoon water. Limnol. Oceanogr. 48(2): 723-734.

Buiteveld, H., J. H. M. Hakvoort and M. Donze, 1994. The optical properties of pure water. Proc. SPIE2258, Ocean Optics XII, 174. doi:10.1117/12.190060.

Bushaw, K. L., R. G. Zepp, M. A. Tarr, D. Schulz-Jander, R. A. Bourbonniere, R. E. Hodson, W. L. Miller, D. A. Bronk and M. A. Moran, 1996. Photochemical release of biologically available nitrogen from aquatic dissolved organic matter. Nature 381: 404-407.

Calbet, A., M. D. Agersted, S. Kaartvedt, M. Møhl, E. F. Møller, S. Enghoff-Poulsen, M. L. Paulsen, I. Solberg, K. W. Tang, K. Tönnesson, D. E. Raitsos and T. G. Nielsen, 2015. Heterogeneous distribution of plankton within the mixed layer and its implications for bloom formation in tropical seas. Sci. Rep.: 5,11240

Chau, K. W. & H. Jin, 2002. Two-layered, 2D unsteady eutrophication model in boundary-fitted coordinate system. Marine Pollution Bulletin, 45: 300-310.

Chen, W.-B., W.-C. Liu & M.-H. Hsu, 2011. Water quality modelling in a tidal estuarine system using three dimensional model. Environmental Engineering Science, 28: 443-459.

Clark, D. R., A. P. Rees and I. Joint, 2008. Ammonium regeneration and nitrification rates in the oligotrophic Atlantic Ocean: Implications for new production estimates. Limnol. Oceanogr. 53(1): 52-62.

Corredor, J. E., R. W. Howarth, R. R. Twilley and J. M. Morell, 1999. Nitrogen cycling and anthropogenic impact in the tropical interamerican seas. Biogeochemistry 46: 163-178.

Cugier, P., G. Billen, J. F. Guillaud, J. Garnier and A. Ménesguen, 2005. Modelling the eutrophication of Seine Bight (France) under historical, present and future riverine nutrient loading. Journal of Hydrology, 304: 381-396.

Curry, R, 2013. Hydrobase 3. www.whoi.edu/science/PO/hydrobase/php/index.php.

del Barrio Fernández, P., A. García Gómez, J. García Alba, C. Álvarez Díaz & J. A. Revilla Cortezón, 2012. A model for describing the eutrophication in a heavily regulated coastal lagoon. Application to the Albufera of Valencia (Spain). Journal of Environmental Management, 112: 340-352.

Deltares, 2014. Delft3D-FLOW, simulation of multi-dimensional hydrodynamic flows and transport phenomena, including sediments. User Manual. Version 3.15.34158. 710 p.

Deltares, 2011. Process library: detailed description of processes, technical reference manual, water quality and aquatic ecology, version 4.00. Deltares. 370 p.

Downing, J. A., 1997. Marine nitrogen:phosphorus stoichiometry and the global N:P cycle. Biogeochemistry 37: 237-252.

Duarte, C. M., D. J. Conley, J. Carstensen and M. Sánchez-Camacho, 2009. Return to Neverland: Shifting baselines affect eutrophication restoration targets. Estuaries and Coasts, 32: 29–36.

Dugdale, R. C. and J. J. Goering, 1967. Uptake of new and regenerated forms of nitrogen in primary productivity. Limnol. Oceanogr. 12: 196-206.

El-Rayis, O. A., 1998. Environmental conditions of two Red Sea coastal lagoons in Jeddah. 2. Nutrients, J. KAU: Mar. Sci. 9: 49-59.

El-Rayis, O. A. and M. O. Moammar, 1998. Environmental conditions of two Red Sea coastal lagoons in Jeddah. 1. Hydrochemistry. J. KAU: Mar. Sci. 9:31-47.

El Sayed, M. A., 2002. Nitrogen and phosphorus in the effluent of a sewage treatment station on the eastern Red Sea coast: daily cycle, flux and impact on the coastal area. Intern. J. Environ. Studies, 59(1): 73-94.

Eppley, R. W. and B. J. Peterson, 1979. Particulate organic matter flux and planktonic new production in the deep ocean. Nature 282: 677-680.

Ewea, H. A., 2010. Hydrological analysis of wastewater lake in Jeddah, Saudi Arabia. JKAU: Met., Env. & Arid Land Agric. Sci. 21(1), 125-144.

European Parliament and Council, 2000. Directive 2000/60/EC of the European Parliament and of the Council of 23 October 2000 establishing a framework for Community action in the field of water policy. OJL 327, 73 pp.

Fabricius, K. E., 2005. Effects of terrestrial runoff on the ecology of corals and coral reefs: review and synthesis. Mar. Pollut. Bull. 50: 125-146.

Fenton, M., S. Geiselhart, E. J. Rohling and Ch. Hemleben, 2000. Aplanktonic zones in the Red Sea. Marine Micropaleontology 40: 277-294.

Furnas, M.J., 1990. In situ growth rates of marine phytoplankton: approaches to measurement, community and species growth. Journal of Plankton Research, 12: 1117-1151.

Garcia, H. E., R. A. Locarnini, T. P. Boyer, J. I. Antonov, M. M. Zweng, O. K. Baranova and D. R. Johnson, 2010. World Ocean Atlas 2009. Volume 4: Nutrients (phosphate, nitrate, silicate). S. Levitus (ed.) NOAA Atlas NESDIS 71, U.S. Government Printing Office, Washington D.C., 398 pp.

Gordon, N., D. L. Angel, A. Neori, N. Kress and B. Kimor, 1994. Heterotrophic dinoflagellates with symbiotic cyanobacteria and nitrogen limitation in the Gulf of Aqaba. Mar. Ecol. Prog. Ser. 107: 83-88.

Grasshoff, K., 1969. Zur Chemie des Roten Meeres und des inneren Golfs von Aden nach Beobachtungen von Forschungsschiff Meteor während der Indischen Expedition 1964/65. Meteor Forschungsergebnisse, Reihe A6.

Grasshoff, K., K. Kremling and M. Ehrhardt (eds.), 1999. Methods of seawater analysis. 3rd completely revised and extended edition. Wiley-VCH, 600 pp.

Greening, H. and A. Janicki, 2006. Toward reversal of eutrophic conditions in a subtropical estuary: water quality and seagrass response to nitrogen loading reductions in Tampa Bay, Florida, USA. Environmental Management, 38: 163-78. DOI: 10.1007/s00267-005-0079-4

Guildford, S. J. and R. E. Hecky, 2000. Total nitrogen, total phosphorus, and nutrient limitation in lakes and oceans: Is there a common relationship? Limnol. Oceanogr., 45(6), 1213-1223.

Håkanson, L., A. C. Bryhn and J. K. Hytteborn, 2007. On the issue of limiting nutrient and predictions of cyanobacteria in aquatic systems. Science of the Total Environment, 379: 89-108.

Hall, J., S.V. Smith and P.R. Boudreau (eds.), 1996. Report on the International Workshop on Continental Shelf Fluxes of Carbon, Nitrogen and Phosphorus. LOICZ Reports & Studies No. 9 / JGOFS Report No. 22, ii + 50 pp. LOICZ, Texel, The Netherlands.

Hinrichsen, D., 1998. Coastal waters of the world: trends, threats, and strategies. Chapter 15: The Red Sea and the Gulf of Aden. Island Press, Washington, 195-200.

Hoad, K., S. Robinson and R. Davies, 2010. Automating warm-up length estimation. Journal of the operational research society 61: 1389-1403.

Howarth, R. W. and R. Marino, 2006. Nitrogen as the limiting nutrient for eutrophication in coastal marine ecosystems: Evolving views over three decades. Limnol. Oceanogr., 51(1, part 2), 364-376.

Hughes, B. B., Haskins, J. C., Wasson, K., Watson, E., 2011. Identifying factors that influence expression of eutrophication in a central California estuary. Mar. Ecol. Prog. Ser. 439: 31-43.

Jackson, G. A. and P. M. Williams, 1985. Importance of dissolved organic nitrogen and phosphorus to biological nutrient cycling. Deep-Sea Res. 32 (2): 223-235.

Jeddah Chamber of Commerce and Industry, 2009. Jeddah Guide – Facts and Figures, 411 pp. http://www.jeg.org.sa/data/modules/contents/uploads/infopdf/1090.pdf

Jeddah Municipality, 2009. Jeddah Strategic Plan. www.jeddah.gov.sa\strategy, 429p.

Kara, A. B., P. A. Rochford and H. E. Hurlburt, 2000. An optimal definition for ocean mixed layer depth. J. Geophys. Res. 105(C7): 16803-16821.

Kemp, W. M., J. M. Testa, D. J. Conley, D. Gilbert and J. D. Hagy, 2009. Temporal responses of coastal hypoxia to nutrient loading and physical controls. Biogeosciences, 6: 2985-3008.

Khomayis, H. S. 2002. The Annual Cycle of Nutrient Salts and Chlorophyll a in the Coastal Waters of Jeddah, Red Sea. JKAU: Mar. Sci. 13: 131-145.

Kinsey, D. W. and Davies, P. J., 1979. Effects of elevated nitrogen and phosphorus on coral reef growth. Limnol. Oceanogr. 24: 935-940.

Kitidis, V., G. Uher, R. C. Upstill-Goddard, R. F. C. Mantoura, G. Spyres and E. M. S. Woodward, 2006. Photochemical production of ammonium in the

oligotrophic Cyprus Gyre (Eastern Mediterranean). Biogeosciences 3: 439-449.

Kitidis, V., G. Uher, E. M. S. Woodward, N. P. J. Owens and R. C. Upstill-Goddard, 2008. Photochemical production and consumption of ammonium in a temperate river-sea system. Mar. Chem. 112: 118-127.

Koropitan, A. F., M. Ikeda, A. Damar & Y. Yamanaka, 2009. Influences of physical processes on the ecosystem of Jakarta Bay: a coupled physical – ecosystem model experiment. ICES Journal of Marine Science, 66: 336-348.

Lapointe, B. E. and M. W. Clark, 1992. Nutrient inputs from the watershed and coastal eutrophication in the Florida Keys. Estuaries 15 (4): 465-476.

Lapointe, B. E., 1997. Nutrient threholds for bottom-up control of macroalgal blooms on coral reefs in Jamaica and southeast Florida. Limnol. Oceanogr. 42 (5, part 2), 1119-1131.

Letscher, R. T., D. A. Hansell, C. A. Carlson, R. Lumpkin, and A. N. Knapp, 2013. Dissolved organic nitrogen in the global surface ocean: Distribution and fate. Global Biogeochem. Cycles, 27: 141–153. doi:10.1029/2012GB004449.

Locarnini, R. A., A. V. Mishonov, J. I. Antonov, T. P. Boyer, H. E. Garcia, O. K. Baranova, M. M. Zweng & D. R. Johnson, 2010. World Ocean Atlas 2009, Volume 1: Temperature. S. Levitus, Ed. NOAA Atlas NESDIS 68, U.S. Government Printing Office, Washington, D.C., 184 pp.

Lomas, M. W. and F. Lipschultz, 2006. Forming the primary nitrite maximum: Nitrifiers of phytoplankton? Limnol. Oceanogr. 51: 2453-2467.

Lopes, J. F., C. I. Silva & A. C. Cardoso, 2008. Validation of a water quality model for the Ria de Aveiro lagoon, Portugal. Environmental Modelling & Software, 23: 479-494.

Lopes, J. F., M. A. Almeida & M. A. Cuhna, 2010. Modelling the ecological patterns of a temperate lagoon in a very wet spring season. Ecological Modelling, 221: 2302-2322.

Lucas, L. V., J. K. Thompson and L. R. Brown, 2009. Why are diverse relationships observed between phytoplankton biomass and transport time? Limnology and Oceanography, 54: 381-390.

Lucea, A., C. M. Duarte, S. Agustí and M. Søndergaard, 2003. Nutrient (N, P and Si) and carbon partitioning in the stratified NW Mediterranean. J. Sea Res. 49(3): 157-170.

Mackey, K. R. M., L. Bristow, D. R. Parks, M. A. Altabet, A. F. Post and A. Paytan, 2011. The influence of light on nitrogen cycling and the primary nitrite maximum in a seasonally stratified sea. Progress in Oceanography 91: 545-560.

Madah, F., R. Mayerle, G. Bruss and J. Bento, 2015. Characteristics of tides in the Red Sea Region, a numerical model study. Open Journal of Marine Science 5: 193-209.

Magram, S. F., 2009. A Review on the Environmental Issues in Jeddah, Saudi Arabia with Special Focus on Water Pollution. J. Environ. Sci. Technol. 2: 120-132. doi:10.3923/jest.2009.120.132

Mandura, A. S., 1997. A mangrove stand under sewage pollution stress: Red Sea. Mangroves Salt Marshes 1: 255-262.

Marubini, F. and Davies, P. S., 1996. Nitrate increases zooxanthellae population density and reduces skeletogenesis in corals. Mar. Biol. 127: 319-328.

Meeder, E., K. R. M. Mackey, A. Paytan, Y. Shaked, D. Iluz, N. Stambler, T. Rivlin, A. F. Post and B. Lazar, 2012. Nitrite dynamics in the open ocean – clues from seasonal and diurnal variations. Mar. Ecol. Prog. Ser. 453: 11-26.

Metcalf and Eddy, Inc., 1991. Wastewater engineering: treatment, disposal and reuse. Tchobanoglous and F. L. Burton (eds.), MacGraw-Hill, New York, 1820 pp.

Miller, S., 1983. Photochemistry of natural water systems. Environ. Sci. Technol. 17: 568A-570A.

Mizerkowski, B. D., Hesse, K.-J., Ladwig, N., da Costa Machado, E., Rosa, R., Araujo, T., Koch, D., 2012. Sources, loads and dispersion of dissolved inorganic nutrients in Paranaguá Bay. Ocean Dynamics 62: 1409-1424.

Morcos, S. A., 1970. Physical and chemical oceanography of the Red Sea. Oceanogr. Mar. Biol. Ann. Rev., 8:73-202.

Morell, J. M. and J. E. Corredor, 2001. Photomineralization of fluorescent dissolved organic matter in the OrinocoRiver plume: Estimation of ammonium release. J. Geophys. Res. 106: 16807-16813.

Morel, A. and S. Maritorena, 2001. Bio-optical properties of oceanic waters: A reappraisal. J. Geophys. Res. 106: 7163-7180.

Mudarris, M. S. A. and A. J. Turki, 2006. Sewage water quality and its dilution in the coastal waters of South Corniche, Jeddah, Red Sea. J. KAU: Met., Env. and Arid Land Agric. Sci., 17:115-128.

Naqvi, S. W. A., H. P. Hansen and T. W. Kureishy, 1986. Nutrient uptake and regeneration ratios in the Red Sea with reference to the nutrient budgets. Oceanol. Acta, 9(3):271-275.

Naqvi, S. W. A., H. Naik, A. Pratihary, W. D'Souza, P. V. Narvekar, D. A. Jayakumar, A. H. Devol, T. Yoshinari and T. Saino, 2006. Coastal versus open-ocean denitrification in the Arabian Sea. Biogeosciences 3: 621-633.

National Center for Atmospheric Research Staff (Eds). Last modified 13 Oct 2016. "The Climate Data Guide: SODA: Simple Ocean Data Assimilation." Retrieved from https://climatedataguide.ucar.edu/climate-data/soda-simple-ocean-data-assimilation.

Newell, S. E., A. R. Babbin, A. Jayakumar, and B. B. Ward, 2011. Ammonia oxidation rates and nitrification in the Arabian Sea. Global Biogeochem. Cycles 25, GB4016, doi:10.1029/2010GB003940.

Obernosterer, I. and R. Benner, 2004. Competition between biological and photochemical processes in the mineralization of dissolved organic carbon. Limnol. Oceanogr. 49(1): 117-124.

OSPAR Commission, 2003. OSPAR Integrated Report 2003 on the Eutrophication Status of the OSPAR Maritime Area Based Upon the First Application of the Comprehensive Procedure, Eutrophication Series, www.ospar.org, 59 pp.

Paerl, H., 2008. Nutrient and other environmental controls of harmful cyanobacterial blooms along the freshwater-marine continuum. Advances in Experimental Medicine and Biology, 619: 217-237. doi: 10.1007/978-0-387-75865-7_10.

Painter, S. C., 2011. On the significance of nitrification within the euphotic zone of the subpolar North Atlantic (Iceland basin) during summer 2007. J. Marine Syst. 88: 332-335.

Park, K., H.-S. Jung, H.-S. Kim & S.-M. Ahn, 2005. Three-dimensional hydrodynamic-eutrophication model (HEM-3D): application to Kwang-Yang Bay, Korea. Marine Environmental Research, 60: 171-193.

Peña-García, D., N. Ladwig, A. J. Turki and M. S. Mudarris, 2014. Input and dispersion of nutrients from the Jeddah Metropolitan Area, Red Sea. Marine Pollution Bulletin, 80: 41-51.

Poisson, A., S. Morcos, S. Souvermezoglou, A. Papaud and A. Ivanoff, 1984. Some aspects of biogeochemical cycles in the Red Sea with special reference to new observation made in summer 1982. Deep-Sea Res., 31:707-718.

Pope, R. M. and E. S. Fry, 1997. Absorption spectrum (380–700 nm) of pure water. II. Integrating cavity measurements. Appl. Opt.36: 8710-8723.

Prieur, L. and S. Sathyendranath, 1981. An optical classification of coastal and oceanic waters based on the specific spectral absorption curves of phytoplankton pigments, dissolved organic matter, and other particulate materials. Limnol. Oceanogr. 26(4): 671-689.

Quadfasel, D. and H. Baudner, 1993. Grey-scale circulation cells in the Red Sea. Oceanol. Acta 16, 221-229.

Qurban, M. A., A. C. Balala, S. Kumar, P. S. Bhavya and M. Wafar, 2014. Primary production in the northern Red Sea. J. Marine Syst. 132: 75-82.

Raitsos, D. E., Y. Pradhan, R. J. W. Brewin, G. Stenchikov and I. Hoteit, 2013. Remote Sensing the Phytoplankton Seasonal Succession of the Red Sea. PLoS ONE 8(6): e64909. https://doi.org/10.1371/journal.pone.0064909

Risk, M. J., O. A. Sherwood, R. Nairn and C. Gibbons, 2009. Tracking the record of sewage discharge off Jeddah, Saudi Arabia, since 1950, using stable isotope records from antipatharians. Mar. Ecol Prog. Ser. 497: 219-226.

Röttgers, R. and R. Doerffer, 2007. Measurements of optical absorption by chromophoric dissolved organic matter using a point-source integrating-cavity absorption meter. Limnol. Oceanogr.: Methods 5: 126–135.

Röttgers, R., D. McKee and C. Utschig, 2014. Temperature and salinity correction coefficients for light absorption by water in the visible to infrared spectral region. Opt. Express 22(21): 25093-25108.

Saad, M. A. H. and M. A. Fahmy, 1996. Heavy metal pollution in the coastal Red Sea waters, Jeddah, J. King Abdul Aziz Univ., Mar. Sci. 7: 67-74

Sathyendranath, S., V. Stuart, A. Nair, K. Oka, T. Nakane, H. Bouman, M.-H. Forget, H. Maass & T. Platt, 2009. Carbon-to-chlorophyll ratio and growth rate of phytoplankton in the sea. Marine Ecology Progress Series, 383: 73-84.

Schindler, D. W., 2006. Recent advances in the understanding and management of eutrophication. Limnol. Oceanogr., 51:356-363.

Shaik, E. A., J. C. Roff and N. M. Dowidar, 1986. Phytoplankton ecology and production in the Red Sea off Jiddah, Saudi Arabia. Marine Biology, 92:405-416.

Shawly, H. H., 2008. Urban water-integrated resource planning to meet future demand in Jeddah - Saudi Arabia. Stuttgarter Berichte zur Siedlungswasserwirtschaft 193, 189 pp

Smith, V. H., 2006. Responses of estuarine and coastal marine phytoplankton to nitrogen and phosphorus enrichment. Limnol. Oceanogr., 51(1, part 2), 377-384.

Söderström, J. 1996. The significance of observed nutrient concentrations in the discussion about nitrogen and phosphorus as limiting nutrients for the primary carbon flux in coastal water ecosystems. Sarsia 81: 81-96.

Sofianos, S. S., W. E. Johns and S. P. Murray, 2002. Heat and freshwater budgets in the Red Sea from direct observations at Bab el Mandeb. Deep-Sea Research II, 49(7-8):1323-1340.

Sofianos, S. S. and W. E. Johns, 2003. An Oceanic General Circulation Model (OGCM) investigation of the Red Sea circulation: 2. Three-dimensional circulation in the Red Sea. J. Geophys. Res. 108 (C3): 3066. DOI:10.1029/2001JC001185.

Stedmon, C. A., S. Markager, L. Tranvik, L. Kronberg, T. Slätis and W. Martinsen, 2007. Photochemical production of ammonium and transformation of dissolved organic matter in the Baltic Sea. Mar. Chem. 104: 227-240.

Stramma, L., G. C. Johnson, J. Sprintall and V. Mohrholz, 2008. Expanding Oxygen-Minimum Zones in the Tropical Oceans. Science 320: 655-658.

Suleiman A.Azis, B., Y. Kosaki & M. Ishikawa, 2011. Water environmental conditions in the Jeddah coast. Memoirs of the Osaka Institute of Technology, Series A. 56: 17-21.

SWCC, 2009. Saline Water Conversion Corporation. Annual Report No. 36 (2009), 112p.

Turki, A. J., 2007. Metal speciation (Cd, Cu, Pb and Zn) in Sediments from Al Shabab Lagoon, Jeddah, Saudi Arabia. Journal of King Abdulaziz University: Marine Sciences, 18: 191-210.

Turki, A. J. and M. S. A. Mudarris, 2008. Bacteria and nutrients as pollution indicators in the Al-Nawrus recreational lagoon, Jeddah. JKAU: Mar. Sci., 19:77-93.

Tyrrell, T. and C. S. Law, 1997. Low nitrate:phosphate ratios in the global ocean. Nature 387:793-796.

Tyrrell, T., 1999. The relative influences of nitrogen and phosphorus on oceanic primary production. Nature 400: 525-531.

Tyrrell, T. and M. I. Lucas, 2002. Geochemical evidence of denitrification in the Benguela upwelling system, Cont. Shelf Res. 22: 2497–2511.

UNEP-United Nations Environment Programme, 1985. Management and conservation of renewable marine resources in the Red Sea and Gulf of Aden region. UNEP Regional Seas Reports and Studies No 64. 89 p.

UNEP-United Nations Environment Programme, 1997. Assesment of land-based sources and activities affecting the marine environment in the Red Sea and Gulf of Aden. UNEP Regional Seas Reports and Studies No 166. 67 p.

Vähätalo, A. V., M. Salkinoja-Salonen, P. Taalas and K. Salonen, 2000. Spectrum of the quantum yield for photochemical mineralization of dissolved organic carbon in a humic lake. Limnol. Oceanogr. 45: 664-676.

Vähätalo, A. V. and R. G. Zepp, 2005. Photochemical mineralization of dissolved organic nitrogen to ammonium in the Baltic Sea. Environ. Sci. Technol. 39: 6985-6992.

Wafar, M., M. A. Qurban, M. Ashraf. K. P. Manikandan, A. V. Flandez and A. C. Balala, 2016. Patterns of distribution of inorganic nutrients in Red Sea and their implications to primary production. Journal of Marine Systems 156: 86-98.

Wang, X. J., Behrenfeld, M., Le Borgne, R., Murtugudde, R., Boss, E., 2009. Regulation of phytoplankton carbon to chlorophyll ratio by light, nutrients and temperature in the Equatorial Pacific Ocean: a basin scale model. Biogeosciences 6: 391-404.

World Ocean Review, 2010. Maribus gGmbh, Hamburg. 232p.

Yool, A., A. P. Martin, C. Fernández and D. R. Clark, 2007. The significance of nitrification for oceanic new production. Nature 447: 999-1002.

Zhan, P., A. C. Subramanian, F. Yao, and I. Hoteit, 2014. Eddies in the Red Sea: A statistical and dynamical study, J. Geophys. Res. Oceans, 119, 3909–3925, doi:10.1002/2013JC009563.

APPENDIX A: SPECIFIC CONTRIBUTIONS

The contributions of the authors to a manuscript published as part of the doctoral program are indicated as follow:

Peña-García, D., N. Ladwig, A. J. Turki & M. S. Mudarris, 2014. Input and dispersion of nutrients from the Jeddah Metropolitan Area, Red Sea. Mar. Pollut. Bullet. 80(1-2):41-51.

Specific contributions: D. Peña-García prepared the concept of the paper, calculated the loads, analyzed and interpreted the data, and wrote the original manuscript and further revisions. N. Ladwig did the spatial interpolation, discussed and analysed the data, contributed to the manuscript and the writing. A. J. Turki and M. S. Mudarris contributed to the manuscript.

Part of the previous mentioned publication is within the thesis.

APPENDIX B: SWORN DECLARATION

David Peña-García

Carrera 7 # 106-25

Bogotá, Colombia

Declaration for my dissertation entitled:

"Nutrient gradients in the Red Sea: The coastal area off Jeddah and the Central Red Sea"

Dear Sir/Madam,

I hereby declare that, apart from the supervisor's guidance, the content and design of the thesis is all my own work. The thesis has been submitted neither partially nor wholly as part of a doctoral degree to another examining body, and no academic degree has ever been withdrawn. It has neither been published nor submitted for publication. I also assure that the thesis has been prepared subject to the Rules of Good Scientific Practice of the German Research Foundation.

Bogotá, Colombia, 11th July 2021

Place and date Signature